

UCSF

UC San Francisco Electronic Theses and Dissertations

Title

The design and development of new inhibitor scaffolds that broaden the scope of analog-sensitive kinase technology

Permalink

<https://escholarship.org/uc/item/6pq7g474>

Author

Lopez, Michael Steven

Publication Date

2013

Peer reviewed|Thesis/dissertation

The design and development of new inhibitor scaffolds that broaden
the scope of analog-sensitive kinase technology

by

Michael S. Lopez

DISSERTATION

Submitted in partial satisfaction of the requirements for the degree of

DOCTOR OF PHILOSOPHY

in

Chemistry and Chemical Biology

in the

GRADUATE DIVISION

of the

Copyright 2013

by

Michael S. Lopez

Dedication

I absolutely must thank my beautiful, funny, and amazing wife Amanda for her unconditional love and unyielding support throughout graduate school. I would also like to thank my parents Steve and Esther Lopez for instilling within me the value of hard work.

Acknowledgements

Thank you to Professor Kevan Shokat and Professor David Morgan for outstanding mentorship. Also, thanks to Professor Charles Craik for serving on my thesis committee and playing a very significant role as an unofficial mentor.

Graduate school was an amazing time due to the camaraderie of many classmates and labmates. In particular, thanks to Dr. Joseph Kliegman, Dr. Gregory Ducker, Dr. Nicholas Hertz, Dr. Alexander Warkentin, and Dr. (anticipated) Samuel Myers for making grad school definitely-not-boring!

I would like to acknowledge collaborators for their specific contributions to each project:

Professor Chao Zhang – Design and synthesis of benzyl-PP compounds described in Chapter 2

Professor Arvin Dar – Mentorship during my rotation and for solving X-ray co-crystal structures of 3MB-PP1 and 1NM-PP1 bound to Src-AS1 (Chapter 2)

Professor Michael J. Eck – for solving the co-crystal structure of 1NA-PP1 bound to Src-AS1 (Chapter 2)

Dr. Jonathan Choy – original synthesis of Star 1 and Star 2 (Chapter 3)

Dr. Ulf Peters – for teaching me X-ray crystallography

Dr. Martin Sos – Constructing the NIH 3T3 cell lines expressing Kif5b-Ret-WT and Kif5b-Ret-AS2

Professor L. David Sibley – drug treatment of mice for PK studies (Chapter 4)

Dr. Alexander Warkentin – proliferation assays of Flt3-driven cell lines (Chapter 4)

Chapter 2 of this thesis contains portions of work previously published as *Structure-guided inhibitor design expands the scope of analog-sensitive kinase technology*. ACS Chem. Biol. 2013.

I would also like to acknowledge the National Science Foundation for supporting me with an NSF Graduate Research Fellowship.

Abstract

Engineered analog-sensitive (AS) protein kinases have emerged as powerful tools for dissecting phospho-signaling pathways, for elucidating the cellular function of individual kinases, and for deciphering unanticipated effects of clinical therapeutics. A crucial and necessary feature of this technology is a bioorthogonal small molecule that is innocuous towards native cellular systems but can potently inhibit the engineered kinase. In an effort to generalize this method we report the development of two new AS kinase inhibitors. First we describe 3MB-PP1, an inhibitor that targets recalcitrant AS kinases that are not sensitive to other known AS-kinase inhibitors. Second, we report the design and development of a new class of inhibitors, termed staralogs, which are uniquely specific for AS kinases. Staralogs extend the scope of the AS technique to include kinases, such as EphA4, that are sensitive to other AS kinase inhibitors even in their un-engineered Wild-Type (WT) form. Finally, we use lessons learned from the development of staralogs to design a new molecule, Star 23, that is an extremely selective and potent inhibitor of Flt3 kinase, a validated drug target for the treatment of acute myeloid leukemia (AML). We suggest Star 23 may serve as a superior therapeutic agent because it does not target the homologous kinase, c-Kit, whose activity is required for the regeneration of healthy white blood cells necessary for a patient's complete remission.

Table of Contents

Preface.....	1
Chapter 1. Introduction.....	1
Overview of analog-sensitive (AS) technology.....	1
The gatekeeper residue controls the size of the ATP-binding pocket of protein kinases.....	3
Generating a functional AS kinase.....	4
AS kinases are powerful tools for studying phospho-signaling pathways in cells.....	7
AS kinases in living multi-cellular organisms.....	8
The present state of AS-kinase inhibitors.....	9
Chapter 2. Structure-guided design of benzyl-pyrazolopyrimidine inhibitors allows targeting of resistant AS kinases.....	10
Introduction.....	10
X-ray crystal structures of PP inhibitors bound to Src-AS1 reveal mechanism of enhanced efficacy of 3MB-PP1.....	10
Structure-guided inhibitor design yields more potent, selective, and general AS-kinase inhibitors.....	14
Selectivity profiles of PP inhibitors.....	15
Conclusion.....	19
Experimental Methods.....	21
Chapter 3. Staurosporine-derived analog-sensitive kinase inhibitors expand the scope of AS technology.....	29
Introduction.....	29
C7-substituted indolocarbazole derivatives complement the gatekeeper mutation in Src kinase.....	31
Simple polar groups rescue activity of staralog inhibitors toward AS kinases bearing an alanine gatekeeper residue.....	33
Structural basis of Star 12 binding.....	36
Staralogs are bioorthogonal AS-kinase inhibitors.....	38
Staralogs expand the scope of AS-kinase technology.....	39
Conclusion.....	42
Experimental Methods.....	43
Chapter 4. Future directions and conclusions.....	66
Introduction.....	66
Optimizing the <i>in vivo</i> properties of PP inhibitors.....	66
Re-purposing staralogs as therapeutic Flt3 inhibitors.....	69
Staralogs are potent Flt3 inhibitors.....	70
Star 23 is a potent Flt3 inhibitor in cells.....	72
Star 23 selectively targets human AML cells over Kit or Bcr-Abl-driven cell lines.....	72
Star 23 is extremely selective for Flt3 over other human kinases.....	74
Conclusion.....	76
Experimental Methods.....	77
Appendix 1. Tables of published analog-sensitive kinases.....	80
Appendix 2. PP inhibitor profiling data.....	85
Appendix 3. Staralog inhibitor profiling data.....	100
References.....	111

Tables and Figures

Table 1. IC ₅₀ values for Star 12 against a representative set of PP-sensitive kinases	38
Figure 1. Overview of AS-kinase technology.....	2
Figure 2. PP1 binds kinases with medium size gatekeeper residues	3
Figure 3. Sequence alignment of the hinge region of diverse kinases.....	6
Figure 4. X-ray co-crystal structures of 1NA-PP1, 1NM-PP1, or 3MB-PP1 bound to Src-AS1 ..	12
Figure 5. Chemical structures of PP compounds	13
Figure 6. Activity of PP compounds against Fyn and Src kinases	15
Figure 7. Off-target activity of PP compounds <i>in vitro</i> and in cells	18
Figure 8. Design of staralog inhibitors and structure-activity relationships of the C7-position....	32
Figure 9. Synthetic approach for construction of staralog derivatives	33
Figure 10. Synthetic approach for installing N12 and N13 substituents	34
Figure 11. Panel of staralogs bearing N12 or N13 substituents.....	35
Figure 12. X-ray co-crystal structure of Star 12 bound to Src-AS1	36
Figure 13. Overlay of X-ray co-crystal structure of Star 12/Src-AS1 with staurosporine/Src-WT	37
Figure 14. Representative sequence alignment of kinases from diverse families and organisms highlights the conservation of Asn 391	37
Figure 15. Inhibition profiles of Star 12, staurosporine, 1NA-PP1, 1NM-PP1, and 3MB-PP1 against ~ 300 kinases	39
Figure 16. Staralogs are potent and selective inhibitors of AS kinases in cells.....	41
Figure 17. PP inhibitors designed to have enhanced metabolic stability and retain potency	67
Figure 18. Serum half-life concentration in mice treated with 3CIB-PP1 or GXJ-184.....	68
Figure 19. Dose-response curves and IC ₅₀ values for staralogs against Flt3 kinase.....	71
Figure 20. Star 23 activity against Flt3-driven Ba/F3 cells	72
Figure 21. Dose-dependent proliferation of leukemia cell lines in the presence of PKC412, CGP52421, or Star 23	73
Figure 22. Selectivity of Star 23	75

Chapter 1 – Introduction

Overview of analog-sensitive (AS) kinase technology

Eukaryotic protein kinases catalyze the transfer of phosphate from ATP to serine, threonine or tyrosine residues on substrate proteins. The resulting phosphorylation event constitutes a critical mode of post-translational protein modification and a core mechanism for cellular signal transduction. Nearly every physiological process in eukaryotic cells involves phospho-signaling networks and many human diseases occur when these pathways are dysregulated¹. Potent and selective inhibitors of protein kinases are valuable tools for probing these networks and for elucidating the cellular functions of individual kinases². However, due to the large number of protein kinases in a cell and their highly homologous active sites, it has proven challenging to find specific inhibitors for many individual kinases³. Our laboratory has developed a chemical-genetic technique that enables systematic generation of highly specific inhibitors for individual kinases⁴. This approach combines the advantages of a small molecule inhibitor (temporal resolution, reversibility, etc.) with the specificity of a genetic manipulation. When a residue at a structurally conserved position in the kinase active site (termed the gatekeeper⁵) is mutated from the natural bulky amino acid side chain (methionine, leucine, phenylalanine, threonine, etc.) to smaller glycine or alanine, a novel pocket that is not found in wild-type (WT) kinases is created within the ATP-binding site. Such an engineered kinase is termed an Analog Sensitive (AS) kinase because it can be potently and specifically targeted by inhibitor analogs that contain a bulky substituent complementing the enlarged ATP-binding pocket⁶.

A major goal of our laboratory is to extend AS-kinase technology to the entire kinome; the fact that nearly all kinases contain a bulky gatekeeper residue suggests this undertaking is possible in principle. However, two criteria must be satisfied for a particular kinase-of-interest (KOI) to be amenable to the approach. First, the kinase must tolerate mutation of the gatekeeper residue to glycine or alanine without severe loss of catalytic activity or cellular function. Second, a potent and bioorthogonal small molecule inhibitor of the AS kinase must be identified. In the course of our studies we have encountered a number of kinases that do not meet one or both of the criteria; they are either intolerant of the gatekeeper mutation or insensitive to available

pyrazolo[3,4-*d*]pyrimidine (PP) inhibitors. We have developed a systematic workflow to overcome each of these limitations as they present themselves (Fig. 1A). For example, if the kinase does not tolerate a glycine gatekeeper, which provides the maximal expansion of the ATP pocket, the larger amino acid alanine may be used instead (Fig. 1B). We have also demonstrated that the introduction of second-site suppressor mutations can be employed to rescue the activity of weakened AS kinases⁷ (Fig. 1C). In extreme cases where second-site suppressor mutations fail to rescue activity a second approach termed an Electrophile-sensitive (ES) kinase may be used⁸. In ES kinases the gatekeeper is mutated to cysteine instead of alanine or glycine, thereby retaining a more hydrophobic residue at the gatekeeper position, maintaining the integrity of the hydrophobic spine of the kinase⁹ and thus enhancing enzyme activity, while sensitizing the ES kinase to PP-inhibitors bearing an appropriately positioned electrophile. Once an active AS or ES kinase has been engineered, a potent and selective AS kinase or ES-kinase inhibitor must be identified from a small library of PP molecules based on the semi-promiscuous tyrosine kinase inhibitor PP1 (Figure 2A).

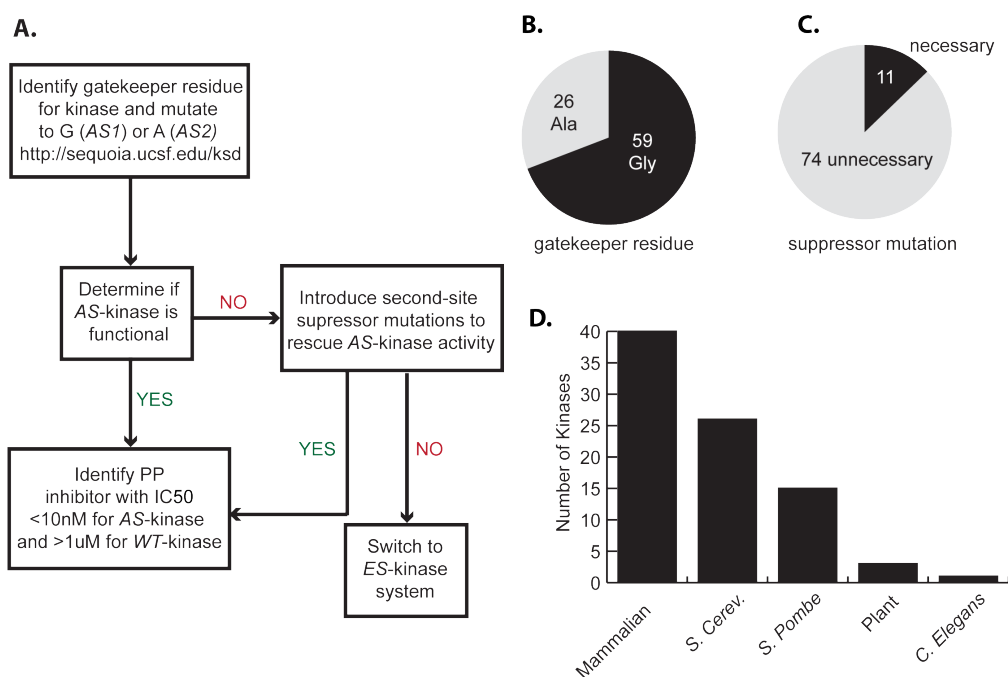


Figure 1. Overview of AS-kinase technology (A) Flow-chart outlines systematic approach for application of AS-kinase technology. (B) The pie chart illustrates the number of reported AS kinases with alanine, A, or Glycine, G, gatekeeper residues. (C) The number of reported AS kinases that require suppressor mutations to rescue activity. (D) The bar graph denotes the number of AS kinases that have been reported in peer-reviewed publications for each class of kinase.

The gatekeeper residue controls the size of the ATP-binding pocket of protein kinases. PP1 was initially identified as a potent ATP-competitive inhibitor of Src-family kinases¹⁰. However, Liu and Shokat *et al* used bioinformatics and site-directed mutagenesis to demonstrate that PP1 was capable of binding any kinase with a small amino acid residue (Thr, Val, Ala, Gly) at the position analogous to Src T338¹¹. The initial classification of PP1 as a Src-family kinase inhibitor simply reflected the fact that many Src family kinases have threonine residues at this position. The Src T338 site is now called the gatekeeper residue because the size of this residue's side chain determines the volume of the hydrophobic pocket at the rear of the ATP-binding site. Thus, kinases with small gatekeeper residues are able to accommodate ligands with large bulky groups such as the C3-tolyl ring of PP1 that cannot bind to kinases with larger gatekeepers. This phenomenon has been exploited by medicinal chemists for the design of selective inhibitors of kinases with small and medium gatekeeper residues¹². Importantly, Lui and Shokat recognized the potential for any kinase to be made sensitive or resistant to inhibitors such as PP1 by choosing the appropriate gatekeeper and exchanging it for the native residue with site-directed mutagenesis. They also noted that kinases sensitive to PP1 become resistant upon mutation of the gatekeeper residue to isoleucine, thereby predicting resistance that would later emerge in the clinic¹³.

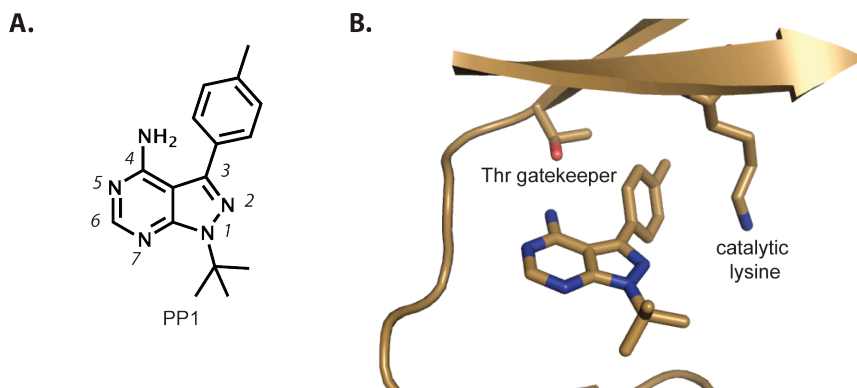


Figure 2. PP1 binds kinases with medium size gatekeeper residues. (A) Chemical structure of PP1. (B) X-ray co-crystal structure of PP1 bound to Hck kinase. The C3-tolyl group of PP1 is wedged between the gatekeeper threonine and the catalytic lysine residue.

The co-crystal structure of PP1 bound to a Src family kinase, Hck, showed that the pyrazolopyrimidine core of PP1 mimics the adenine ring of ATP in its binding to the nucleobase pocket while the *p*-tolyl group at the C3 position projects into a deep hydrophobic pocket situated between the gatekeeper T338 and the catalytic lysine residue K295 (Figure 2B)¹⁴. Based on this crystal structure, it was predicted that PP1 analogs with an enlarged C3 substituent would suffer a steric clash with the native gatekeeper residue in WT kinases. However, mutation of the gatekeeper to glycine or alanine, which are exceedingly rare in the human kinome, should create extra space to accommodate the enlarged C3 substituent. Thus, the same phenomenon that results in the selectivity of PP1 for a subset of WT kinases can be used to create inhibitors with selectivity for unnatural kinases engineered to contain glycine or alanine gatekeepers. It has been demonstrated that potent and specific inhibitors can be readily identified for various AS kinases by screening a small panel of PP derivatives with enlarged C3 substituents⁴. INA-PP1 and 1NM-PP1 were initially found to be the most effective inhibitors for AS kinases and have been used to target numerous AS kinase alleles from a variety of organisms and kinase families⁴.

Generating a functional AS kinase. As illustrated by the flowchart in Figure 1A, we have developed a systematic approach for engineering functional AS kinases. The first step is to correctly identify the gatekeeper residue of the kinase-of-interest (KOI). This can be done by submitting the amino acid sequence of the KOI kinase domain to the Kinase Database at <http://sequoia.ucsf.edu/ksd/>. Additionally, the amino acid sequence of the KOI kinase domain can be aligned with c-Src and other protein kinases to identify the position equivalent to Src T338 (Figure 3). Typically, the gatekeeper residue is preceded by two hydrophobic amino acids (I336 and V337 in Src) and followed by an acidic residue (E339 in Src) and another hydrophobic amino acid (Y340 in Src). While atypical kinases may require additional structural information to accurately identify the gatekeeper, this simple sequence alignment is usually sufficient for canonical tyrosine and serine/threonine protein kinase.

One of the most commonly encountered obstacles in the creation of AS kinases is the loss of stability or activity that may result from mutation. The gatekeeper residue of protein kinases contributes to the hydrophobic spine of the kinase domain and plays an important role in

promoting enzymatic activity⁹. Thus, mutation of this position to a smaller residue may disrupt this structural feature and lead to a reduction in the catalytic efficiency of the AS kinase. For example, mutation of the budding yeast kinase Cdc28 from the native phenylalanine gatekeeper to glycine results in a ten-fold reduction in ATP affinity and a six-fold reduction in k_{cat} ⁴. Fortunately, this reduction in activity is often acceptable and can be tested directly by examining the ability of the AS allele to complement loss of the WT gene. In cases where compromised kinase activity is prohibitive, our lab has developed a series of steps to remedy this limitation.

The glycine gatekeeper mutation (AS1) creates the maximal expansion of the ATP-binding pocket and typically also maximizes sensitivity to AS-kinase inhibitors. However, if the AS1 kinase suffers a prohibitive reduction in activity, the alanine gatekeeper (AS2) can be employed to increase enzyme activity while retaining sensitivity to AS-kinase inhibitors. Additionally, Zhang *et al* identified second-site suppressor mutations in the five-stranded anti-parallel β sheet of the N-terminal lobe of the kinase domain that enhance the stability and activity of AS kinases⁷. In certain cases, the activity of impaired AS-kinases can also be rescued by rational substitution of residues that are not conserved in closely related, well-behaved AS kinases¹⁵. Taken together, these mutations represent a general and systematic approach for engineering functional AS kinases capable of complementing the WT gene while retaining sensitivity to a specific inhibitor. Nearly all kinases that we have attempted to engineer into AS form have been successful with the proper choice of gatekeeper residue and the addition of second-site suppressors when necessary. However, our lab has developed a cysteine gatekeeper approach that can be used in cases where glycine or alanine are absolutely not tolerated⁸. This species of engineered kinase is termed an Electrophilic Sensitive (ES) kinase and relies on inhibitors that target the cysteine gatekeeper through covalent chemistry. The cysteine gatekeeper has a larger, more non-polar side chain that maintains the integrity of the hydrophobic spine and retains or enhances kinase activity. The expansion of the ATP-binding pocket of ES kinases is minimal; however, the unique reactivity of the cysteine thiol allows covalent targeting of the gatekeeper with appropriate electrophilic inhibitors. Like glycine and alanine, cysteine gatekeepers are exceedingly rare in the human kinome thereby reducing the chances of off-target activity of ES-kinase inhibitors. The irreversible nature of covalent inhibitors also provides unique experimental advantages. For example, an ES kinase might be

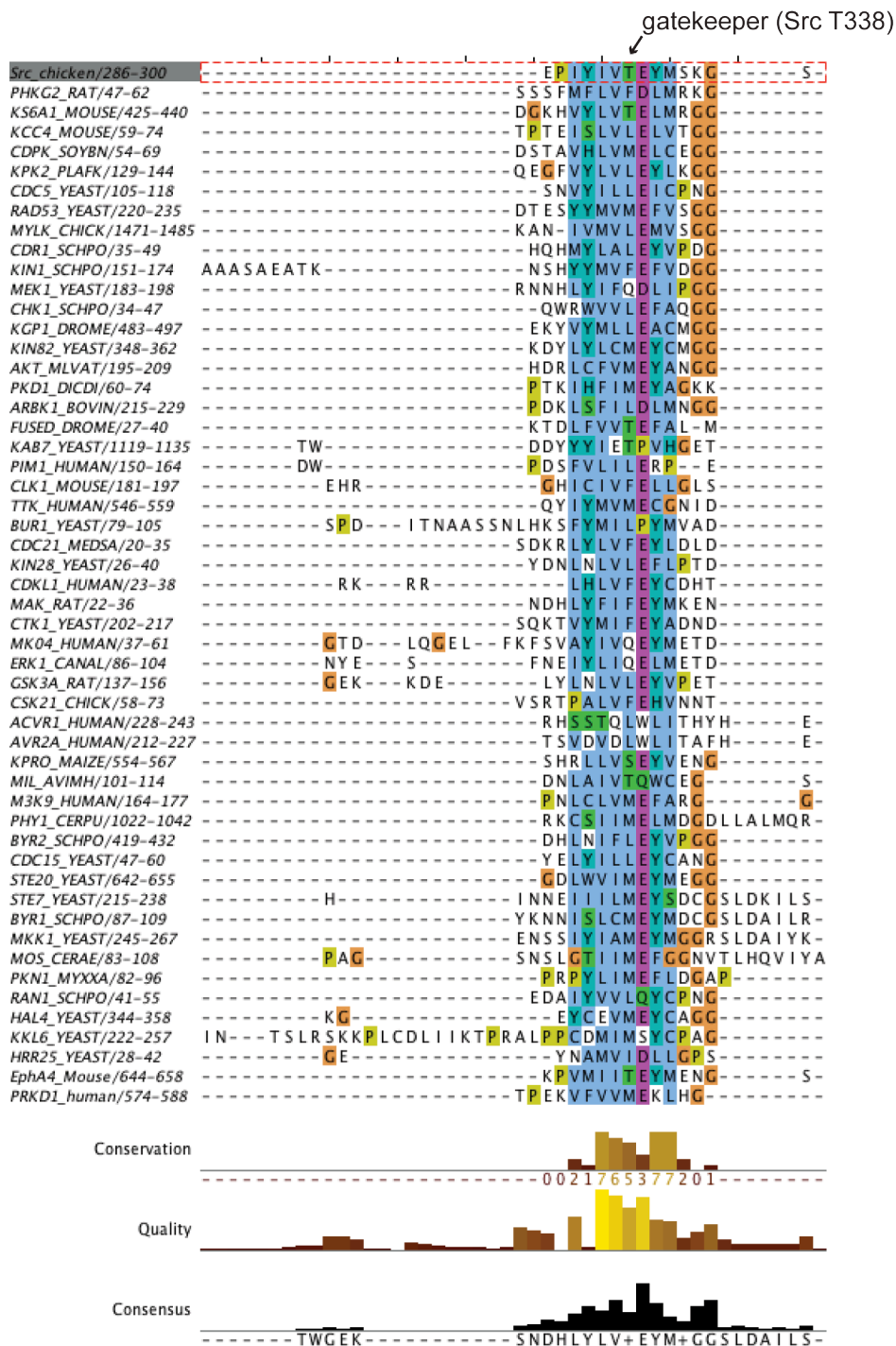


Figure 3. Sequence alignment of the hinge region of diverse kinases. The gatekeeper residue varies amongst kinases, but nearly always follows two aliphatic residues and precedes an acidic residue.

titrated with inhibitor to identify the precise activity threshold required for a specific function. Another exciting advantage of this technique is the potential to target two different engineered kinases with orthogonal inhibitors. Taken together, glycine, alanine and cysteine gatekeeper residues can be used in combination with appropriate second-site suppressor mutations to engineer nearly any kinase into a functional enzyme that is sensitive to specific small molecule inhibition.

AS kinases are powerful tools for studying phospho-signaling pathways in cells. AS technology is most commonly used to study kinase-signaling pathways in single-cell eukaryotes, such as yeast, or in cell lines derived from multi-cellular organisms such as mice and humans. This allows ease of genetic manipulations and avoids the complication of pharmacokinetics (PK) and pharmacodynamics (PD) that are encountered when using small molecules in intact multi-cellular organisms. There are, however, considerable differences in the cell-permeability of AS-kinase inhibitors amongst different cell types. Mammalian cells are fairly permeable to small organic molecules and thus AS-kinase inhibitors can often be used at relatively low concentrations between 100 nM and 5 μ M (Appendix 1). In contrast, the thick cell wall of plant cells and the abundant drug transporters present in yeast often require AS kinase inhibitors to be used at much higher concentrations (up to 100 μ M) despite the fact that yeast and plant kinases are likely to have similar sensitivity to these inhibitors *in vitro*.

The genetic tractability of yeast and their ability to exist in a stable haploid state has led to widespread use of AS technology in both *S. cerevisiae* and *S. pombe*. For example, there are 113 conventional protein kinase genes in budding yeast¹⁶ and the AS technique has been applied to 26 individual kinases (Appendix 1) thereby covering 23% of the yeast kinome. More recently, Gregan and co-workers developed functional AS alleles and identified suitable inhibitors for 13 of the 17 essential kinases in *S. pombe*¹⁷. Some of the key discoveries made with various AS kinases in yeast include the large-scale identification of Cdc28 substrates¹⁸ and the discovery of the allosteric activation of the RNase activity of Ire1 upon ligand binding to the ATP-binding site within its kinase domain¹⁹. Recently, Kliegman and co-workers managed to combine AS technology with the power of large-scale yeast genetics by crossing an AS-Tor2 *S. cerevisiae*

strain with a library of deletion strains and measuring dose-dependent genetic interactions between AS-Tor2 inhibition and each deleted gene (Joseph Kliegman, personal communication). In summary, the ease of yeast genetics presents a simple system in which the AS technique can be used to elucidate fundamental eukaryotic kinase-signaling pathways.

Over 40 mouse or human AS kinases have been reported in peer-reviewed publications thereby making mammalian cells the most commonly studied with AS technology. In many cases, a disease-causing kinase allele may be dominant, allowing simple over-expression of the AS mutant in an appropriate cell line for investigation. In other cases, the WT kinase gene must be replaced with the AS allele. Although genetic manipulation of mammalian cells is often more difficult than in yeast, they offer the opportunity to address many questions most relevant to human disease. For example, Wong *et al* used an AS mutant of the disease-causing fusion protein Bcr-Abl to demonstrate that inhibition of this kinase alone was not sufficient to eliminate all myeloproliferative disorder cell populations²⁰. This was an important discovery as it revealed that the off-target effects of the clinical therapeutic imatinib are, in fact, required for effective treatment of heterogeneous Chronic Myeloid Leukemia cell populations. AS kinases have also been used to shed light on fundamental processes of mammalian biology and development. An AS mutant of Zap70, for example, has been used to identify its role in T cell receptor and CD28 super agonist signaling, and to determine which functions are dependent on kinase activity. Thus, the use of AS kinases in mammalian tissue culture is a powerful method for investigating fundamental biological processes and the molecular basis of human disease.

AS kinases in living multi-cellular organisms. Many developmental processes can only be studied in the context of an intact organism. Furthermore, therapeutic drug targets can only truly be validated by inhibition *in vivo*. Thus, several AS kinases have been introduced into mice and used to study the *in vivo* biology or pharmacology of kinase signaling pathways. The *in vivo* use of AS kinases presents the additional challenges of achieving optimal PK and PD properties for small molecule inhibitors. While the properties of current AS kinase inhibitors have not been optimized for *in vivo* efficacy, they are nevertheless sufficient for use with several AS kinases in mice. For example, Wright and co-workers generated mice that are homozygous for an AS

mutant of Ret kinase in order to study the role of GDNF signaling in spermatogenesis. Taconis is a company that generates mice bearing homozygous AS kinase alleles, which they refer to as ASKA mice. Presumably, their target consumers are biotech and pharmaceutical companies who wish to validate specific kinases as therapeutic targets before investing the time and money required for the development of viable drug compounds. Although the effectiveness of their ASKA mice is not subject to peer review, they claim to have generated functional ASKA mice for the following kinases: Akt1, Gsk α , Gsk3 β , Ntrk1, Ntrk2, Src, Btk, Map3k5, EphB4, Mapk14, PdgfrB, Met, and Rps6kb1 (<http://www.taconic.com>). It is likely that such a large number of ASKA mice suggests a strong unmet need in drug target validation. In both drug development enterprises and academic investigations it is clear that many important questions can only be addressed *in vivo* and that AS-kinase technology may play an important role in furthering these studies.

The present state of AS-kinase inhibitors. A necessary tool for studying AS kinases in any system is a potent and selective small molecule inhibitor. As mentioned above, 1NA-PP1 and 1NM-PP1 were initially identified to be the most potent and selective inhibitors for diverse AS kinases. However, we have encountered a number of cases where 1NA-PP1 and 1NM-PP1 were not efficacious because of a lack of potency for the AS kinase or because of off-target inhibition of WT kinases. In this thesis I describe my work to develop new PP inhibitors that allow targeting of resistant AS kinases. I also describe a new set of inhibitors based on the natural product staurosporine that are extremely selective and allow targeting of AS kinases whose WT alleles are sensitive to PP analogs. Finally, I present some preliminary work aimed at repurposing AS-kinase inhibitors as therapeutic inhibitors of disease causing kinases.

Chapter 2 – Structure-guided Design of Benzyl-Pyrazolopyrimidine Inhibitors Allows Targeting of Resistant Analog-sensitive Kinases

Introduction

In the course of our studies we have encountered a number of AS kinases that are insensitive to 1NA-PP1 and 1NM-PP1, thereby precluding the application of our chemical genetic technique. Our initial hypothesis was that the PP structure was sub-optimal for some kinases and thus we sought alternative scaffolds that might be complementary or even superior to PP. For example, we used an inhibitor based on the aminoindazole scaffold (a known Akt binder) to target AS Akt alleles^{21,22}. However, this molecule and its derivatives were largely inactive towards other AS kinases (unpublished results). We also attempted to design AS-kinase inhibitors based on purine, pyrimidine, and quinazoline scaffolds^{23,24}, but these molecules also proved to be largely ineffective against diverse AS kinases. Since the PP scaffold has so far proven to be the most general for AS kinases, we embarked on a medicinal chemistry effort to find a new PP analog capable of targeting recalcitrant AS kinases. The result of this undertaking was the identification of a new molecule 3MB-PP1 that has enhanced potency against a diverse set of AS kinases, including several that were insensitive to all previously known AS-kinase inhibitors^{17,21,25,26}. The focus of this study is to understand the mechanism of efficacy of 3MB-PP1 by analysis of co-crystal structures of Src-*AS1* kinase bound to 3MB-PP1, 1NA-PP1, or 1NM-PP1. We then use insights gained from these structures to design next-generation PP inhibitors with increased potency and selectivity for AS kinases.

Results and Discussion

X-ray Crystal Structures of PP Inhibitors Bound to Src-AS1 Reveal Mechanism of Enhanced Efficacy of 3MB-PP1. We previously reported that 3MB-PP1 and a closely related analog **16** (Figure 4A, 5) are capable of targeting several AS kinases that are impervious to 1NA-PP1 and 1NM-PP1^{17,21,25,26}. In order to better understand the enhanced efficacy of 3MB-PP1 and the potential deficiencies of 1NA-PP1 and 1NM-PP1 in targeting divergent AS kinases, we

solved co-crystal structures of Src-AS1 (T338G) in complex with 1NA-PP1, 1NM-PP1 or 3MB-PP1 (Figure 4C). Comparison of the Src-AS1 structures to the previously solved Src-WT/AMP-PNP complex reveals little movement of protein backbone atoms (with an RMSD of 0.22 Å) upon introduction of the gatekeeper mutation T338G, indicating that the mutation does not perturb the overall structure of the Src protein (Figure 4B). The most notable effect of the T338G mutation in Src is the expanded ATP-binding pocket that we hypothesized would accommodate bulky groups at the C3 position of PP1. Next we created an overlay of the Src-AS1 structures with that of the highly homologous tyrosine kinase Hck bound to PP1 (Figure 4C). We found that the PP analogs share nearly identical binding orientations and hydrogen bond interactions with the hinge region of the kinase. As predicted, the bulky naphthyl, naphthylmethyl and 3'-methylbenzyl substituents of 1NA-PP1, 1NM-PP1 and 3MB-PP1, respectively, project toward the gatekeeper and occupy the pocket created by the T338G mutation. While PP1 is accommodated in the ATP pocket of Hck, it is clear that all three AS-kinase inhibitors are prevented from binding due to a steric clash with the Thr gatekeeper residue; however, the degree of clash varies amongst the compounds. Specifically, the naphthyl ring of 1NA-PP1 (Figure 4C, green) appears to have minimal overlap with the surface of the gatekeeper side chain, while the clash between the gatekeeper and 1NM-PP1 (Figure 4C, purple) is maximal and that with 3MB-PP1 (Figure 4C, yellow) is intermediate. The minimal clash between 1NA-PP1 and a Thr gatekeeper explains why 1NA-PP1 has weak activity towards WT-kinases with small gatekeeper residues but not towards kinases with larger Ile or Phe gatekeeper residues⁴. In contrast, the C5' position of 1NM-PP1 projects deep into the gatekeeper side chain surface of Hck, thus explaining the enhanced orthogonality of 1NM-PP1 towards WT kinases relative to 1NA-PP1.

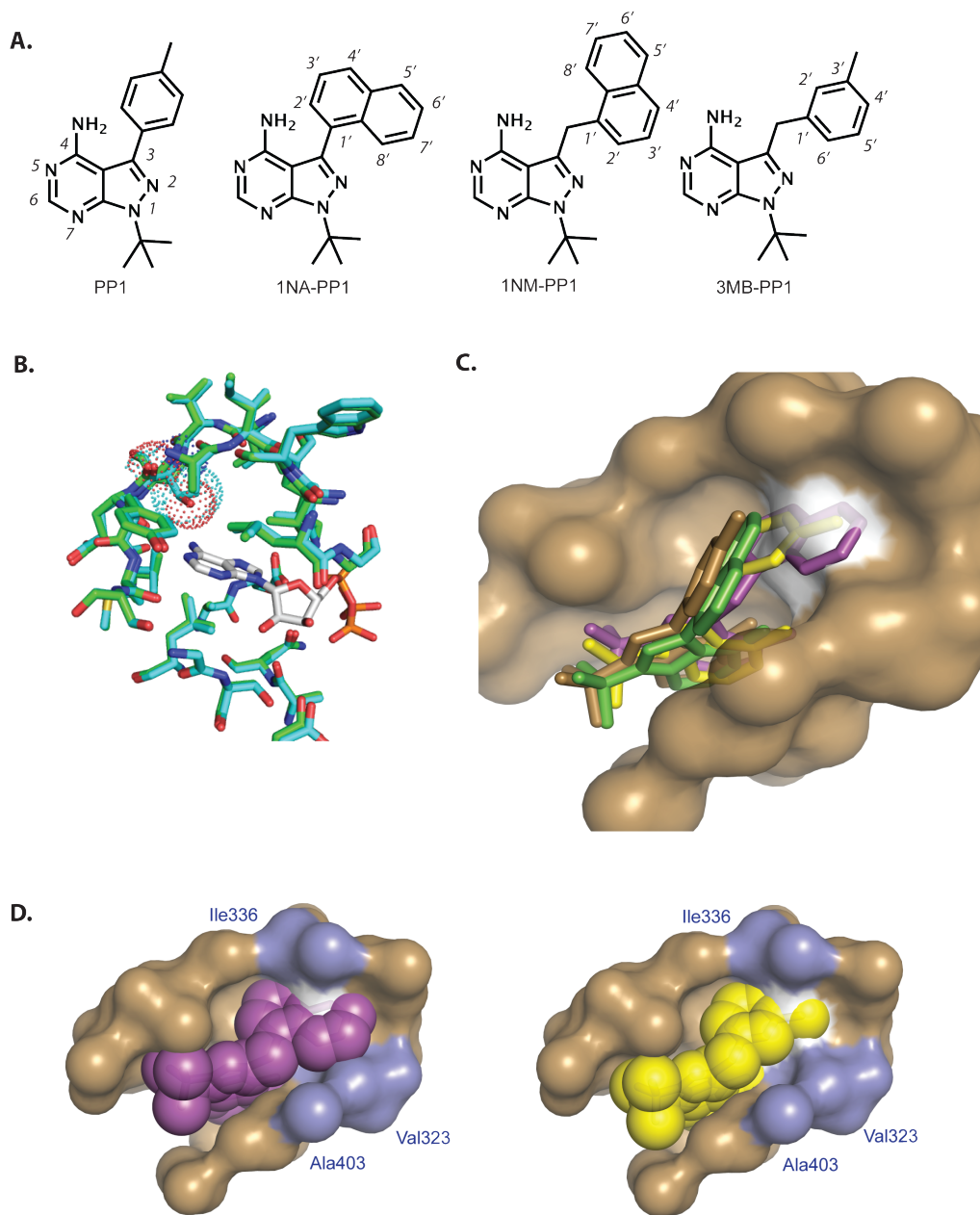


Figure 4. X-ray co-crystal structures of 1NA-PP1, 1NM-PP1, or 3MB-PP1 bound to Src-AS1. (A) PP1 is a promiscuous kinase inhibitor that targets kinases with medium size gatekeeper residues (Thr, Val, Ser). 1NA-PP1, 1NM-PP1 and 3MB-PP1 are three of the most commonly used AS-kinase inhibitors. (B) Overlay of Src-WT (teal) and Src-AS1 (green) with the WT-gatekeeper surface illustrated in dots and the Src-WT ligand AMP-PNP (white). (C) Overlay of 1NA-PP1 (green), 1NM-PP1 (pink) and 3MB-PP1 (yellow) with the PP1/Hck-WT structure (brown). The surface of the gatekeeper residue is highlighted in white. (D) Overlay of Hck ATP pocket surface with 3MB-PP1 (right, yellow spheres) and 1NM-PP1 (left, pink spheres). Surface of residues V323, I336 and A403 are highlighted in blue.

A key feature of both 1NM-PP1 and 3MB-PP1 is the methylene linker between the aryl ring and the heterocyclic core of the PP scaffold. This linkage imbues the molecules with rotational freedom that allows for optimal orientation of the bulky phenyl and naphthyl rings in the gatekeeper pocket, thereby maximizing potential affinity interactions with the enlarged ATP pocket of AS kinases. Simultaneously, the methylene linker ensures that the bulky aryl groups project more deeply into the gatekeeper pocket, resulting in greater steric clash with the gatekeeper side chain of WT-kinases. The 3'-methyl group of 3MB-PP1 and C5' of 1NM-PP1 appear to occupy the same position within the ATP binding pocket and provide the most direct steric clash with the gatekeeper side chain. An important difference between 3MB-PP1 and 1NM-PP1, however, is that the additional atoms of the naphthyl ring of 1NM-PP1 (C6', C7', and C8') provide additional clash with the Hck gatekeeper, but also appear to overlap with the surface of other residues in the ATP binding pocket (V323, I336 and A403; Figure 4D). We hypothesize that subtle differences in the ATP binding sites of divergent kinases might alleviate or escalate this undesired interaction and, in extreme cases, prevent 1NM-PP1 from binding to the AS kinase despite the enlarged gatekeeper pocket. In fact, it has been demonstrated that some kinases bearing larger amino acids at the position analogous to Ala 403 can be further sensitized to PP derivatives by mutation of that position to alanine²⁷.

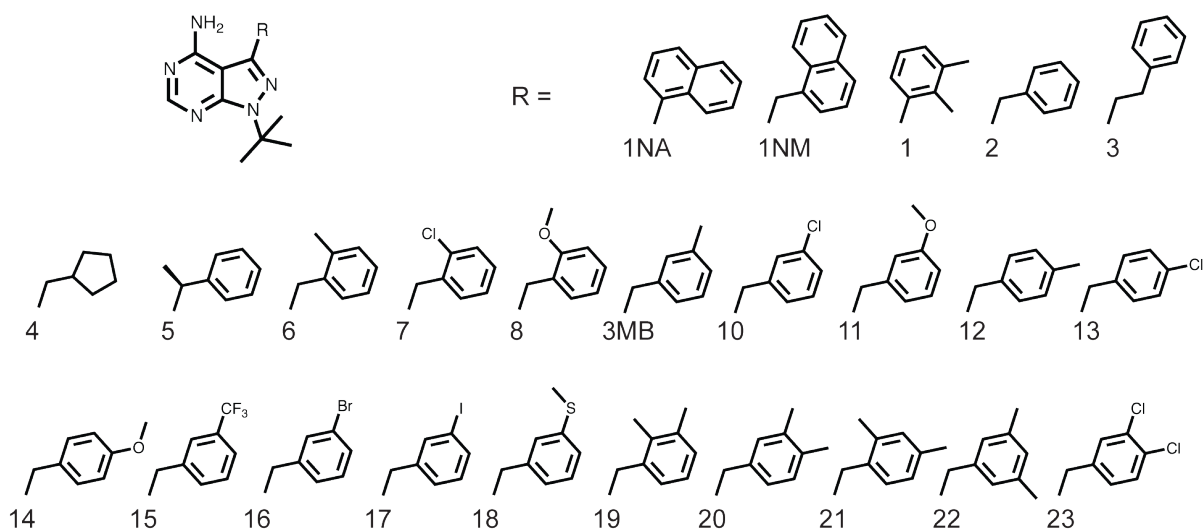


Figure 5. Chemical structures of PP compounds

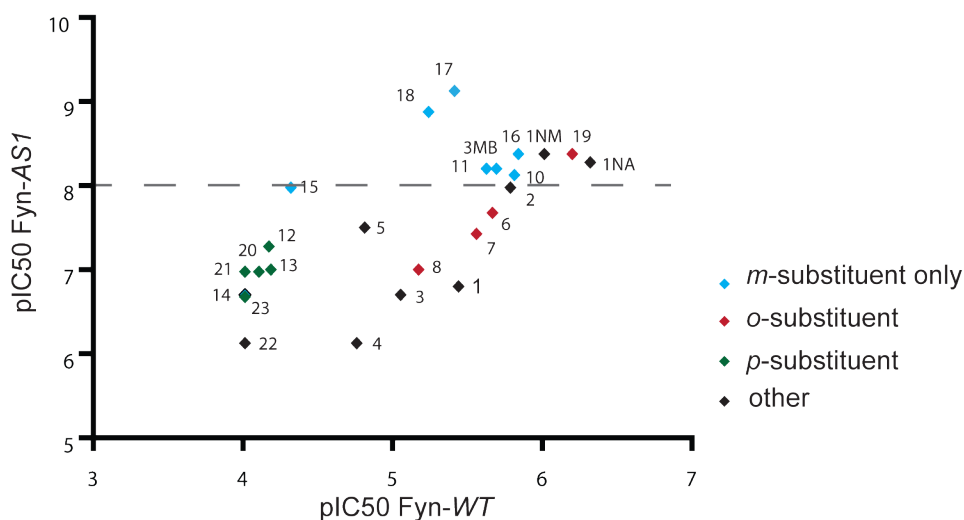
Structure-guided Inhibitor Design Yields More Potent, Selective, and General AS-kinase

Inhibitors. Next we sought to test our hypothesis that the benzyl moiety is the optimal orthogonality element for PP AS-kinase inhibitors as well as to design more potent, selective and general AS-kinase inhibitors using our enhanced understanding of 3MB-PP1 as a guide. Thus, we synthesized a panel of PP derivatives based largely on the benzyl PP scaffold with various substituents designed to project into the gatekeeper pocket, as does the methyl group of 3MB-PP1 (Figure 5). The PP analogs were synthesized in four steps using a previously described route⁶ and were analyzed for potency and selectivity towards Fyn-AS1 over Fyn-WT. We chose Fyn, a Src family tyrosine kinase, because it is a potent target of PP1⁵; thus, an inhibitor of AS kinases that does not target WT-Fyn would ensure that potency was not gained at the expense of selectivity. We plotted the negative logarithm of the IC₅₀ value (pIC₅₀) of each compound for Fyn-AS1 against the pIC₅₀ for Fyn-WT to illustrate the potency and selectivity of the inhibitors (Figure 6A). Strikingly, all of the new PP's with pIC₅₀ (Fyn-AS1) ≥ 8 contain the *m*-substituted benzyl functional group. Increasing the linkage between the aryl group and the heterocyclic core from one methylene to two (**3**) or removing the methylene group altogether (**1**) results in a dramatic decrease in activity. Remarkably, all compounds that are mono-substituted at the C3' position of the benzyl group are quite potent and selective inhibitors of Fyn-AS1. C2'-substituted benzyl PP inhibitors (**6-8**) showed decreasing potency with increasing size of the substituent, indicating an unfavorable steric clash that can be minimized with smaller substituents. Molecules with substituents at the C4' position (**12-14**) display an even more dramatic decrease in potency towards both Fyn alleles. Taken together, these results confirm that the C3'-substituted benzyl PP structure is an ideal scaffold for AS-kinase inhibitors.

Notably, two C3'-benzyl PP's, **17** and **18**, stand out as being the most potent and selective inhibitors of Fyn-AS1; these molecules contain larger, more polarizable groups relative to 3MB-PP1. We wished to verify that the enhanced efficacy of these compounds was a general phenomenon and not unique to Fyn, so we measured their ability to target Src-WT, Src-AS1 (SrcT338G), and Src-AS2 (SrcT338A). Once again, **17** and **18** have poor (IC₅₀ > 10 μM) activity towards the WT-kinase but are the most potent inhibitors for the kinase bearing a glycine

gatekeeper. **17** and **18** are less potent towards Src-AS2, suggesting the iodo and thiomethyl substituents may ideally complement the space created by a glycine gatekeeper but are perhaps

A.



B.

	1NA	1NM	2	3MB	10	11	15	16	17	18	19
Src-WT	900	1200	1500	2300	1200	2000	50000	1500	4000	6000	900
Src-AS1	1.5	2	8	3	4	3	6	2	0.4	0.7	1
Src-AS2	1	15	9	6	7	9	58	10	13	30	3

IC₅₀ (nM)

Figure 6. Activity of PP analogs against Fyn and Src kinases. (A) The pIC₅₀ of each compound for Fyn-AS1 is plotted against the pIC₅₀ for Fyn-WT to illustrate the potency and selectivity of PP inhibitors. The dotted grey line indicates threshold for compounds with suitable potency (pIC₅₀ > 8) against Fyn-AS1. (B) IC₅₀ values for select PP's against Src-WT, Src-AS1 and Src-AS2. IC₅₀ values were determined from a single dose-response measurement.

too large to fit in the smaller ATP pocket created by the alanine gatekeeper. Taken together, our results suggest that the C3'-substituted PP core is the optimal scaffold for AS-kinase inhibitors; however, the substituent that best complements a particular AS kinase might vary.

Selectivity Profiles of PP Inhibitors. A crucial property that an effective AS-kinase inhibitor must possess is selectivity; it must potently inhibit the activity of an AS kinase but not affect

WT-kinases or other endogenous proteins. We and others have previously reported that 1NA-PP1 and 1NM-PP1 are very selective but imperfect AS-kinase inhibitors, as they weakly target some WT-kinases^{4,28}. To gain a more comprehensive understanding of the off-target effects of our AS-kinase inhibitors we tested the ability of 1 μ M 1NA-PP1, 1NM-PP1, 3MB-PP1, **17** and **18** to inhibit the activity of several hundred WT-kinases *in vitro* and found that several are indeed sensitive to one or more PP inhibitors (Appendix 2). This is a very high standard for selectivity as AS-kinase inhibitors typically have IC₅₀ values < 100 nM towards AS kinases and the cellular concentration of the competitor ligand ATP is relatively high (1-10mM)²⁹. Nonetheless, we wished to determine if off-target inhibition of WT-kinases by PP compounds is significant in the broad panel of AS-technology. We asked which of the WT-kinases targeted by our PP inhibitors are likely to be inhibited in cells at concentrations typically used in chemical genetic experiments. To this end we first measured IC₅₀ values for 1NA-PP1, 1NM-PP1 and 3MB-PP1 against a representative subset of the PP-sensitive WT-kinases identified in our screen (Figure 7A, B). We found that kinases inhibited greater than 80% in our screen generally have IC₅₀ values less than 100 nM, while those inhibited between 40-80% have IC₅₀ values ranging between 100 nM and 1.5 μ M (Figure 7B). The correlation between the fractional kinase activity determined in our screen and the measured IC₅₀ values gives us confidence that data from the screen can be used to accurately predict the *in vitro* potency of our inhibitors against a large portion of the kinome.

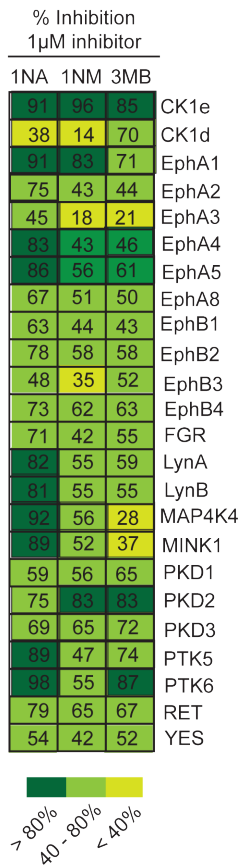
To address whether PP-sensitive WT-kinases are likely to be bona fide targets in cells we calculated the predicted EC₅₀ values for each inhibitor/kinase pair using the Cheng Prusoff equation (Figure 7B) which relates the measured IC₅₀ value, the K_M of the enzyme for ATP, and the cellular concentration of ATP which we assume to be ~5mM^{30,31}. PP-inhibitors are typically used in mammalian cells at concentrations between 500 nM and 5 μ M (Appendix 1). We calculated that many of the identified PP-sensitive WT-kinases would only be targeted in cells at concentrations greater than 5 μ M and we therefore predicted their cellular inhibition should be minimal under typical experimental conditions.

We sought to confirm that weak *in vitro* inhibition of WT-kinases by PP molecules is not a practical impediment to our technique by demonstrating the analog-sensitive approach can be

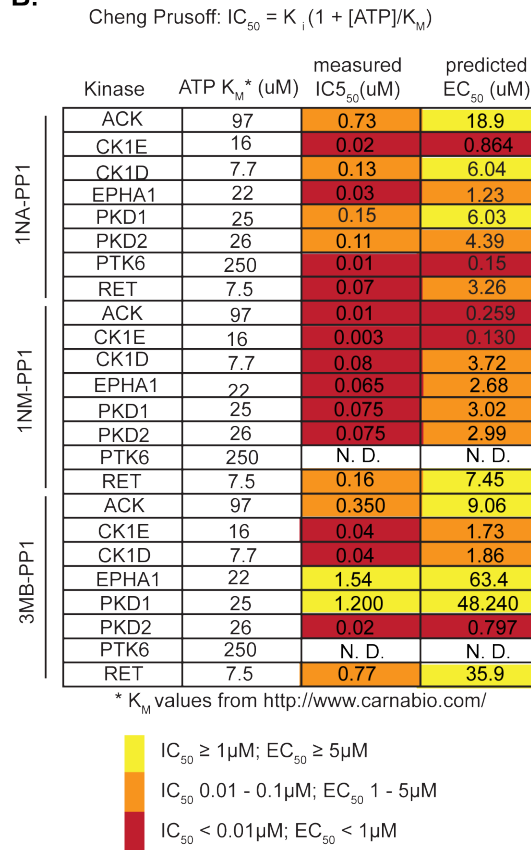
applied to Protein Kinase D1 (Pkd1), one of the few kinases inhibited by all PP analogs tested. This unusual sensitivity to PP analogs may be due to a lysine residue at position 667 that occurs in all three Pkd family members in place of a conserved hydrophobic amino acid found in nearly all other kinases. K667 is located in the hinge region of the kinase domain and it is possible that this amino acid side chain allows greater flexibility in the inhibitor binding orientation although this remains to be tested. Pkd1 is a widely expressed Ser/Thr protein kinase involved in a number of physiological processes including the trafficking of membrane proteins in neurons³². We transfected HEK 293T cells with Pkd1-AS2 (M665A) or Pkd1-WT and found that a concentration of 1 μ M 1NA-PP1 completely abrogates autophosphorylation by the analog-sensitive allele but not the wild type kinase, despite the fact that Pkd1-WT is inhibited by 1NA-PP1 *in vitro* with an IC₅₀ of 150 nM (Fig. S1). We wished to examine the effects of 1NA-PP1 on a physiological function of Pkd1 and thus we examined the localization of the Pkd1-WT and Pkd1-AS2 in the presence of inhibitor. Kinase-dead alleles of Pkd1 have been shown to constitutively localize to the *trans*-Golgi network (TGN) and TGN-derived vesicles³³. We co-expressed Venus-tagged Pkd1-WT and Pkd1-AS2 in neurons and assessed puncta formation in the presence of 1 μ M 1NA-PP1 and found that Venus-Pkd1-WT neurons were unaffected, while Venus-Pkd1-AS2 recapitulated the kinase-dead phenotype, forming discrete puncta after one hour of inhibitor treatment (Figure 7C).

The example of Pkd1 demonstrates that kinases predicted to be targeted by PP inhibitors in cells with EC₅₀ values greater than several micromolar are unlikely to be inhibited under the typical conditions of chemical genetic experiments. Additionally, 1NA-PP1 and 3MB-PP1 have been used to selectively target AS alleles of Ret, EphB2, EphB3 and EphB4 in cells and mice despite weak inhibition of their WT-alleles *in vitro*^{34,35}. Thus, many of the WT-kinases identified as targets of 1NA-PP1, 1NM-PP1 or 3MB-PP1 in our screen and in the work of others are not likely to be bona fide targets in a cellular context.

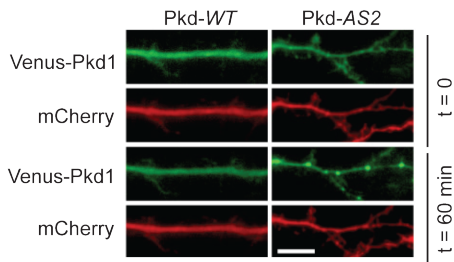
A.



B.



C.



D.

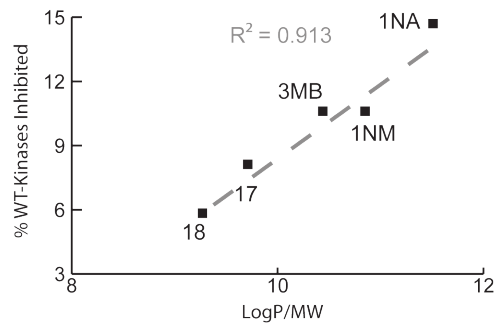


Figure 7. Off-target activity of PP compounds *in vitro* and in cells (A) Fraction of activity of wild-type PP-sensitive kinases inhibited by 1uM 1NA-PP1, 1NM-PP1 and 3MB-PP1. (B) IC_{50} values were measured for 1NA-PP1, 1NM-PP1 and 3MB-PP1 towards eight WT-kinases. The Cheng-Prusoff equation and K_M values of each kinase for ATP were used to calculate predicted EC_{50} values for 1NA-PP1, 1NM-PP1, and 3MB-PP1 towards eight WT-kinases. (C) Neurons were transfected with Venus-Pkd1-WT or Venus-Pkd1-AS2, treated with DMSO or 1uM 1NA-PP1, and analyzed for puncta formation. (D) The fraction of WT-kinases inhibited by 40% or more was plotted as a function CLogP value for 1NA-PP1, 1NM-PP1, 3MB-PP1, 17 and 18.

As discussed above, weak *in vitro* inhibition of WT-kinases by PP inhibitors is unlikely to be relevant in cells due to competition with the high concentration of ATP. However, we postulate that such weak inhibition might serve as a proxy measurement for overall promiscuity of molecules towards unrelated proteins in a cell. Specifically, PP inhibitors that bind to fewer WT-kinases are less likely to bind to diverse proteins including metabolic enzymes capable of inactivating drug molecules *in vivo*. An important physical property that contributes to the promiscuity of small molecule inhibitors is lipophilicity; lipophilic molecules tend to bind non-specifically to hydrophobic regions of proteins such as ligand binding sites³⁶. Furthermore, lipophilic molecules are more likely to have poor bioavailability, poor solubility and to form aggregates that may non-specifically inhibit unrelated enzymes³⁷. We found that the promiscuity of our PP inhibitors was related to both the lipophilicity and the molecular weight of the molecule; larger molecules (greater molecular weight) are less promiscuous while more lipophilic molecules (greater LogP) tend to be more promiscuous. We plotted the fraction of WT-kinases whose activity is inhibited by 40% or more as a function of LogP/MW for 1NA-PP1, 1NM-PP1, 3MB-PP1, **17**, and **18**, and discovered this yields a linear relationship (Figure 7D). This observation was surprising as we initially expected 1NM-PP1 to be the most selective inhibitor due to the greater steric clash between the naphthyl moiety and the ATP-binding pocket observed in the overlay of the 1NM-PP1/Src-AS1 and the Hck structures. In fact 3MB-PP1 has a selectivity profile that is similar to 1NM-PP1, while **17** and **18** inhibit a much smaller fraction of WT-kinases. We interpret these results to reflect the fact that two mechanisms of selectivity are at work; increasing size of the functional group that projects towards the gatekeeper contributes to selectivity as we originally designed. However, minimizing lipophilicity also contributes by reducing non-specific affinity of the molecules for the hydrophobic ATP binding pocket of kinases. This discovery highlights the importance of a more comprehensive evaluation of drug molecules that incorporates consideration of physical properties such as lipophilicity in addition to the more obvious metrics of on-target potency (IC_{50} , EC_{50} , etc).

Conclusion.

We have reported the mechanism of enhanced efficacy of the AS-kinase inhibitor 3MB-PP1 as well as the design and development of new, more potent and selective AS-kinase inhibitors. We employed X-ray crystallography to decipher the binding modes of 1NA-PP1, 1NM-PP1, and

3MB-PP1 and discovered that the methylene linker of benzyl PP analogs projects the phenyl group towards the gatekeeper, preventing binding to most WT-kinases while providing rotational flexibility that allows optimal orientation to complement the enlarged ATP pocket of AS kinases. We used insights gained from these structures to design a small panel of benzyl-PP's and discovered two molecules, **17** and **18** that are the most potent and selective AS-kinase inhibitors yet developed. The increased potency and reduced off-target effects of the new PPs offer a major advantage when targeting an individual AS kinase in cells or organisms that express hundreds of native kinases. Recent studies have identified 3MB-PP1 and **16** as capable of targeting at least 10 AS v kinases that are resistant to inhibition by any other known PP analog^{17,21,25,26}. Importantly, these kinases are from several different organisms and span four of the seven major kinase families (CMGC, STE, AGC, and TK) suggesting the enhanced efficacy of the inhibitors is not unique to the tyrosine kinases described in this report. We also examined the potential limitations presented by off-target inhibition of WT-kinases by PP inhibitors and discovered that many of the WT-kinases inhibited *in vitro* are unlikely to be targeted under cellular conditions. We have combined 1NA-PP1 and 1NM-PP1 with a panel of 3-substituted benzyl PP molecules to create a repertoire of potent and selective AS-kinase inhibitors that allows us to extend AS-kinase technology to the edges of the kinome and propels us towards the larger goal of understanding the logic of cellular signal transduction.

Experimental Methods:

Kinase inhibition assays *in vitro*

Fyn Kinase. Glutathione S-transferase (GST) fused Fyn proteins were expressed in *E. coli* and purified on glutathione beads as described previously⁶. In the Fyn kinase assay, various concentrations of inhibitor were incubated with 50 mM Tris (pH 8.0), 10 mM MgCl₂, 1.6 mM glutathione, 1 mg/mL BSA, 0.1 mg/mL peptide substrate (IYGFEFKKK), 3.3% DMSO, and 11 nM (2 μCi) [γ -³²P]ATP (6000 Ci/mmol, NEN), and Fyn kinase in a total volume of 30 μL for 30 min. Reaction mixtures (27 μL) were spotted onto a phosphocellulose disk, and washed with 0.5% H₃PO₄. The transfer of ³²P was measured by standard scintillation counting. IC₅₀ values were defined to be the concentration of inhibitor at which the radioactivity counts remaining on the phosphocellulose disk were inhibited by 50%.

Src Kinase. 6xHis-tagged Src (257-533) was expressed in BL-21 *ecoli* cells as previously described³⁸. Kinase reaction was carried out as described for Fyn kinase above.

CK1δ and CK1ε. Casein Kinase 1δ (catalog # PV3665) and Casein Kinase 1ε (catalog # PV3500) were purchased from Life Technologies and assayed under the following conditions: 50mM TRIS (pH 8.0), 10mM MgCl₂, 0.4 mg/mL casein, 2.5 mM DTT, 2% DMSO, 5nM kinase, 100μM ATP, 0.1 mg/mL BSA, 1μCi ³²P-ATP and various concentrations of inhibitors.

PKD1 and PKD2. PKD1 (catalog # PV3791) and PKD2 (catalog # PV3758) were purchased from Life Technologies and assayed under the following conditions: 50 mM TRIS (pH 8.0), 10 mM MgCl₂, 2mM DTT, 2% DTT, 0.1 mg/mL BSA, 100 μM ATP, 3 μCi ³²P-ATP, 7 nM kinase and various concentrations of inhibitors.

RET and ACK. RET (catalog # PV3819) and ACK (catalog # PV4807) were purchase from Life Technologies and assayed under the following conditions: 50 mM TRIS (pH 8.0), 10 mM MgCl₂, 2 mM DTT, 0.1 mg/mL BSA, 2% DMSO, 200 μM Abltide, 10 nM kinase, 100 μM ATP, 1μCi ³²P-ATP and variable concentrations of inhibitors.

EPHA1 and PTK6. EPHA1 (catalog # 3841) and PTK6 (catalog # 3291) were purchased from Life Technologies and assayed under the following conditions: 50 mM TRIS (pH 8.0), 10 mM MgCl₂, 2.5 mM DTT, 0.1 mg/mL BSA, 2% DMSO, 0.2 mg/mL poly[Glu, Tyr] 4:1, 2 nM kinase, 100 μM ATP, 1μCi ³²P-ATP and variable concentrations of inhibitors.

Protein crystallization

Src-*AS1* co-crystal structure with 1NA-PP1. The structure of 1NA-PP1 in complex with Src-*AS1* (residues 83–533, including the SH3, SH2, kinase, and tail regions) was determined essentially as previously described for an N6-Benzyl-ADP complex³⁹. Briefly, the Src-*AS1* protein, homogeneously phosphorylated on Tyr 527, was concentrated to 10–15 mg/ml in storage buffer (20 mM HEPES [pH 7.6], 100 mM NaCl, and 10 mM DTT), and combined with a slight molar excess of 1NA-PP1. The complex was crystallized in hanging drops at 22°C by combining 2 μl of the above solution with 1 μl of a well solution (50 mM PIPES [pH 6.5], 12% PEG4000, 10 mM DTT). Crystals were briefly transferred to a buffer containing crystallization solution plus 20% glycerol and frozen at –165°C. Diffraction data were recorded with a Princeton 2k CCD detector on the A1 beamline at CHESS. All diffraction data were integrated and scaled with the programs DENZO and SCALEPACK. The structure was determined by molecular replacement using PDB entry 2SRC as a search model and refined using Refmac. Data collection and refinement statistics are available in Table S3.

Src-*AS1* co-crystal structures with 1NM-PP1 and 3MB-PP1. The kinase domain of c-Src-*AS1* was expressed and purified as previously described²⁴. Src-drug complexes were formed by mixing 10mM DMSO stocks of the drug compounds into 100 mM Src, 100 mM NaCl, 50 mM Tris [8.0], 2 mM DTT, and 5 % glycerol at room temperature. Crystals were obtained in hanging drops of a 1:1 mixture (protein-drug and mother liquor) by vapor diffusion atop a mother liquor solution of 100 mM MES [6.5], 50 mM NaAc, 12% glycerol, and 6% PEG 4000. Just prior to data collection, crystals were flash frozen in mother liquor containing 25% glycerol. Data for the 1NM-PP1 and 3MB-PP1 structures were collected at the Advanced Light Source, beam lines 8.2.2 and 8.2.1, respectively. Data were processed using HKL2000. Molecular replacement solutions for the 1NM-PP1 and 3MB-PP1 structures were solved using Phaser in the CCP4 program suite with chain A of c-Src (PDB ID: 1YOJ) as the search model. Structures were

optimized through iterative rounds of manual fitting in Coot and using maximum likelihood refinement protocols in Refmac. Coordinate and topology files for the ligands 1NM and 3MB were derived in PRODRG.

X-ray Crystallography Data Collection and Refinement Statistics

	Data Collection		
Structure	Src-1NA	Src-1NM	Src-3MB
Space Group	P212121	P1	P1
Unit Cell Dimensions	a= 50.96, b=72.72 , c=171.98 , $\alpha=90$, $\beta=90$, $\gamma=90$	a=42.3 , b=62.7 , c=74.3 , $\alpha=100.4$, $\beta=91.0$, $\gamma=90.1$	a=42.0 , b=55.8 , c=63.0 , $\alpha=90.0$, $\beta=90.1$, $\gamma=88.9$
Number protein molecules/assymetric unit	1	2	2
X-ray Source	CHESS A1	ALS 5.0.1	ALS 5.0.1
Resolution (Å)	2.3	2.84	2.4
Total Reflections	101969	16738	21085
Unique Reflections	28882	16738	18807
Completeness (%)	98.7 (99.6 in 2.38-2.3 shell)	94.7	95.1
	Model Refinement		
Resolution (Å)	25-2.3	32.93-2.84	33.87-2.41
Rwork/Rfree	0.213/0.25	0.230/0.287	0.232/0.281
Rmsd from ideality in bond length (Å)	0.018	0.008	0.014
Rmsd from ideality in Angles (°)	1.38	1.12	1.4
Number of Protein Atoms In Model	3607	3874	7685

Number of Drug atoms In Model	24	50	43
Number of waters	278	37	46
Favored/Allowed/Outliers in the Ramachandran Plot (%)	97.3/2.7/0	95.6/4.4/0	96.6/3.4/0

Compound Characterization

1-tert-Butyl-3-(2,3-dimethylphenyl)-1H-pyrazolo[3,4-d]pyrimidin-4-ylamine (1). White powder; ^1H NMR (CDCl_3 , 400 MHz) δ 1.81 (s, 9H), 2.17 (s, 3H), 2.33 (s, 3H), 5.25 (br s, 2H), 7.20 (m, 3H), 8.31 (s, 1H); ^{13}C NMR (CDCl_3 , 100 MHz) δ 16.5, 20.6, 29.3, 60.3, 100.9, 125.9, 127.9, 130.7, 132.6, 136.2, 138.2, 142.0, 153.7, 154.6, 157.8; HRMS (EI) molecular ion calculated for $\text{C}_{17}\text{H}_{21}\text{N}_5$ 295.17970, found 295.17968.

3-Benzyl-1-tert-butyl-1H-pyrazolo[3,4-d]pyrimidin-4-ylamine (2). White powder; ^1H NMR (CDCl_3 , 400 MHz) δ 1.79 (s, 9H), 4.29 (s, 2H), 4.89 (br s, 2H), 7.20 (d, $J = 7$ Hz, 2H), 7.25 (t, $J = 7$ Hz, 1H), 7.32 (t, $J = 7$ Hz, 2H), 8.23 (s, 1H); ^{13}C NMR (CDCl_3 , 100 MHz) δ 29.2, 35.2, 59.9, 100.7, 127.3, 128.4, 129.4, 138.2, 140.9, 154.5, 154.7, 157.6; HRMS (EI) molecular ion calculated for $\text{C}_{16}\text{H}_{19}\text{N}_5$ 281.16405, found 281.16410.

1-tert-Butyl-3-phenethyl-1H-pyrazolo[3,4-d]pyrimidin-4-ylamine (3). White powder; ^1H NMR (CDCl_3 , 400 MHz) δ 1.74 (s, 9H), 3.11 (t, 2H), 3.22 (t, 2H), 6.32 (s, 2H), 7.17 (d, 2H), 7.25 (m, 3H), 8.17 (s, 1H); ^{13}C NMR (CDCl_3 , 100 MHz) δ 29.2, 31.3, 34.8, 61.1, 99.7, 126.7, 128.5, 128.8, 140.6, 143.2, 147.8, 152.3, 155.1; HRMS (EI) molecular ion calculated for $\text{C}_{17}\text{H}_{21}\text{N}_5$ 295.17970, found 295.17888.

1-tert-Butyl-3-cyclopentylmethyl-1H-pyrazolo[3,4-d]pyrimidin-4-ylamine (4). White powder; ^1H NMR (CDCl_3 , 400 MHz) δ 1.28 (m, 2H), 1.53 (m, 2H), 1.65 (m, 2H), 1.71 (m, 2H), 1.73 (s, 9H), 2.28 (m, 1H), 2.86 (d, $J = 8$ Hz, 2H), 5.69 (br s, 2H), 8.25 (s, 1H); ^{13}C NMR (CDCl_3 , 100 MHz) δ 25.0, 29.2, 32.4, 35.2, 39.7, 59.7, 100.5, 142.1, 153.0, 154.0, 158.0; HRMS (EI) molecular ion calculated for $\text{C}_{15}\text{H}_{23}\text{N}_5$ 273.19535, found 273.19565.

1-tert-Butyl-3-(1-phenethyl)-1H-pyrazolo[3,4-d]pyrimidin-4-ylamine (5). White powder; ^1H NMR (CDCl_3 , 400 MHz) δ 1.71 (d, $J = 7$ Hz, 3H), 1.79 (s, 9H), 4.38 (q, $J = 7$ Hz, 1H), 5.06 (br s, 2H), 7.19 (d, $J = 7$ Hz, 2H), 7.22 (m, 1H), 7.30 (t, $J = 7$ Hz, 2H), 8.16 (s, 1H); ^{13}C NMR (CDCl_3 , 100 MHz) δ 21.0, 29.1, 40.1, 60.0, 100.0, 127.2, 127.4, 129.3, 144.5, 145.2, 153.6, 154.5, 157.3; HRMS (EI) molecular ion calculated for $\text{C}_{17}\text{H}_{21}\text{N}_5$ 295.17970, found 295.18043.

1-tert-Butyl-3-(2-methylbenzyl)-1H-pyrazolo[3,4-d]pyrimidin-4-ylamine (6). White powder; ^1H NMR (CDCl_3 , 400 MHz) δ 1.77 (s, 9H), 2.30 (s, 3H), 4.25 (s, 2H), 5.09 (br s, 2H), 6.98 (d, $J = 8$ Hz, 1H), 7.14 (m, 3H), 8.20 (s, 1H); ^{13}C NMR (CDCl_3 , 100 MHz) δ 19.8, 29.1, 33.1, 59.9, 100.9, 126.7, 127.3, 128.3, 130.8, 136.1, 136.8, 140.6, 154.3, 154.5, 157.8; HRMS (EI) molecular ion calculated for $\text{C}_{17}\text{H}_{21}\text{N}_5$ 295.17970, found 295.17922.

1-tert-Butyl-3-(2-chlorobenzyl)-1H-pyrazolo[3,4-d]pyrimidin-4-ylamine (7). White powder; ^1H NMR (CDCl_3 , 400 MHz) δ 1.78 (s, 9H), 4.38 (s, 2H), 5.41 (br s, 2H), 7.00 (dd, $J_1 = 7$ Hz, $J_2 = 2$ Hz, 1H), 7.15 (m, 2H), 7.39 (dd, $J_1 = 8$ Hz, $J_2 = 2$ Hz, 1H), 8.22 (s, 1H); ^{13}C NMR (CDCl_3 , 100 MHz) δ 29.1, 31.9, 60.0, 100.7, 127.4, 128.4, 129.6, 130.1, 133.3, 135.6, 139.4, 154.4, 154.5, 157.7; HRMS (EI) molecular ion calculated for $\text{C}_{16}\text{H}_{18}\text{N}_5\text{Cl}$ 315.12507, found 315.12449.

1-tert-Butyl-3-(2-methoxybenzyl)-1H-pyrazolo[3,4-d]pyrimidin-4-ylamine (8). White powder; ^1H NMR (CDCl_3 , 400 MHz) δ 1.77 (s, 9H), 3.89 (s, 3H), 4.25 (s, 2H), 5.77 (br s, 2H), 6.89 (m, 2H), 7.18 (m, 2H), 8.20 (s, 1H); ^{13}C NMR (CDCl_3 , 100 MHz) δ 27.4, 29.2, 55.5, 59.8, 100.4, 110.8, 121.5, 126.5, 128.0, 130.6, 141.1, 154.3, 154.3, 155.7, 158.0; HRMS (EI) molecular ion calculated for $\text{C}_{17}\text{H}_{21}\text{N}_5\text{O}$ 311.17461, found 311.17545.

1-tert-Butyl-3-(3-methylbenzyl)-1H-pyrazolo[3,4-d]pyrimidin-4-ylamine (3MB). White powder; ^1H NMR (CDCl_3 , 400 MHz) δ 1.79 (s, 9H), 2.29 (s, 3H), 4.24 (s, 2H), 4.95 (br s, 2H), 6.99 (d, $J = 7$ Hz, 1H), 7.00 (s, 1H), 7.06 (d, $J = 8$ Hz, 1H), 7.20 (t, $J = 8$ Hz, 1H), 8.22 (s, 1H); ^{13}C NMR (CDCl_3 , 100 MHz) δ 21.4, 29.2, 35.1, 59.9, 100.7, 125.4, 128.1, 129.1, 129.1, 138.1, 139.0, 141.1, 154.4, 154.7, 157.7; HRMS (EI) molecular ion calculated for $\text{C}_{17}\text{H}_{21}\text{N}_5$ 295.17970, found 295.17981.

1-(tert-butyl)-3-(3-chlorobenzyl)-1H-pyrazolo[3,4-d]pyrimidin-4-amine (10). White powder; ^1H NMR (CDCl_3 , 400 MHz) δ 1.79 (s, 9H), 3.79 (s, 3H), 3.25 (s, 2H), 7.06 (d, 1H), 7.19 (m,

3H), 8.26 (s, 1H); ^{13}C NMR (CDCl_3 , 100 MHz) δ 29.2, 34.8, 60.1, 77.2, 100.6, 126.4, 127.5, 128.5, 130.4, 135.1, 139.8, 140.2, 154.6, 157.5; HRMS (EI) molecular ion calculated for $\text{C}_{16}\text{H}_{19}\text{N}_5^{35}\text{Cl}$ 316.1324, found 316.1314.

3-(3-Methoxybenzyl)-1-*tert*-butyl-1*H*-pyrazolo[3,4-*d*]pyrimidin-4-ylamine (11). White powder; ^1H NMR (CDCl_3 , 400 MHz) δ 1.79 (s, 9H), 3.74 (s, 3H), 4.25 (s, 2H), 4.89 (s, 2H), 6.72 (s, 1H), 6.79 (m, 2H), 7.22 (s, 1H), 8.24 (s, 1H); ^{13}C NMR (CDCl_3 , 100 MHz) δ 29.4, 35.4, 55.4, 60.1, 100.9, 112.5, 114.7, 120.8, 130.5, 140.1, 141.0, 154.7, 154.9, 157.8, 160.5; HRMS (EI) molecular ion calculated for $\text{C}_{17}\text{H}_{21}\text{N}_5\text{O}$ 311.1824, found 311.1835.

1-*tert*-Butyl-3-(4-methylbenzyl)-1*H*-pyrazolo[3,4-*d*]pyrimidin-4-ylamine (12). White powder; ^1H NMR (CDCl_3 , 400 MHz) δ 1.79 (s, 9H), 2.30 (s, 3H), 4.24 (s, 2H), 4.94 (br s, 2H), 7.08 (d, $J = 8$ Hz, 2H), 7.11 (d, $J = 8$ Hz, 2H), 8.21 (s, 1H); ^{13}C NMR (CDCl_3 , 100 MHz) δ 21.0, 29.2, 34.8, 59.9, 100.6, 128.3, 130.0, 135.1, 136.9, 141.3, 154.5, 154.7, 157.7; HRMS (EI) molecular ion calculated for $\text{C}_{17}\text{H}_{21}\text{N}_5$ 295.17970, found 295.18068.

1-*tert*-Butyl-3-(4-chlorobenzyl)-1*H*-pyrazolo[3,4-*d*]pyrimidin-4-ylamine (13). White powder; ^1H NMR (CDCl_3 , 400 MHz) δ 1.77 (s, 9H), 4.25 (s, 2H), 5.16 (br s, 2H), 7.11 (d, $J = 8$ Hz, 2H), 7.27 (d, $J = 8$ Hz, 2H), 8.22 (s, 1H); ^{13}C NMR (CDCl_3 , 100 MHz) δ 29.1, 34.5, 60.0, 100.6, 129.3, 129.6, 133.1, 136.6, 140.1, 154.5, 154.6, 157.6; HRMS (EI) molecular ion calculated for $\text{C}_{16}\text{H}_{18}\text{N}_5\text{Cl}$ 315.12507, found 315.12545.

1-*tert*-Butyl-3-(4-methoxybenzyl)-1*H*-pyrazolo[3,4-*d*]pyrimidin-4-ylamine (14). White powder; ^1H NMR (CDCl_3 , 400 MHz) δ 1.78 (s, 9H), 3.76 (s, 3H), 4.22 (s, 2H), 4.91 (br s, 2H), 6.84 (d, $J = 9$ Hz, 2H), 7.11 (d, $J = 9$ Hz, 2H), 8.22 (s, 1H); ^{13}C NMR (CDCl_3 , 100 MHz) δ 29.2, 34.3, 55.2, 59.9, 100.6, 114.6, 129.4, 130.0, 141.4, 154.5, 154.7, 157.6, 158.7; HRMS (EI) molecular ion calculated for $\text{C}_{17}\text{H}_{21}\text{N}_5\text{O}$ 311.17461, found 311.17454.

3-(3-Trifluoromethylbenzyl)-1-*tert*-butyl-1*H*-pyrazolo[3,4-*d*]pyrimidin-4-ylamine (15). White powder; ^1H NMR (CDCl_3 , 400 MHz) δ 1.789 (s, 9H), 4.349 (s, 2H), 4.917 (s, 2H), 7.360 (d, 1H), 7.430 (t, 1H), 7.506 (s, 1H), 7.516 (d, 1H), 8.262 (s, 1H); ^{13}C NMR (CDCl_3 , 100 MHz) δ 29.144, 34.961, 60.172, 77.205, 100.601, 124.108, 125.042, 129.640, 131.265, 131.652, 139.124,

139.474, 154.646, 154.699, 157.387; ESI-HRMS [MH]⁺ calculated for C₁₇H₁₈F₃N₅ 350.1587, found 350.1581.

3-(3-Bromobenzyl)-1-*tert*-butyl-1*H*-pyrazolo[3,4-*d*]pyrimidin-4-ylamine (16). White powder; ¹H NMR (CDCl₃, 400 MHz) δ 1.79 (s, 9H), 4.28 (s, 2H), 5.73 (s, 2H), 7.13 (d, 1H), 7.20 (t, 1H), 7.36 (s, 1H), 7.40 (d, 1H), 8.21 (s, 1H); ¹³C NMR (CDCl₃, 100 MHz) δ 29.2, 34.7, 60.8, 100.1, 123.5, 126.9, 130.7, 130.8, 131.4, 140.0, 141.0, 151.5, 153.8, 156.0; HRMS (EI) molecular ion calculated for C₁₆H₁₈BrN₅ 359.07456, found 359.07423.

3-(3-Iodobenzyl)-1-*tert*-butyl-1*H*-pyrazolo[3,4-*d*]pyrimidin-4-ylamine (17). White powder; ¹H NMR (CDCl₃, 400 MHz) δ 1.79 (s, 9H), 4.24 (s, 2H), 4.90 (s, 2H), 7.04 (t, 1H), 7.13 (d, 1H), 7.58 (s, 1H), 7.60 (d, 1H), 8.26 (s, 1H); ¹³C NMR (CDCl₃, 100 MHz) δ 29.4, 34.9, 60.3, 95.4, 100.8, 127.8, 131.0, 136.6, 137.5, 140.0, 140.8, 154.8, 154.9, 157.7; HRMS (EI) molecular ion calculated for C₁₆H₁₈IN₅ 407.0685, found 407.0705.

3-(3-Methylthiolbenzyl)-1-*tert*-butyl-1*H*-pyrazolo[3,4-*d*]pyrimidin-4-ylamine (18). White powder; ¹H NMR (CDCl₃, 400 MHz) δ 1.791 (s, 9H), 2.414 (s, 3H), 4.250 (s, 2H), 4.886 (s, 2H), 6.937 (d, 1H), 7.097 (s, 1H), 7.123 (d, 1H), 7.225 (t, 1H), 8.243 (s, 1H); ¹³C NMR (CDCl₃, 100 MHz) δ 15.567, 29.190, 35.105, 60.013, 77.205, 100.685, 124.924, 125.076, 126.283, 129.602, 138.942, 139.853, 140.468, 154.585, 154.767, 157.585; HRMS (EI) [MH]⁺ calculated for C₁₇H₂₁N₅S 328.1577, found 328.1583.

1-*tert*-Butyl-3-(2,3-dimethylbenzyl)-1*H*-pyrazolo[3,4-*d*]pyrimidin-4-ylamine (19). White powder; ¹H NMR (CDCl₃, 400 MHz) δ 1.78 (s, 9H), 2.19 (s, 3H), 2.28 (s, 3H), 4.28 (s, 2H), 4.86 (s, 2H), 6.88 (d, 1H), 7.02 (t, 1H), 7.08 (d, 1H), 8.23 (s, 1H); ¹³C NMR (CDCl₃, 100 MHz) δ 15.3, 20.6, 29.2, 34.0, 59.9, 100.9, 126.1, 126.3, 129.2, 135.7, 136.0, 137.8, 141.1, 154.4, 154.6, 157.7; HRMS (EI) molecular ion calculated for C₁₈H₂₃N₅ 309.19535, found 309.19515.

1-*tert*-Butyl-3-(3,4-dimethylbenzyl)-1*H*-pyrazolo[3,4-*d*]pyrimidin-4-ylamine (20). White powder; ¹H NMR (CDCl₃, 400 MHz) δ 1.79 (s, 9H), 2.20 (s, 3H), 2.21 (s, 3H), 4.21 (s, 2H), 5.45 (s, 2H), 6.91 (d, 1H), 6.96 (s, 1H), 7.07 (d, 1H), 8.18 (s, 1H); ¹³C NMR (CDCl₃, 100 MHz) δ 19.4, 19.8, 29.2, 34.8, 60.4, 100.2, 125.7, 129.6, 130.6, 135.0, 136.0, 137.9, 142.4, 151.5, 153.9, 156.4; HRMS (EI) molecular ion calculated for C₁₈H₂₃N₅ 309.19535, found 309.19542.

1-tert-Butyl-3-(2,5-dimethylbenzyl)-1H-pyrazolo[3,4-d]pyrimidin-4-ylamine (21). White powder; ^1H NMR (CDCl_3 , 400 MHz) δ 1.79 (s, 9H), 2.20 (s, 3H), 2.25 (s, 3H), 4.22 (s, 2H), 4.94 (s, 2H), 6.81 (s, 1H), 6.98 (d, 1H), 7.08 (d, 1H), 8.23 (s, 1H); ^{13}C NMR (CDCl_3 , 100 MHz) δ 19.3, 21.0, 29.2, 33.1, 59.9, 100.9, 128.1, 129.1, 130.9, 133.6, 135.9, 136.3, 140.9, 154.3, 154.6, 157.7; HRMS (EI) molecular ion calculated for $\text{C}_{18}\text{H}_{23}\text{N}_5$ 309.19535, found 309.19386.

1-tert-Butyl-3-(3,5-dimethylbenzyl)-1H-pyrazolo[3,4-d]pyrimidin-4-ylamine (22). White powder; ^1H NMR (CDCl_3 , 400 MHz) δ 1.80 (s, 9H), 2.25 (s, 6H), 4.20 (s, 2H), 5.00 (s, 2H), 6.80 (s, 2H), 6.88 (s, 1H), 8.22 (s, 1H); ^{13}C NMR (CDCl_3 , 100 MHz) δ 21.3, 29.2, 35.1, 59.9, 100.7, 126.2, 129.0, 138.0, 138.9, 141.3, 154.4, 154.7, 157.7; HRMS (EI) molecular ion calculated for $\text{C}_{18}\text{H}_{23}\text{N}_5$ 309.19535, found 309.19439.

1-tert-Butyl-3-(3,4-dichlorobenzyl)-1H-pyrazolo[3,4-d]pyrimidin-4-ylamine (23). White powder; ^1H NMR (CDCl_3 , 400 MHz) δ 1.79 (s, 9H), 4.24 (s, 2H), 5.07 (s, 2H), 7.02 (dd, 1H), 7.29 (d, 1H), 7.37 (d, 1H), 8.26 (s, 1H); ^{13}C NMR (CDCl_3 , 100 MHz) δ 29.1, 34.3, 60.2, 100.6, 127.6, 130.2, 131.0, 131.4, 133.2, 138.4, 139.2, 154.6, 154.7, 157.5; HRMS (EI) molecular ion calculated for $\text{C}_{16}\text{H}_{17}\text{N}_5\text{Cl}_2$ 349.08610, found 349.08621.

Chapter 3 – Staurosporine-derived analog-sensitive kinase inhibitors expand the scope of AS technology

Introduction

Protein kinases are key signaling enzymes involved in nearly every physiological process in eukaryotes. A major challenge in biomedical research is to elucidate kinase-mediated signaling pathways and to understand how human diseases arise from their misregulation. Small molecule inhibitors are invaluable tools for studying kinase-signaling events as they allow rapid inactivation of kinase activity in cells and thereby enable the study of essential kinases⁴⁰ and the dissection of events that occur on a time scale of seconds to minutes². However, it remains difficult to identify specific inhibitors of individual kinases due to the high degree of conservation of the ATP-binding pocket throughout the human kinome (~520 kinases)¹. Our lab has developed a systematic method for generating specific inhibitors of individual kinases by using genetic engineering to sensitize a single kinase to inhibition by a highly selective ATP-competitive molecule^{4,6}. Specifically, the inhibitor is designed to form a steric clash with a conserved residue in the ATP-binding pocket, termed the gatekeeper, which prevents inhibitor binding. In contrast, the gatekeeper residue of the AS kinase is mutated from the larger native amino acid (Thr, Leu, Phe, etc) to glycine or alanine thereby sensitizing it to inhibition by the bulky analog. This chemical-genetic approach combines the specificity of genetics with the temporal resolution and reversibility of pharmacology.

A central design feature of this technology is the use of a bioorthogonal small molecule that does not bind to WT kinases but potently inhibits the activity of the AS mutant. We have demonstrated that pyrazolopyrimidine analogs fulfill these requirements for many kinases and have successfully applied this chemical genetic technique to more than 80 kinases from diverse species and kinase families. Recently, however, we discovered that the commonly used AS kinase inhibitors 1NA-PP1, 1NM-PP1, and 3MB-PP1 target a subset of WT kinases with weak to moderate potency^{28,41}. This does not preclude application of the analog-sensitive approach to most kinases because potential off-target effects of these molecules are accounted for when WT cells are treated with the inhibitor. However, if the KOI is, itself, sensitive to the PP, the window

of selectivity for the AS allele may narrow and it may not be possible to completely abrogate AS kinase activity without also reducing that of the WT allele. Additionally, if a PP-sensitive kinase is involved in the same pathway as the AS kinase, unintentional inhibition might compromise or complicate a chemical genetic analysis. Thus we sought to identify a new inhibitor that would retain potency and generality towards engineered AS kinases while remaining inactive toward all other human kinases.

The ideal starting scaffold from which to design an AS kinase inhibitor is a molecule that binds a maximum number of kinases but can be modified to introduce an orthogonality element that disrupts binding unless the kinase bears a complementary mutation. The indolocarbazole natural product staurosporine is an attractive option as it potently targets ~80% of protein kinases⁴². Staurosporine also adopts a well-defined and conserved binding mode in the ATP pocket of divergent kinases as evidenced by numerous X-ray co-crystal structures⁴³. Furthermore, previous studies of the related molecule, K252a, have identified the C7 atom of the indolocarbazole as an ideal position at which functional groups can be introduced to prevent binding to WT kinases through steric clash with the gatekeeper residue (Figure 8A, B)^{4,44}. Staurosporine and K252a each contain a different carbohydrate moiety bridging the N12 and N13 atoms that contributes to the affinity of the molecules for the ATP-binding pocket of protein kinase. The different interactions of each sugar may account for the far greater number of kinases targeted by staurosporine⁴² and the poor generality of C7-modified K252a analogs towards diverse AS kinases (unpublished data). The carbohydrate functional groups of both staurosporine⁴⁵ and K252a⁴⁶ are challenging to synthesize and therefore not ideal for the construction of a panel of AS-kinase inhibitors or for the large-scale synthesis required for *in vivo* studies.

To develop a synthetically tractable surrogate for staurosporine, we asked if the non-glycosylated indolocarbazole could serve as the basis of a new scaffold for AS kinase inhibitors. Here we report the synthesis of carbohydrate-free staurosporine analogs, termed staralogs, and their structure-activity relationships toward a subset of AS kinases. We also show that simple polar groups at the N12 position form a novel interaction with a conserved asparagine residue and recover the potency that is lost by removal of the sugar group. Finally, we demonstrate the

staralogs are uniquely selective inhibitors and are capable of targeting kinases that have thus far eluded the application of AS-kinase technology.

Results and Discussion

C7-substituted indolocarbazole derivatives complement the gatekeeper mutation in Src kinase. Removal of the staurosporine sugar ring (K252c) led to complete loss of activity towards the tyrosine kinase Src-WT, as well as Src-AS1 (glycine gatekeeper) and Src-AS2 (alanine gatekeeper), confirming previous reports that affinity interactions provided by the sugar are critical to inhibitor binding (Figure 8C)⁴⁷. Despite this severe loss in potency for the parent aglycone, K252c, we reasoned that introduction of new substituents at C7 might complement the engineered pocket and enhance potency without the sugar moiety. Thus we prepared a panel of staralogs using a synthetic strategy whereby the (S)-configuration of the C7-substituent is introduced from commercially available L-amino acids (Figure 9)⁴⁴. We found that several alkyl or aryl groups indeed rescued activity toward Src-AS1 but not Src-AS2 or Src-WT. The most potent staralogs (**Star 1**, **Star 3**, **Star 4**) bear *iso*-butyl, *n*-butyl, and *n*-propyl groups at the C7 position. Larger groups, such as benzyl (**Star 2**) and cyclohexylmethyl (**Star 5**), were much less potent, presumably due to steric clash of these larger groups with the surface of the expanded gatekeeper pocket. Conversely, staralogs with C7 substituents that do not project as deeply into the expanded ATP binding pocket were also less potent (Figure 8C, **Star 6 – 9**). We interpreted these structure-activity relationships as evidence that a complementary hydrophobic interaction exists between the C7 group of the staralog and the gatekeeper pocket. This interaction provides a significant and necessary contribution to inhibitor binding in the absence of sugar affinity elements.

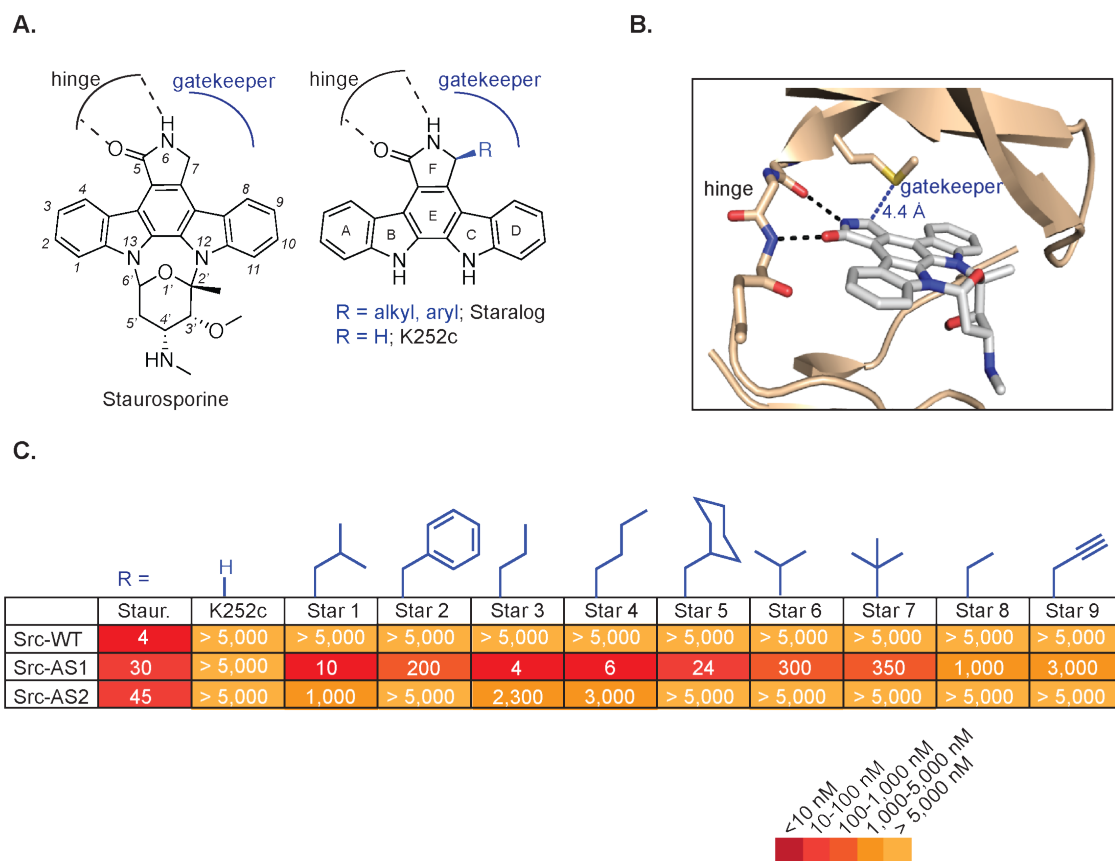


Figure 8. Design of staralog inhibitors and structure-activity relationships of the C7-position. (A) Structure of staurosporine (left) and engineered staralog inhibitors (right) with kinase hinge-binding interaction and gatekeeper pocket illustrated in black and blue, respectively. (B) X-ray co-crystal structure of staurosporine bound to Protein Kinase C θ ^{47,48} with hinge interaction highlighted in black and the distance between C7-position of staurosporine and the Met gatekeeper side chain highlighted in blue. (C) IC₅₀ values for staralog inhibitors against Src-WT, Src-AS1, and Src-AS2 kinases.

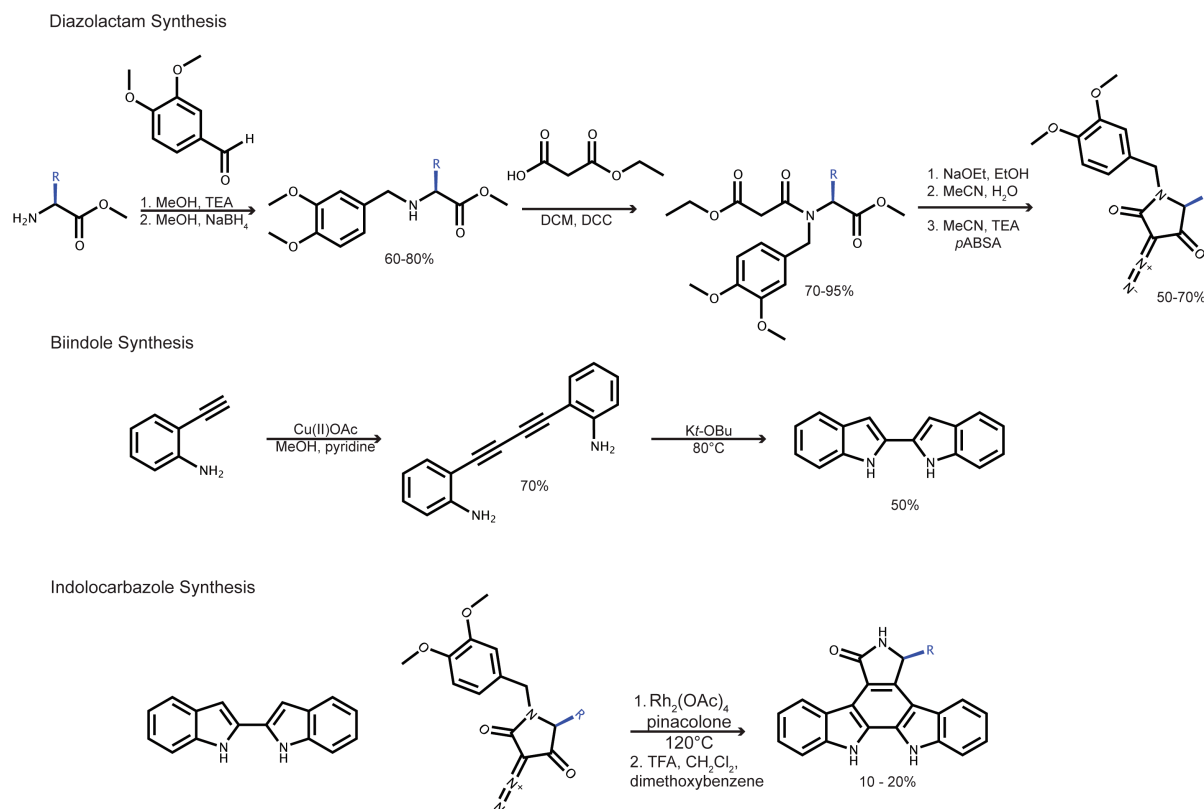


Figure 9. Synthetic approach⁴⁴ for construction of staralog derivatives. Diazolactam derivatives are synthesized from appropriate commercially available L-amino acid methyl esters. Biindole is prepared in two steps from 2-alkynyl aniline. Indolocarbazole is formed via a rhodium catalyzed coupling of the diazolactam and biindole building blocks.

Simple polar groups rescue activity of staralog inhibitors toward AS kinases bearing an alanine gatekeeper residue. Some kinases suffer decreased stability or activity upon mutation of the gatekeeper residue to glycine but are more tolerant of an alanine substitution^{8,9}. Thus, an ideal AS kinase inhibitor must be able to target kinases with either a glycine (AS1) or alanine (AS2) gatekeeper. Although several molecules in our initial panel are potent Src-AS1 inhibitors, none were able to target Src-AS2. We hypothesized that the larger methyl side chain of the alanine gatekeeper decreases the size of the gatekeeper pocket thereby reducing the potential affinity of this hydrophobic interaction. We sought to identify other positions on the staralog scaffold that could be altered to increase inhibitor affinity and allow for targeting of AS kinases bearing an alanine gatekeeper. Since removal of the sugar group from staurosporine led to a significant decrease in potency towards Src-WT (Figure 8C), we asked if restoring one or more

of the sugar affinity elements might be key to enhancing staralog potency towards kinases with a larger alanine gatekeeper.

We sought to retain the synthetic tractability of our simplified staralog derivatives while regaining the affinity interactions provided by the carbohydrate portion of staurosporine. We synthesized a new panel of staralogs that retain the C7-*iso*-butyl element of **Star 1** but also contain simple polar groups at either the N12 or N13 positions (Figure 10, 11). These groups were designed to mimic the affinity elements of the staurosporine sugar as revealed by various co-crystal structures and could be installed in one or two synthetic steps (Figure 10).

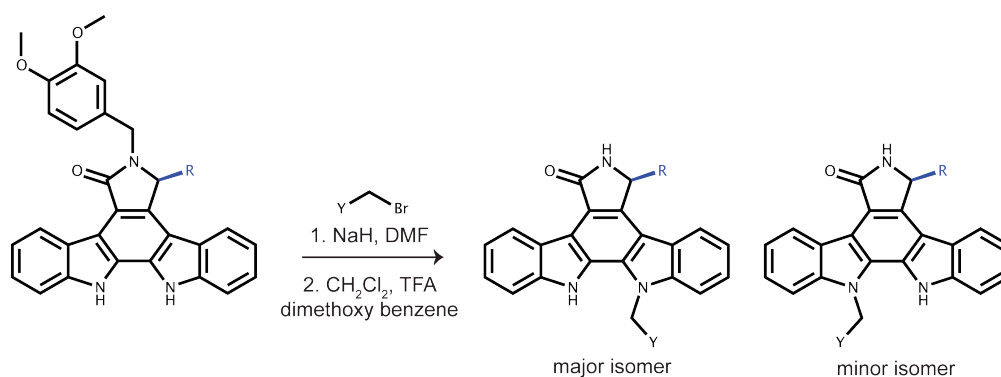


Figure 10. Synthetic approach⁴⁹ for installing N12 and N13 substituents. Major product is alkylation at N12 and minor product is alkylation at N13. 3,4-dimethoxybenzyl group as well as other Y-protecting groups (Boc, etc.) were removed with TFA in methylene chloride and scavenger dimethoxy benzene. Regiochemistry of the alkylations were determined by ¹H NMR (described in ref. 3) and relative shift by liquid chromatography where the major isomer (N12-alkylated) migrated more quickly than the minor isomer (N13-alkylated). Finally, the regiochemistry was further confirmed by X-ray co-crystallography of **Star 12** (Figure 3) and **Star 16** (unpublished data) bound to Src-AS1.

We synthesized derivatives bearing alkyl amines, alcohols, ethers or pyridine groups to mimic potential affinity interactions provided by the C4'-methylamine, C3'-methylether, and O1'-cyclic ether of the sugar group. These derivatives retained selectivity for Src-AS1 over the wild-type kinase and some showed modest improvements in potency towards Src-AS2. The N12-butylamine derivative (**Star 12**), however, yielded a marked improvement (> ten-fold) in potency toward both Src-AS1 and Src-AS2, while remaining inactive (IC₅₀ > 5 μM) toward Src-WT. Reducing the alkyl linker of **Star 12** by one carbon (**Star 17**) decreased the potency of the inhibitor toward Src-AS2 by more than ten-fold. Such a precise structure-activity relationship

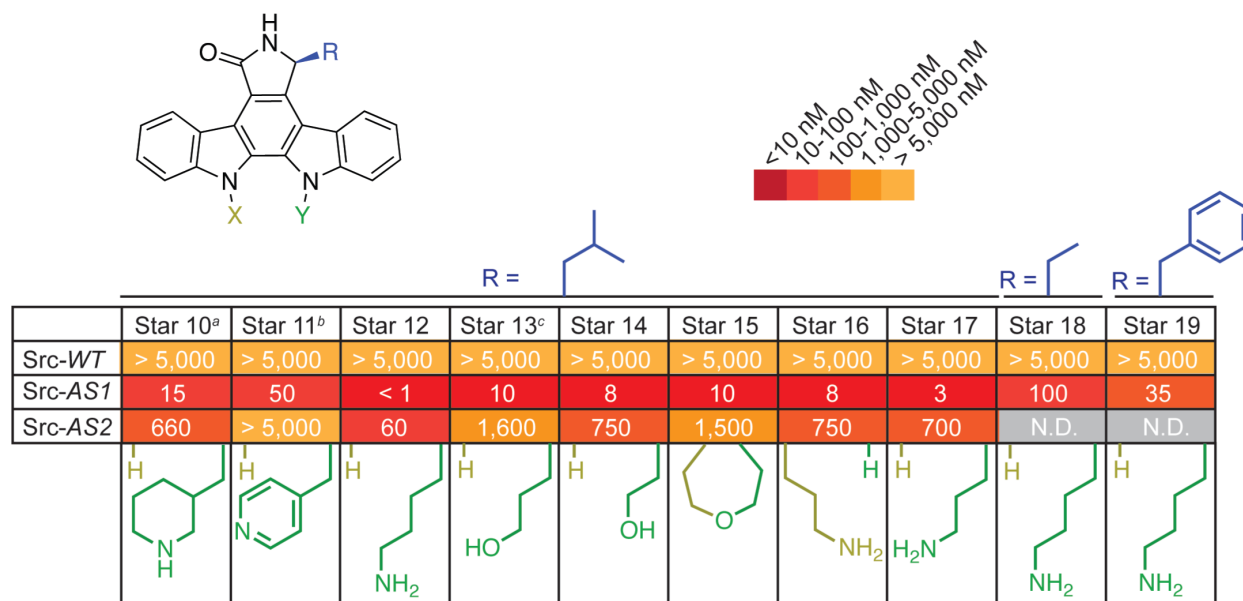


Figure 11. Panel of staralogs bearing N12 or N13 substituents. IC₅₀ values (nM) against Src-WT, Src-AS1, and Src-AS2. *a.* **Star 10** is a mixture of regioisomers (1:3 N13:N12 substitution) *b.* **Star 11** is a mixture of regioisomers (1:3 N13:N12 substitution) *c.* **Star 13** is a mixture of regioisomers (1:2 N13:N12 substitution).

suggests the N12-butylamine of **Star 12** provides a specific affinity interaction with Src kinase and does not simply alter a general property, such as solubility, of staralogs.

We anticipate that individual AS kinases will exhibit varying sensitivity to the size and shape of the C7-orthogonality element. Thus, we asked if the affinity enhancement of the N12-butylamine group was unique to staralogs bearing the C7-*iso*-butyl modification or if it would enhance the potency of staralogs with other C7-substitutions. To test this we synthesized two molecules, each bearing the N12-butylamine in combination with a C7-group that is either smaller (ethyl, **Star 18**) or larger (benzyl, **Star 19**) than the *iso*-butyl group of **Star 12** (Figure 8C). The potency towards Src-AS1 was enhanced ten-fold for **Star 18** over **Star 8** and nearly six-fold for **Star 19** over **Star 2**. The precision of the structure-activity relationship at the N12-position and the enhancement of potency by N12-butylamine in diverse staralogs suggest that this group is a versatile affinity element for staralog inhibitors.

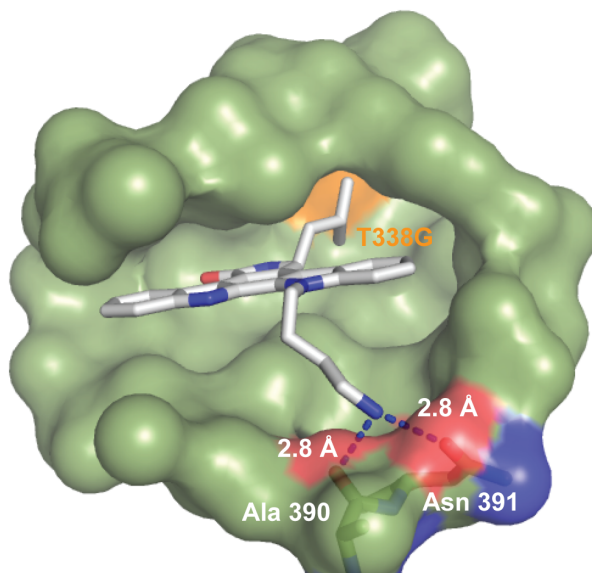


Figure 12. X-ray co-crystal structure of **Star 12** bound to the kinase domain of Src-AS1. The *iso*-butyl group of **Star 12** projects towards the expanded gatekeeper pocket (orange). The N12-butylamine group forms hydrogen bonds with side chain of Asn 391 and the backbone carbonyl of Ala 390.

Structural basis of Star 12 binding. To understand the structural mechanism by which the N12-butylamine enhances inhibitor binding we solved a 2.7 Å X-ray co-crystal structure of **Star 12** bound to the kinase domain of Src-AS1 (Figure 12). In agreement with previously published structures of staurosporine bound to protein kinases, the lactam ring (Ring F) of the indolocarbazole forms hydrogen bond interactions with the backbone amides of E339, Y340, and M341 in the hinge region of the ATP binding pocket (Figure 13). As predicted, the C7-*iso*-butyl group projects directly toward the gatekeeper pocket and occupies the cavity created by mutation of the threonine gatekeeper to glycine (Figure 12, 13). An overlay of the **Star 12**/Src-AS1 structure with that of staurosporine bound to Src-WT^{41,48} reveals that **Star 12** rings A, B and F occupy similar positions as those of staurosporine. Unexpectedly, the bulky C7-*iso*-butyl group of **Star 12** forces rings E, C and D to project below the plane of staurosporine resulting in a binding mode that appears tilted to minimize steric clash with the gatekeeper pocket (Figure 13).

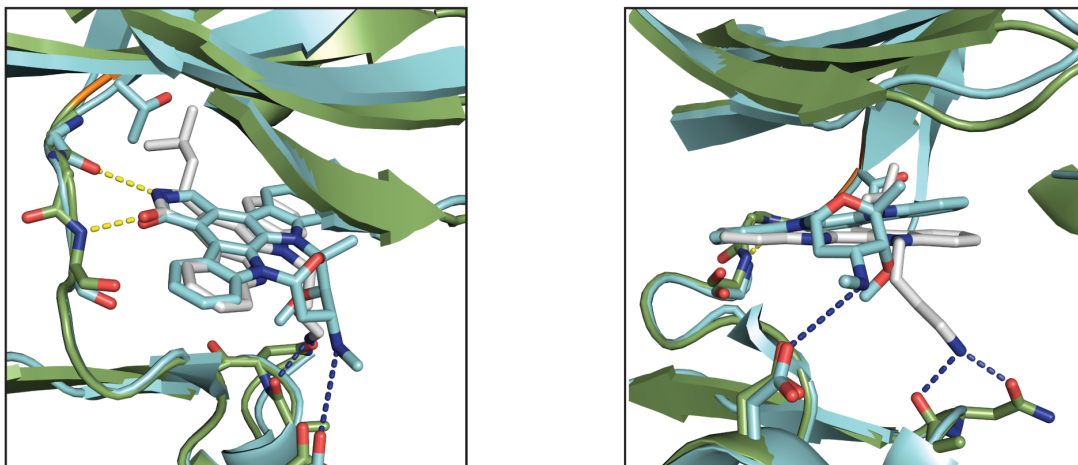


Figure 13. Overlay of X-ray co-crystal structure of Star 12/Src-AS1 with staurosporine/Src-WT⁵⁰. Left: Rings F and A of both inhibitors occupy similar positions and maintain the hinge-binding interaction between ring F and the backbone amides of residues. Right: Rings C and D dip below the plane of staurosporine.

Despite the predicted flexibility of a four-methylene linker, clear electron density reveals the N12-butylamine to be rigid and bent, allowing the formation of hydrogen bonds with the side chain of Asn391 and the backbone amide carbonyl of Ala390 (Figure 12, 13). This observation is significant as it may explain why the butylamine group has such a profound influence on inhibitor affinity and why this effect is lost when the alkyl linker is shortened. We had initially installed polar groups at the N12 and N13 positions in an effort to mimic the affinity interactions of the staurosporine sugar. However, the A390/N391 hydrogen bonds observed are not found in any other crystal structure of staurosporine bound to a protein kinase. It is possible that this unique interaction is made possible by the tilted orientation of **Star 12** relative to staurosporine. Importantly, Asn391 is completely conserved throughout protein kinases (Figure 14) suggesting this key affinity interaction may be a general feature applicable to staralog binding to any AS kinase.

conserved Asn 391
↓

Src_gga	M	N	Y	V	H	R	D	L	R	A	A	N	I	L	V	G
CDPK_gmx	L	G	V	M	H	R	D	L	K	P	E	N	F	L	F	D
CDKL1_hsa	H	N	C	I	H	R	D	V	K	P	E	N	I	L	I	T
Cdc5_sce	R	R	V	I	H	R	D	L	K	L	G	N	I	F	F	D
KPRO_zma	C	L	E	W	H	C	D	V	K	P	E	N	I	L	L	D
PKN1_mxa	R	G	I	V	H	R	D	L	K	P	D	N	I	F	L	V

non-conserved conserved

Figure 14. Representative sequence alignment of kinases from diverse families and organisms highlights the conservation of Asn391.

	CK1ε	CKδ	Pkd1	Pkd2	Ack	EphA1	Ptk6	Ret
IC50 (nM)	>5,000	>5,000	1,600	>5,000	1,200	>5,000	>5,000	>5,000

Table 1. IC50 values for **Star 12** against a representative set of PP-sensitive kinases.

Staralogs are bioorthogonal AS-kinase inhibitors. The primary goal of developing staralogs is to expand the scope of AS-kinase technology by creating more selective inhibitors that do not target WT-kinases inherently sensitive to PP analogs. To evaluate our progress towards this objective we measured *in vitro* IC50 values for **Star 12** against a panel of PP-sensitive WT-kinases (Table 1). One or more of the three commonly used AS -kinase inhibitors, 1NA-PP1, 1NM-PP1 and 3MB-PP1, inhibit each of the PP-sensitive kinases at concentrations between one and several hundred nanomolar^{41,43}. Strikingly, **Star 12** exhibits enhanced selectivity and does not potently target any of these PP-sensitive WT kinases. The observation that **Star 12** is a potent inhibitor of AS kinases but is orthogonal with PP-sensitive WT kinases suggests it may be capable of selectively targeting AS alleles of PP-sensitive kinases, thereby expanding this technology to include a previously intractable subset of enzymes.

Although **Star 12** does not target PP-sensitive WT kinases, we examined the possibility that a new subset of the kinome might be inherently sensitive to C7-modified staralogs. For example, staurosporine was originally reported to be a potent inhibitor of Protein Kinase C^{41,43}, and thus we asked if staralogs might retain activity against some WT kinases with intrinsic sensitivity to a staurosporine-derived molecule. We analyzed 308 human kinases by measuring the fraction of activity inhibited by 1μM **Star 12** (Figure 15, Appendix 3). Strikingly, a concentration of 1 μM **Star 12** did not inhibit a single kinase by more than 80% and thus displayed remarkable and unprecedented selectivity for an AS kinase inhibitor. By comparison, 1NA-PP1, 1NM-PP1, and 3MB-PP1 inhibit 4.5%, 1.2% and 1.2% of kinases, respectively⁴¹. Using the same metric, staurosporine and K252a target 72% and 49%, respectively, of all protein kinases at a concentration of 500 nM⁴².

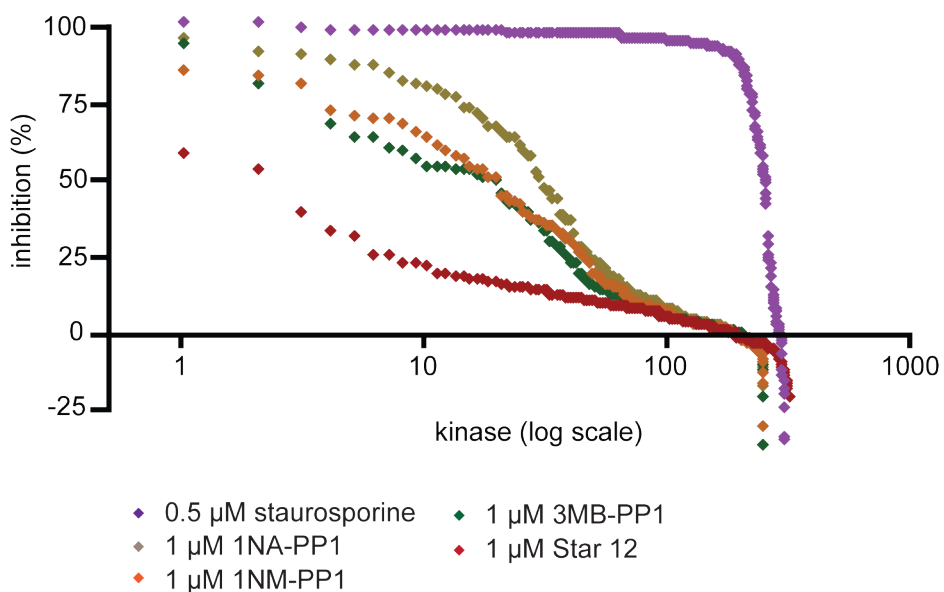


Figure 15. Inhibition profiles of **Star 12** (red), staurosporine (purple), 1NA-PP1 (brown), 1NM-PP1 (orange), and 3MB-PP1 (green) towards ~300 kinases. Kinases were ordered from most-to-least inhibited for each drug and plotted with the X-axis formatted in log-scale.

Staralogs expand the scope of AS kinase technology. An important application of AS -kinase technology is to decipher the roles of individual kinases in cellular signaling pathways relevant to human diseases. Thus, it is critical a new inhibitor scaffold be membrane-permeable and capable of targeting AS kinases in intact mammalian cells. To determine if staralogs meet this requirement we measured the ability of **Star 1**, **Star 17**, and **Star 12** to inhibit v-Src-WT or v-Src-AS1 in stably transfected mouse 3T3 cells (Figure 16A). All three staralogs completely inhibit v-Src-AS1 mediated phosphorylation in cells at concentrations below 1 μ M. **Star 12** was the most potent inhibitor, while **Star 17** exhibited intermediate potency, and **Star 1** was the weakest. These observations indicate that the structural changes that enhance inhibitor affinity *in vitro* do not have counterproductive effects on the cell-permeability of the molecules. Unlike the promiscuous tyrosine kinase inhibitor PP1, **Star 12** had little effect on v-Src-WT-mediated phosphorylation in, confirming the selectivity of **Star 12** extends to cellular conditions.

EphA4 is a receptor tyrosine kinase involved in neuronal development and axon guidance in mammals^{51,52} and has recently been identified as a potential therapeutic target for the treatment of amyotrophic lateral sclerosis (ALS)^{35,51}. EphA4 belongs to the ephrin (Eph) receptor

family of 16 tyrosine kinases, a branch of the kinome that is inherently sensitive to the PP inhibitor scaffold. Some family members, such as EphB1, EphB2, and EphB3, retain a differential of sensitivity for the AS allele over the WT allele that is sufficient to allow the application of our chemical genetic technique^{35,41}. Meanwhile, others, such as EphA4, have eluded AS technology due to their inherent sensitivity to PP inhibitors. To determine if staralogs are capable of extending AS-kinase technology to EphA4, we measured the ability of several staralogs to target EphA4-AS1 in HEK-293T cells (Figure 16B). While **Star 12** exhibited activity towards EphA4-AS1, we found that **Star 17** was in fact the most potent staralog derivative, completely inhibiting the AS kinase without affecting the WT kinase at a concentration of 10 μ M (Figure 16B). 1NA-PP1, in contrast, inhibited EphA4-WT activity at concentrations at which inhibition of the AS allele was incomplete. Thus, the enhanced selectivity of staralogs may allow for the extension of AS-kinase technology to EphA4 and potentially the entire Eph family of kinases. In particular, staralog inhibitors may be used to target EphA4-AS1 in ALS mouse models to clarify the potential of EphA4 as a therapeutic drug target.

To explore the generality of staralog inhibitors we asked if we could identify potent inhibitors of two other PP-sensitive kinases, Pkd1 and Ret. Although AS versions of these kinases have been successfully targeted with 1NA-PP1, it was also observed that the WT kinases are also weakly inhibited at higher drug concentrations^{21,41}. Thus, staralogs might serve as complementary or superior alternative inhibitors when studying these kinases and their orthologs. Although **Star 18**, **Star 12**, and **Star 19** did not show activity towards Pkd1-AS2, **Star 12** was able to target over-expressed Pkd1-AS1 in HEK-293T cells (Figure 16C). By contrast, both **Star 12** and, to a lesser extent **Star 18**, were capable of potently inhibiting Ret-AS2 in mouse 3T3 cells (Figure 16D). Thus, from a small panel of staralogs we identified potent inhibitors of Src-AS1, Src-AS2, EphA4-AS1, Pkd1-AS1 and Ret-AS2. These molecules represent a versatile inhibitor scaffold with unique selectivity amongst AS-kinase inhibitors and they may enable the application of AS-kinase technology to previously intractable PP-sensitive kinase such as EphA4. Furthermore, **Star 12** is the first reported AS-kinase inhibitor that is completely orthogonal with all human kinases examined.

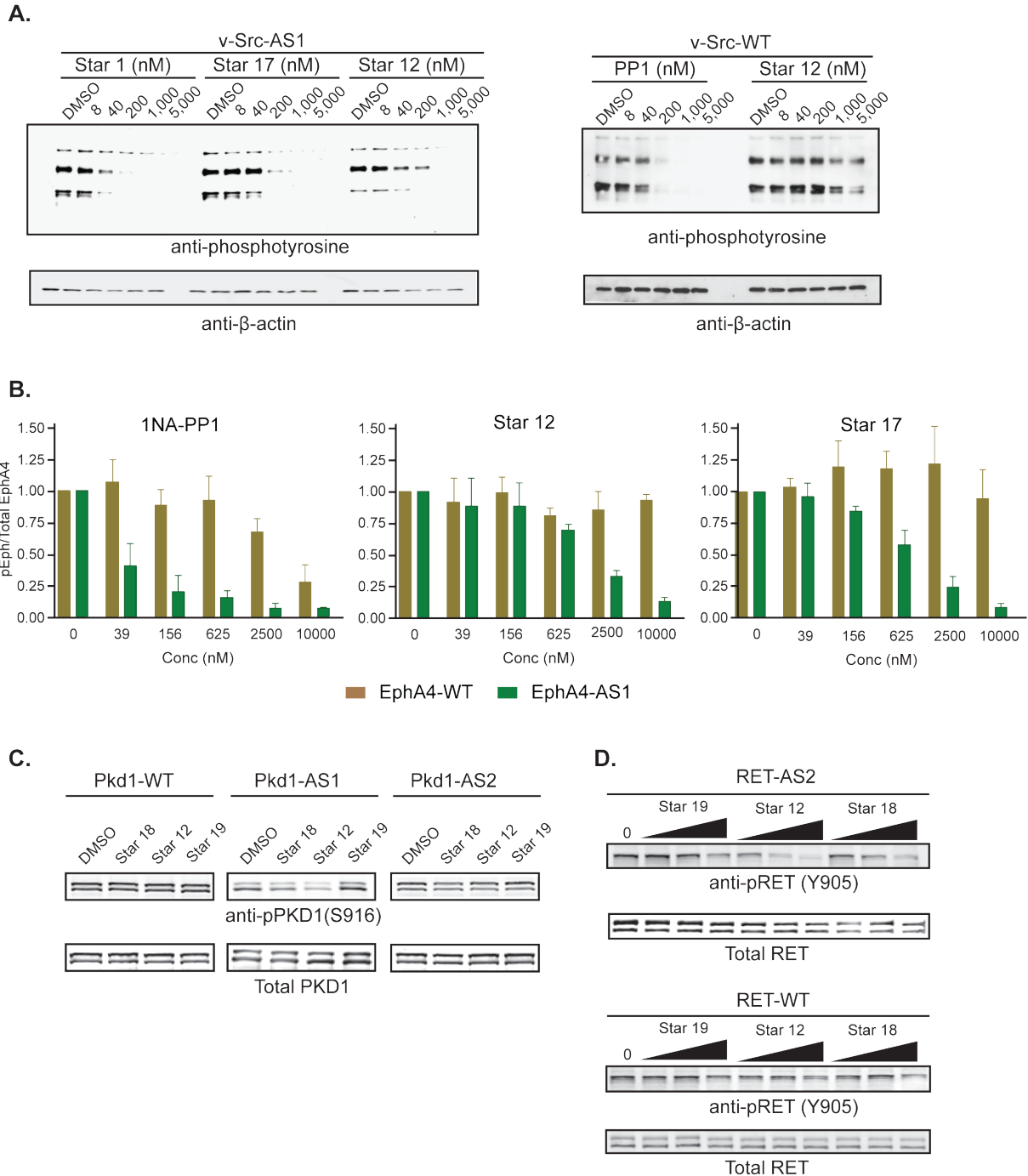


Figure 16. Staralogs are potent and selective inhibitors of AS kinases in cells. (A.) 3T3 mouse cells over-expressing v-Src-AS1 or v-Src-WT were treated with varying concentrations and analyzed for inhibition of tyrosine phosphorylation. (B.) HEK-293T cells were transfected with EphA4-WT or EphA4-AS1, treated with inhibitors and analyzed for EphA4 auto-phosphorylation. Error bars are the SEM of three separate experiments. (C.) HEK-293T cells were transfected with Pkd1-WT, Pkd1-AS1, or Pkd1-AS2, treated with 5μM inhibitor, and analyzed for Pkd auto-phosphorylation at S916. (D.) 3T3 mouse cells expressing Kif5b-Ret-AS2 or Kif5b-Ret-WT were treated with the indicated inhibitors (10μM, 3.3μM, and 1.1μM) and analyzed for Ret auto-phosphorylation at Y905.

Conclusion

Orthogonal small molecule inhibitors of engineered AS kinases are powerful tools for elucidating the cellular roles of individual kinases and deciphering paradoxical effects of clinical therapeutics²¹. The potential impact of the AS approach grows commensurately with advances^{6,53} in gene-editing technology as they allow for replacement of WT-kinase genes with AS alleles in cells and *in vivo*. The ability to target AS kinases with a selective inhibitor provides the unique advantages of a chemical tool (reversibility, temporal resolution, etc.) while retaining the specificity of a genetic manipulation. An essential feature of AS kinase technology is that the small molecule inhibitor must potently target the engineered kinase at a concentration at which the WT is unaffected. Although PP inhibitors satisfy this requirement for the majority of kinases, a small subset has been identified that are inherently sensitive to PP inhibitors. In this report we have introduced a panel of (S)-C7-substituted indolocarbazoles, termed staralogs, which overcome the limited selectivity of PP inhibitors and expand the potential scope of AS kinase technology to PP-sensitive kinases such as EphA4. Furthermore, **Star 12** is the first AS kinase inhibitor that does not inhibit any known WT kinase. The inhibitors described here now form a core piece of the repertoire of the chemical tool kit necessary for the chemical genetic investigation of protein kinases.

Experimental Methods:

***In Vitro* Kinases Assays:**

Src Kinase. 6xHis-tagged Src (257-533), Src-AS1 (T338G), and Src-AS2 (T338A) were expressed in BL-21 *E. coli* cells as previously described³⁸. Kinase activity was assayed under the following conditions: 2nM Src kinase, 50mM TRIS (pH 8.0), 10mM MgCl₂, 100μM Src peptide substrate (IYGEFKKK), 100μM ATP, 0.5μCi ³²P-ATP, 2% DMSO, and variable concentrations of inhibitors (5 μM to 1.2 nM). 2 μL of the reaction mixture was placed onto P81 paper at various time points and evaporated under a heat lamp for 5 min. The P81 paper was washed with 1% phosphoric acid, dried, and exposed to phosphor-imaging screen. Radioactivity was measured using a Typhoon fluorescence imager (Molecular Dynamics) and IC₅₀ values were determined by fitting the data to a sigmoid function in Prism 4.0 (GraphPad Software).

CK1δ and CK1ε. Casein Kinase 1δ (catalog # PV3665) and Casein Kinase 1ε (catalog # PV3500) were purchased from Life Technologies and assayed under the following conditions: 50mM TRIS (pH 8.0), 10mM MgCl₂, 0.4 mg/mL casein, 2.5 mM DTT, 2% DMSO, 5nM kinase, 100μM ATP, 0.1 mg/mL BSA, 1μCi ³²P-ATP and various concentrations of inhibitors (5 μM to 1.2 nM). 2 μL of the reaction mixture was placed onto P81 paper at various time points and evaporated under a heat lamp for 5 min. The P81 paper was washed with 1% phosphoric acid, dried, and exposed to phosphor-imaging screen. Radioactivity was measured using a Typhoon fluorescence imager (Molecular Dynamics) and IC₅₀ values were determined by fitting the data to a sigmoid function in Prism 4.0 (GraphPad Software).

PKD1 and PKD2. PKD1 (catalog # PV3791) and PKD2 (catalog # PV3758) were purchased from Life Technologies and assayed under the following conditions: 50 mM TRIS (pH 8.0), 10 mM MgCl₂, 2mM DTT, 2% DTT, 0.1 mg/mL BSA, 100 μM ATP, 3 μCi ³²P-ATP, 7 nM kinase and various concentrations of inhibitors (5 μM to 1.2 nM). 2 μL of the reaction mixture was placed onto P81 paper at various time points and evaporated under a heat lamp for 5 min. The P81 paper was washed with 1% phosphoric acid, dried, and exposed to phosphor-imaging screen. Radioactivity was measured using a Typhoon fluorescence imager (Molecular Dynamics) and IC₅₀ values were determined by fitting the data to a sigmoid function in Prism 4.0 (GraphPad Software).

RET and ACK. RET (catalog # PV3819) and ACK (catalog # PV4807) were purchased from Life Technologies and assayed under the following conditions: 50 mM TRIS (pH 8.0), 10 mM MgCl₂, 2 mM DTT, 0.1 mg/mL BSA, 2% DMSO, 200 μM Abltide, 10 nM kinase, 100 μM ATP, 1 μCi ³²P-ATP and variable concentrations of inhibitors (5 μM to 1.2 nM). 2 μL of the reaction mixture was placed onto P81 paper at various time points and evaporated under a heat lamp for 5 min. The P81 paper was washed with 1% phosphoric acid, dried, and exposed to phosphor-imaging screen. Radioactivity was measured using a Typhoon fluorescence imager (Molecular Dynamics) and IC₅₀ values were determined by fitting the data to a sigmoid function in Prism 4.0 (GraphPad Software).

EPHA1 and PTK6. EPHA1 (catalog # 3841) and PTK6 (catalog # 3291) were purchased from Life Technologies and assayed under the following conditions: 50 mM TRIS (pH 8.0), 10 mM MgCl₂, 2.5 mM DTT, 0.1 mg/mL BSA, 2% DMSO, 0.2 mg/mL poly[Glu, Tyr] 4:1, 2 nM kinase, 100 μM ATP, 1 μCi ³²P-ATP and variable concentrations of inhibitors (5 μM to 1.2 nM). 2 μL of the reaction mixture was placed onto P81 paper at various time points and evaporated under a heat lamp for 5 min. The P81 paper was washed with 1% phosphoric acid, dried, and exposed to phosphor-imaging screen. Radioactivity was measured using a Typhoon fluorescence imager (Molecular Dynamics) and IC₅₀ values were determined by fitting the data to a sigmoid function in Prism 4.0 (GraphPad Software).

Cellular Kinases Assays:

v-Src-WT and v-Src-AS1

NIH-3T3 cell lines transformed with v-Src gatekeeper variants were prepared using the procedure of Bishop et al.⁵⁴. 5x10⁵ cells were seeded in each well of a 6-well dish and grown overnight at 37°C with 5% CO₂ in Dulbecco's Modified Eagle Medium (DMEM) supplemented with 10% Fetal Bovine Serum (FBS). The next day the medium was removed and replaced with 1.5ml of fresh DMEM (+10% FBS) containing inhibitor and a final concentration of 1% DMSO. The cells were incubated with drug medium for 1.5 hours, washed with cold PBS, and lysed with 150 μL buffer (50 mM Tris (pH 7.4), 150 mM NaCl, 1 mM EDTA, 1 mM EGTA, 1 mM Na₃VO₄, 10 mM sodium-β-glycerophosphate, 1% triton, 50 mM NaF, 5 mM sodium pyrophosphate, 0.27 M sucrose, 50 mM benzamidine, 1 complete mini protease inhibitor tablet (Roche), 1 mM PMSF, 1 PhosSTOP (Roche) phosphatase inhibitor tablet, 0.1 mg/ml RNase A,

and 0.1 mg/ml DNase I), normalized for concentration and analyzed by Western blot for global phosphotyrosine levels (4G10, Millipore, 1:5000) and β -actin (β -actin Antibody, Cell Signaling, 1:1000).

EphA4-WT and EphA4-AS1

3×10^5 HEK-293T cells were seeded into each well of a six-well tissue culture plate and grown in 2 mL DMEM (+10% FBS) at 37°C under 5% CO₂ for 12-18 hrs. pCS2+ plasmids containing full length EphA4-WT or EphA4-AS1(T640G) were transfected into HEK 293T cells using Lipofectamine®, LTX and PLUS reagent (Life Technologies) and the cells returned to 37°C 5% CO₂ incubator for 12-18 hrs. The next day the medium was removed and replaced with 1.5ml of fresh DMEM (+10% FBS) containing inhibitor and a final concentration of 1% DMSO. The cells were incubated with drug medium for 1.5 hours, washed with cold PBS, and lysed with 150 μ L buffer (50 mM Tris (pH 7.4), 150 mM NaCl, 1 mM EDTA, 1 mM EGTA, 1 mM Na₃VO₄, 10 mM sodium- β -glycerophosphate, 1% triton, 50 mM NaF, 5 mM sodium pyrophosphate, 0.27 M sucrose, 50 mM benzamidine, 1 complete mini protease inhibitor tablet (Roche), 1 mM PMSF, 1 PhosSTOP (Roche) phosphatase inhibitor tablet, 0.1 mg/ml RNase A, and 0.1 mg/ml DNase I), normalized for concentration and analyzed by Western blot for pEph (provided by Greenberg Lab⁵⁵, 1:1000) and total EphA4 (anti-EphA4, Santa Cruz Biotechnology, 1:1000).

Pkd1-WT, Pkd1-AS1, and Pkd1-AS2

3×10^5 HEK-293T cells were seeded into each well of a six-well tissue culture plate and grown in 2 mL DMEM (+10% FBS) at 37°C under 5% CO₂ for 12-18 hrs. Venus-Pkd1-WT, Venus-Pkd1-AS1 (M665G), or Venus-Pkd1-AS2 (M665A)⁴¹ were transfected into HEK 293T cells using Lipofectamine®, LTX and PLUS reagent (Life Technologies) and the cells returned to 37°C 5% CO₂ incubator for 12-18 hrs. The next day the medium was removed and replaced with 1.5ml of fresh DMEM (+10% FBS) containing inhibitor and a final concentration of 1% DMSO. The cells were incubated with drug medium for 1.5 hours, washed with cold PBS, and lysed with 150 μ L buffer (50 mM Tris (pH 7.4), 150 mM NaCl, 1 mM EDTA, 1 mM EGTA, 1 mM Na₃VO₄, 10 mM sodium- β -glycerophosphate, 1% triton, 50 mM NaF, 5 mM sodium pyrophosphate, 0.27 M

sucrose, 50 mM benzamidine, 1 complete mini protease inhibitor tablet (Roche), 1 mM PMSF, 1 PhosSTOP (Roche) phosphatase inhibitor tablet, 0.1 mg/ml RNase A, and 0.1 mg/ml DNase I), normalized for concentration and analyzed by Western blot for pS916 Pkd1 (Cell Signaling # 2051, 1:1000) and total Pkd1 (Cell Signaling # 2052, 1:1000).

Kif5b-Ret-WT and Kif5b-Ret-AS2

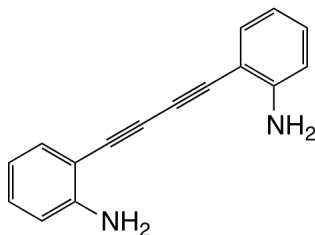
The KIF5B-RET WT cDNA was cloned into pBABE-Puro vectors using SLIC-cloning⁵⁶ and the V804A-AS mutation was introduced by site-directed mutagenesis. Replication-incompetent retroviruses were produced in Phoenix-Eco HEK 293T cells. Supernatant was filtered and used at 1:2 dilutions for transduction of NIH3T3 cells that were selected with puromycin (1.0 µg/ml). 5×10^5 cells were seeded in each well of a 6-well dish and grown overnight at 37°C with 5% CO₂ in Dulbecco's Modified Eagle Medium (DMEM) supplemented with 10% Fetal Bovine Serum (FBS) and puromycin. The next day the medium was removed and replaced with 1.5ml of fresh DMEM (+10% FBS, +1µ/mL puromycin) containing inhibitor and a final concentration of 1% DMSO. The cells were incubated with drug medium for 1.5 hours, washed with cold PBS, and lysed with 150 µL buffer (50 mM Tris (pH 7.4), 150 mM NaCl, 1 mM EDTA, 1 mM EGTA, 1 mM Na₃VO₄, 10 mM sodium-β-glycerophosphate, 1% triton, 50 mM NaF, 5 mM sodium pyrophosphate, 0.27 M sucrose, 50 mM benzamidine, 1 complete mini protease inhibitor tablet (Roche), 1 mM PMSF, 1 PhosSTOP (Roche) phosphatase inhibitor tablet, 0.1 mg/ml RNase A, and 0.1 mg/ml DNase I), normalized for concentration and analyzed by Western blot for Ret autophosphorylation (anti-pY905, Cell Signaling # 3221, 1:1000) and total Ret (anti-Ret, Cell Signaling # 3220, 1:1000).

Crystalization and Data Collection

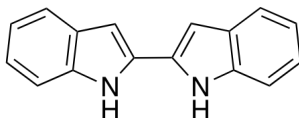
Prior to crystallization, purified c-Src-AS1 was applied to a S200 gel filtration column. Pooled fractions were concentrated to 3-10mg/mL and mixed with **Star 12** (1:1.3 ratio of protein:inhibitor) in 100 mM NaCl, 50 mM Tris [pH 8.0], 5% glycerol, 1 mM DTT, and 4% DMSO. Hanging drops containing 1 µL of kinase-inhibitor complexes were mixed with equal volume of well buffer containing 8% PEG 4K, 50 mM NaAc, 100 mM MES [pH 6.5] and grown at 14°C to yield c-Src-AS1-**Star 12** crystals. Crystals were cryo-protected in well buffer

supplemented with 20% glycerol and flash frozen in liquid nitrogen. Diffraction data were collected at -170°C and processing was carried out using HKL2000 (HKL Research Inc.). The structure was solved by molecular replacement using 1YOJ⁵⁷ lacking the activation segment, helix αC , and ligands as the search model in the program PHASER⁵⁸. Molecular replacement solutions were modified and refined with alternate cycles of manual fitting and building into $|2\text{Fo}-\text{Fc}|$ and composite omit electron density maps using Coot⁵⁹. Refinement of the structures was carried out using Phenix⁶⁰. Data collection and refinement statistics are shown in supplementary Table S1. All structural figures were prepared with PYMOL (The PyMOL Molecular Graphics System, Version 1.5.0.4 Schrödinger, LLC). Structure has been deposited in the Protein Data Bank under ID code 4MCV.

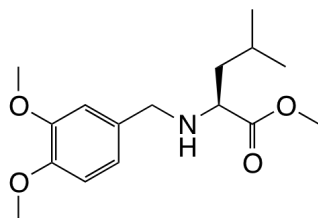
Compound Characterization



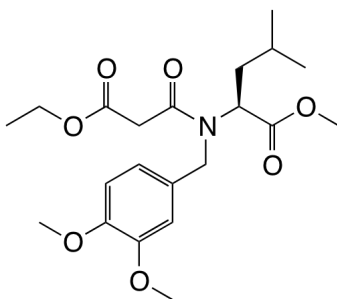
2,2'-(buta-1,3-diyne-1,4-diyl)dianiline ^1H NMR (d_6 DMSO, 400 MHz) δ 5.60 (s, 2H), 6.48 (t, 1H, $J = 8\text{Hz}$), 6.68 (d, 1H, $J = 8\text{Hz}$), 7.07 (t, 1H, $J = 8\text{Hz}$), 7.19 (d, 1H, $J = 8\text{Hz}$); ^{13}C NMR (d_6 DMSO, 400 MHz) δ 79.79, 81.53, 104.83, 115.30, 117.07, 131.95, 133.78, 152.80; LCMS: calculated $[\text{M}+\text{H}]^+ = 233.10$, found = 233.22.



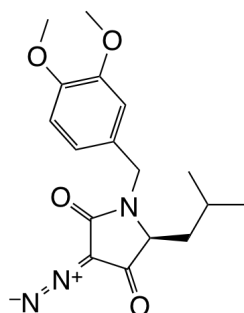
1H,1'H-2,2'-biindole ^1H NMR (d_6 DMSO, 400 MHz) δ 6.89 (s, 2H), 6.98 (t, 2H, $J = 8\text{Hz}$), 7.08 (t, 2H, $J = 8\text{Hz}$), 7.37 (d, 2H, $J = 4\text{Hz}$), 7.53 (d, 2H, $J = 4\text{Hz}$); ^{13}C NMR (d_6 DMSO, 400 MHz) δ 99.05, 111.69, 120.04, 120.67, 122.33, 129.08, 132.05, 137.55; LCMS: calculated $[\text{M}+\text{H}]^+ = 233.10$, found = 233.18.



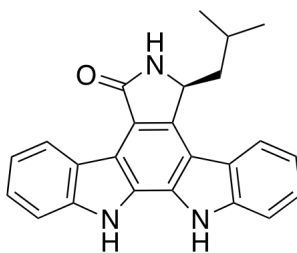
(S)-methyl 2-((3,4-dimethoxybenzyl)amino)-4-methylpentanoate (Star 1a) ^1H NMR (d_6 DMSO, 400 MHz) δ 0.75 (d, 3H, $J = 2\text{Hz}$), 0.82 (d, 3H, $J = 2\text{Hz}$), 1.30 – 1.38 (m, 2H), 1.66 – 1.76 (m, 1H), 2.24 (s, 2H), 3.13 (t, 1H, $J = 8\text{Hz}$), 3.43 (d, 1H, $J = 16\text{Hz}$), 3.62 (d, 1H, $J = 16\text{Hz}$), 3.69 (s, 3H), 3.70 (s, 3H), 6.75 (d, 1H, $J = 8\text{Hz}$), 6.82 (d, 1H, $J = 8\text{Hz}$), 6.89 (s, 1H); ^{13}C NMR (d_6 DMSO, 400 MHz) δ 22.58, 23.34, 25.02, 42.68, 50.30, 51.33, 55.92, 58.82, 112.11, 112.18, 112.32, 120.55, 133.39, 148.34, 149.28, 176.31; LCMS: calculated $[\text{M}+\text{H}]^+ = 296.18$, found = 296.33.



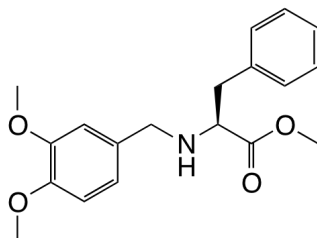
(S)-methyl 2-(N-(3,4-dimethoxybenzyl)-3-ethoxy-3-oxopropanamido)-4-methylpentanoate (Star 1b) ^1H NMR (d_6 DMSO, 400 MHz) δ 0.71 (d, 3H, $J = 4\text{Hz}$), 0.77 (d, 3H, $J = 4\text{Hz}$), 1.13 – 1.20 (3H), 1.46 – 1.53 (m, 2H), 1.73 – 1.75 (m, 1H), 3.50 (s, 3H), 3.67 (d, 2H, $J = 4\text{Hz}$), 3.71 (s, 3H), 3.72 (s, 3H), 4.01 – 4.12 (m, 2H), 6.73 – 6.95 (m, 3H); ^{13}C NMR (d_6 DMSO, 400 MHz) 14.58, 14.62, 22.72, 23.17, 25.09, 38.56, 41.77, 51.19, 52.40, 55.54, 56.04, 56.18, 61.25, 111.75, 112.32, 129.73, 148.81, 149.32, 167.59, 167.99, 171.72; LCMS: calculated $[\text{M}+\text{Na}]^+ = 432.20$, found = 432.33.



(S)-3-diazo-1-(3,4-dimethoxybenzyl)-5-isobutylpyrrolidine-2,4-dione (Star 1c) ^1H NMR (CDCl_3 , 400 MHz) δ 0.80 (d, 3H, $J = 8\text{Hz}$), 0.85 (d, 3H, $J = 8\text{Hz}$), 1.57 – 1.64 (m, 2H), 1.78 – 1.88 (m, 1H), 3.65 – 3.68 (m, 1H), 3.86 (d, 1H, $J = 16\text{Hz}$), 5.12 (d, 1H, $J = 16\text{Hz}$), 6.72 – 6.77 (m, 3H); ^{13}C NMR (CDCl_3 , 400 MHz) δ 0.17, 38.25, 44.46, 56.10, 56.15, 62.16, 111.36, 111.55, 120.92, 128.17, 149.13, 149.63, 161.92, 189.72; LCMS: calculated $[\text{M}+\text{H}]^+ = 331.15$, found = 331.34.

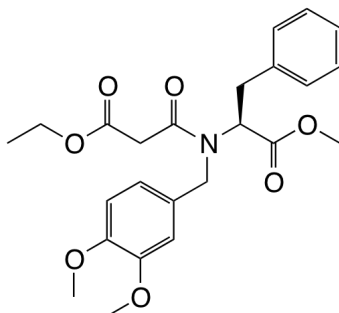


(S)-7-isobutyl-6,7,12,13-tetrahydro-5H-indolo[2,3-a]pyrrolo[3,4-c]carbazol-5-one (Star 1) ^1H NMR (d_6 DMSO, 400 MHz) δ 0.79 (d, 3H, $J = 8\text{Hz}$), 1.19 (d, 3H, $J = 8\text{Hz}$), 1.23 – 1.30 (m, 1H), 1.98 – 2.01 (m, 1H), 2.21 (t, 1H, $J = 12\text{Hz}$), 5.22 (d, 1H, $J = 8\text{Hz}$), 7.18 (t, 1H, $J = 8\text{Hz}$), 7.28 (t, 1H, $J = 8\text{Hz}$), 7.38 (t, 1H, $J = 8\text{Hz}$), 7.43 (t, 1H, $J = 8\text{Hz}$), 7.67 (d, 1H, $J = 8\text{Hz}$), 7.75 (d, 1H, $J = 8\text{Hz}$), 8.80 (d, 1H, $J = 8\text{Hz}$), 8.73 (s, 1H), 9.18 (d, 1H, $J = 8\text{Hz}$); LCMS: calculated $[\text{M}+\text{H}]^+ = 368.17$, found = 367.98.

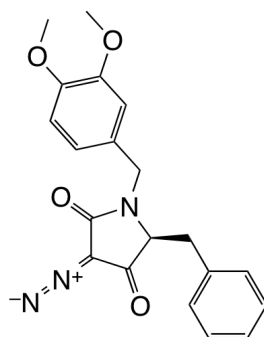


(S)-methyl 2-((3,4-dimethoxybenzyl)amino)-3-phenylpropanoate (Star 2a) ^1H NMR (d_6 DMSO, 400 MHz) δ 2.38 (s, 1H), 2.84 (d, 2H, $J = 8\text{Hz}$), 3.37 (s, 1H), 3.45 (d, 1H, $J = 16\text{Hz}$), 3.53 (s, 3H), 3.62 (s, 3H), 3.65 (d, 1H, $J = 16\text{Hz}$), 3.75 (s, 3H), 6.68 (d, 1H, $J = 8\text{Hz}$), 6.79 (d,

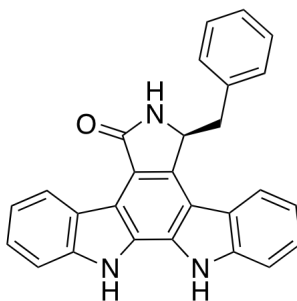
2H, $J = 8\text{Hz}$), 7.14 – 7.25 (m, 5H); ^{13}C NMR (d_6DMSO , 400 MHz) δ 51.09, 51.90, 55.89, 56.61, 62.24, 112.11, 112.13, 120.37, 126.92, 128.71, 129.84, 133.20, 138.61, 148.26, 149.26, 175.11; LCMS: calculated $[\text{M}+\text{H}]^+ = 330.16$, found = 329.95.



(S)-ethyl 3-((3,4-dimethoxybenzyl)(1-methoxy-1-oxo-3-phenylpropan-2-yl)amino)-3-oxopropanoate (Star 2b) ^1H NMR (d_6DMSO , 400 MHz) δ 1.26 (t, 3H, $J = 7.2\text{Hz}$), 1.52 (s, 3H), 3.20 – 3.44 (m, 4H), 3.65 (s, 2H), 3.68 (d, 1H, $J = 16.8\text{Hz}$), 3.79 (s, 3H), 3.83 (s, 3H), 4.17 (q, 2H, $J = 7.2\text{Hz}$), 4.24 (q, 1H, $J = 4.0\text{Hz}$), 4.35 (d, 1H, $J = 16.8\text{Hz}$), 6.57 (dd, 1H, $J = 2\text{Hz}$, $J = 8\text{Hz}$), 6.73 (d, 1H, $J = 8.4\text{Hz}$), 6.76 (d, 1H, $J = 2\text{Hz}$), 7.13 – 7.29 (m, 5H); LCMS: calculated $[\text{M}+\text{H}]^+ = 444.19$, found = 444.00.

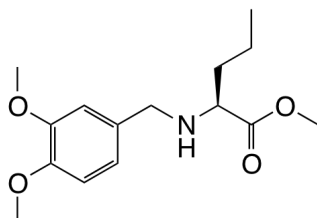


(S)-5-benzyl-3-diazo-1-(3,4-dimethoxybenzyl)pyrrolidine-2,4-dione (Star 2c) ^1H NMR (CDCl_3 , 400 MHz) δ 3.05 (dd, 1H, $J = 5.6\text{Hz}$, $J = 14.4\text{Hz}$), 3.17 (dd, 1H, $J = 4\text{Hz}$, $J = 14.4\text{Hz}$), 3.80 (s, 3H), 3.84 (s, 3H), 5.20 (t, 1H, $J = 4.4\text{Hz}$), 5.18 (d, 1H, $J = 14.8\text{Hz}$), 6.58 – 6.62 (m, 2H), 6.76 (d, 1H, $J = 8\text{Hz}$), 7.08 – 7.10 (m, 2H), 7.23 – 7.29 (m, 3H).

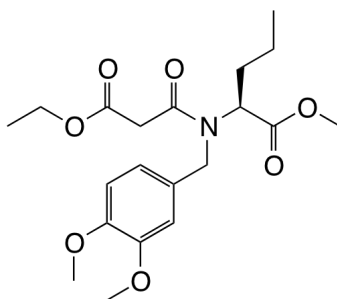


(S)-7-benzyl-6,7,12,13-tetrahydro-5H-indolo[2,3-a]pyrrolo[3,4-c]carbazol-5-one (Star 2) ^1H NMR (d_6DMSO , 400 MHz) δ 3.02 – 3.08 (m, 2H), 3.29 (dd, 1H, $J = 5.6\text{Hz}$, $J = 13.6\text{Hz}$), 5.55 (t,

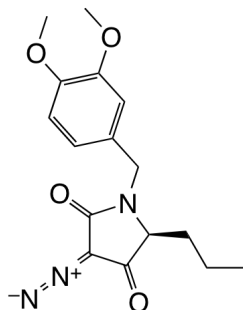
1H, $J = 4.4\text{Hz}$), 6.86 – 6.98 (m, 5H), 7.12 (t, 1H, $J = 7.2\text{Hz}$), 7.34 (m, 2H), 7.47 (t, 1H, $J = 7.6\text{Hz}$), 7.64 (d, 1H, $J = 8\text{Hz}$), 7.78 (d, 1H, $J = 8\text{Hz}$), 8.29 (d, 1H, $J = 7.6$), 8.45 (s, 1H), 9.04 (d, 1H, $J = 7.6$), 11.26 (s, 1H), 11.56 (s, 1H); LCMS: calculated $[M+H]^+ = 402.15$, found = 401.97.



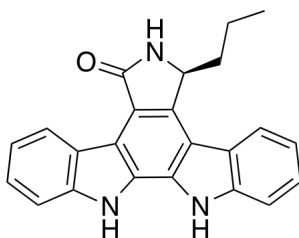
(S)-methyl 2-((3,4-dimethoxybenzyl)amino)pentanoate (Star 3a) ^1H NMR (d_6 DMSO, 400 MHz) δ 0.80 (t, 3H, $J = 8\text{Hz}$), 1.23 – 1.30 (m, 2H), 1.46 – 1.52 (m, 2H), 2.27 (s, 1H), 3.10 (t, 1H, $J = 12\text{Hz}$), 3.42 (d, 1H, $J = 12\text{Hz}$), 3.60 (s, 3H), 3.63 (d, 1H, $J = 12\text{Hz}$), 3.69 (s, 3H), 3.70 (s, 3H), 6.75 (d, 1H, $J = 8\text{Hz}$), 6.82 (d, 1H, $J = 8\text{Hz}$), 6.88 (s, 1H); ^{13}C NMR (d_6 DMSO, 400 MHz) δ 14.35, 19.32, 35.57, 51.33, 51.90, 55.97, 56.15, 60.15, 112.17, 112.33, 120.50, 133.42, 148.30, 149.28, 176.02; LCMS: calculated $[M+H]^+ = 282.16$, found = 282.32.



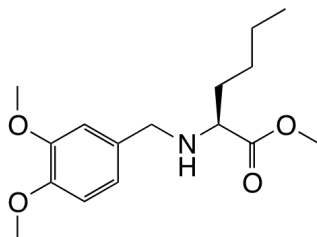
(S)-methyl 2-(N-(3,4-dimethoxybenzyl)-3-ethoxy-3-oxopropanamido)pentanoate (Star 3b) ^1H NMR (d_6 DMSO, 400 MHz) δ 0.66 – 0.79 (m, 3H), 1.12 – 1.17 (m, 5H), 1.63 – 1.81 (m, 2H), 3.32 – 3.51 (m, 1H), 3.48 (s, 3H), 3.71 (s, 3H), 3.72 (s, 3H), 3.99 – 4.11 (m, 2H), 4.23 – 4.29 (m, 1H), 4.42 – 4.56 (2H), 6.76 – 6.97 (m, 3H); ^{13}C NMR (d_6 DMSO, 400 MHz) δ 14.41, 14.49, 19.73, 41.72, 51.80, 52.33, 56.03, 56.17, 59.01, 61.25, 111.74, 112.29, 120.03, 129.78, 148.76, 149.40, 167.41, 168.00, 171.51; LCMS: calculated $[M+H]^+ = 396.19$, found = 396.32.



(S)-3-diazo-1-(3,4-dimethoxybenzyl)-5-propylpyrrolidine-2,4-dione (Star 3c) ^1H NMR (d_6 DMSO, 400 MHz) δ 0.73 (t, 3H, $J = 8\text{Hz}$), 1.09 – 1.14 (m, 2H), 1.65 – 1.70 (m, 2H), 3.70 (s, 3H), 3.71 (s, 3H), 3.83 (t, 1H, $J = 8\text{Hz}$), 4.18 (d, 1H, $J = 16\text{Hz}$), 4.72 (d, 1H, $J = 16\text{Hz}$), 6.81 – 6.89 (m, 3H); ^{13}C NMR (d_6 DMSO, 400 MHz) δ 14.34, 14.73, 16.62, 30.85, 44.37, 56.15, 64.26, 65.56, 112.42, 112.51, 121.00, 129.47, 148.96, 149.49, 162.16, 189.97; LCMS: calculated $[\text{M}+\text{H}]^+ = 318.14$, found = 318.22.

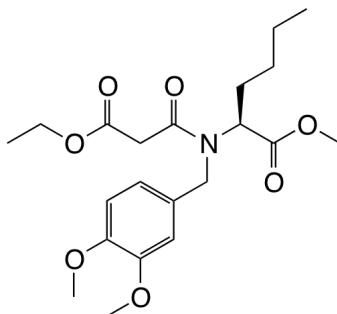


(S)-7-propyl-6,7,12,13-tetrahydro-5H-indolo[2,3-a]pyrrolo[3,4-c]carbazol-5-one (Star 3) ^1H NMR ($\text{CDCl}_3/\text{MeOH}$, 400 MHz) δ 0.89 (t, 3H, $J = 8\text{Hz}$), 1.28-1.32 (m, 1H), 1.50-1.54 (m, 1H), 1.64-1.68 (m, 1H), 3.29 (t, 1H, $J = 4\text{Hz}$), 4.95 (dd, 1H, $J = 4\text{Hz}$, $J = 4\text{Hz}$), 7.21 (t, 1H, $J = 8\text{Hz}$), 7.28 (t, 1H, $J = 8\text{Hz}$), 7.35 (t, 1H, $J = 8\text{Hz}$), 7.43 (t, 2H, $J = 8\text{Hz}$), 7.59 (d, 1H, $J = 8\text{Hz}$), 7.91 (d, 1H, $J = 8\text{Hz}$); ^{13}C NMR ($\text{CDCl}_3/\text{MeOH}$, 400 MHz) δ 13.64, 18.74, 36.03, 57.32, 110.79, 111.57, 114.20, 116.30, 119.34, 120.07, 121.69, 122.77, 123.23, 125.08, 125.35, 125.38, 125.80, 128.88, 138.04, 139.75, 139.93, 174.30; LCMS: calculated $[\text{M}+\text{H}]^+ = 354.14$, found = 354.2.

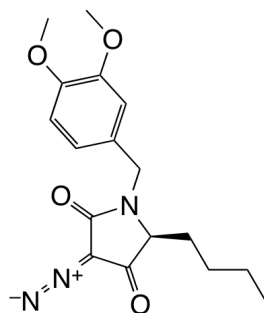


(S)-methyl 2-((3,4-dimethoxybenzyl)amino)hexanoate (Star 4a) ^1H NMR (d_6 DMSO, 400 MHz) δ 0.81 (t, 3H, $J = 8\text{Hz}$), 1.15 – 1.26 (m, 4H), 1.47 – 1.52 (m, 2H), 2.28 (s, 1H), 3.08 (s, 1H), 3.41 (d, 1H, $J = 12\text{Hz}$), 3.59 (s, 3H), 3.64 (d, 1H, $J = 12\text{Hz}$), 3.69 (s, 3H), 3.70 (s, 3H), 6.75 (dd, 1H, $J = 4\text{Hz}$, $J = 8\text{Hz}$), 6.82 (d, 1H, $J = 8\text{Hz}$), 6.88 (d, 1H, $J = 4\text{Hz}$); ^{13}C NMR (d_6 DMSO, 400 MHz) δ 14.47, 22.59, 28.27, 33.11, 51.32, 51.92, 55.97, 56.17, 60.38, 112.18, 112.32,

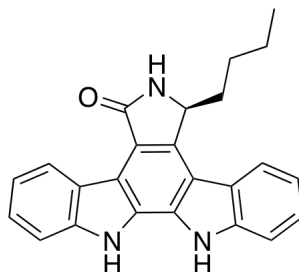
120.50, 133.43, 148.29, 149.27, 176.01; LCMS: calculated $[M+H]^+ = 296.18$, found = 296.33.



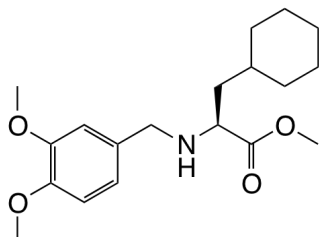
(S)-methyl 2-(N-(3,4-dimethoxybenzyl)-3-ethoxy-3-oxopropanamido)hexanoate (Star 4b) ^1H NMR (d_6 DMSO, 400 MHz) δ 0.65 – 0.75 (m, 3H), 1.10 – 1.18 (m, 6H), 1.63 – 1.67 (m, 1H), 1.69 – 1.81 (m, 1H), 3.34 (d, 1H, $J = 12\text{Hz}$), 3.50 (s, 3H), 3.54 (d, 1H, $J = 16\text{Hz}$), 3.66 – 3.72 (m, 6H), 3.99 – 4.07 (m, 2H), 4.20 – 4.27 (m, 1H), 4.43 – 4.58 (m, 2H), 6.75 – 6.97 (3H); ^{13}C NMR (d_6 DMSO, 400 MHz) δ 14.44, 14.60, 22.65, 28.66, 29.19, 52.34, 56.03, 56.19, 59.27, 61.25, 111.77, 112.31, 120.08, 129.80, 131.36, 148.79, 149.41, 167.40, 168.00, 168.13, 171.52; LCMS: calculated $[M+H]^+ = 432.20$, found = 432.



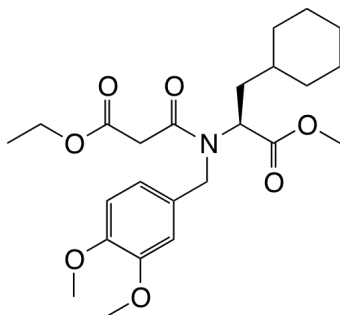
(S)-5-butyl-3-diazo-1-(3,4-dimethoxybenzyl)pyrrolidine-2,4-dione (Star 4c) ^1H NMR (d_6 DMSO, 400 MHz) δ 0.73 (t, 3H, $J = 8\text{Hz}$), 0.98 – 1.16 (m, 4H), 1.67 – 1.71 (m, 2H), 3.71 (s, 6H), 3.85 (t, 1H, $J = 4\text{Hz}$), 4.21 (d, 1H, $J = 16\text{Hz}$), 4.68 (d, 1H, $J = 16\text{Hz}$), 6.82 (d, 1H, $J = 8\text{Hz}$), 6.87 – 6.89 (m, 1H); ^{13}C NMR (d_6 DMSO, 400 MHz) δ 14.34, 14.74, 21.40, 22.61, 25.17, 28.48, 44.47, 56.14, 56.19, 60.41, 64.44, 65.61, 112.44, 112.54, 121.04, 129.55, 148.97, 149.48, 162.21, 189.98; LCMS: calculated $[M+H]^+ = 332.15$, found = 332.26.



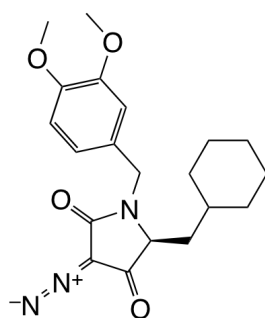
(S)-7-butyl-6,7,12,13-tetrahydro-5H-indolo[2,3-a]pyrrolo[3,4-c]carbazol-5-one (Star 4) ¹H NMR (CDCl₃/MeOH, 400 MHz) δ 0.73 (t, 3H, *J* = 8Hz), 1.07-1.29 (m, 5H), 1.39-1.46 (m, 1H), 2.18 (m, 1H), 4.28 (d, 1H, *J* = 8Hz), 7.16 (t, 2H, *J* = 8Hz), 7.22-7.26 (m, 2H), 7.38 (t, 1H, *J* = 8Hz), 7.50 (d, 1H, *J* = 8Hz), 7.72 (d, 1H, 8Hz), 9.02 (d, 1H, *J* = 8Hz); ¹³C NMR (CDCl₃/MeOH, 400 MHz) δ 13.92, 22.56, 22.66, 33.47, 57.40, 110.93, 111.59, 115.97, 119.43, 120.06, 121.79, 122.71, 122.89, 125.03, 125.07, 125.38, 125.49, 128.69, 137.92, 139.37, 139.62, 174.25; LCMS: calculated [M+H]⁺ = 368.17, found = 368.24.



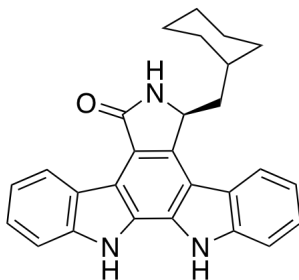
(S)-methyl 3-cyclohexyl-2-((3,4-dimethoxybenzyl)amino)propanoate (Star 5a) ¹H NMR (d₆ DMSO, 400 MHz) δ 0.68 – 0.87 (m, 2H), 1.03 – 1.23 (m, 3H), 1.32 – 1.60 (m, 8H), 2.27 (s, 1H), 3.40 (d, 1H, *J* = 12Hz), 3.59 (s, 3H), 3.65 (d, 1H, *J* = 16Hz), 3.69 (s, 3H), 3.70 (s, 3H), 6.73 (d, 1H, *J* = 8Hz), 6.81 (d, 1H, *J* = 12Hz), 6.88 (s, 1H); ¹³C NMR (d₆DMSO, 400 MHz) δ 26.32, 26.48, 26.70, 32.80, 33.79, 34.31, 51.28, 51.92, 55.93, 56.17, 57.99, 112.10, 112.26, 120.56, 133.42, 148.31, 149.28, 176.40; LCMS: calculated [M+H]⁺ = 336.21, found = 336.69.



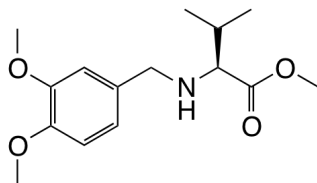
(S)-ethyl 3-((3-cyclohexyl-1-methoxy-1-oxopropan-2-yl)(3,4-dimethoxybenzyl) amino)-3-oxopropanoate (Star 5b) ¹H NMR (d₆ DMSO, 400 MHz) δ 0.66 – 0.74 (m, 2H), 0.94 – 1.11 (m, 4H), 1.11 – 1.17 (m, 3H), 1.35 (d, 1H, *J* = 12.8Hz), 1.43 – 1.64 (m, 5H), 1.70 – 1.77 (m, 1H), 3.43 – 3.56 (m, 1H), 3.50 (s, 3H), 3.71 (s, 3H), 3.72 (s, 3H), 4.02 – 4.11 (m, 2H), 4.39 – 4.70 (m, 2H), 6.73 – 6.94 (m, 3H); ¹³C NMR (d₆DMSO, 400 MHz) δ 26.23, 26.42, 32.99, 33.55, 34.38, 37.05, 41.79, 51.35, 52.43, 55.61, 56.03, 56.23, 56.31, 61.25, 111.85, 112.36, 120.16, 129.79, 148.86, 149.45, 167.59, 168.02, 171.84; LCMS: calculated [M+H]⁺ = 450.24, found = 450.33.



(S)-5-(cyclohexylmethyl)-3-diazo-1-(3,4-dimethoxybenzyl)pyrrolidine-2,4-dione (Star 5c) ¹H NMR (CDCl₃, 400 MHz) δ 0.67 – 0.77 (m, 2H), 0.81 – 0.88 (m, 3H), 1.33 – 1.66 (m, 8H), 3.63 (t, 1H, *J* = 8Hz), 3.75 (s, 6H), 3.83 (d, 1H, *J* = 16Hz), 5.03 (d, 1H, *J* = 16Hz), 6.66 – 6.72 (m, 3H); ¹³C NMR (CDCl₃, 400 MHz) δ 26.10, 26.23, 26.31, 33.44, 33.46, 36.80, 44.50, 56.05, 56.08, 61.86, 65.23, 111.34, 111.52, 120.85, 128.24, 149.06, 149.56, 161.92, 189.65; LCMS: calculated [M+H]⁺ = 372.18, found = 372.26.

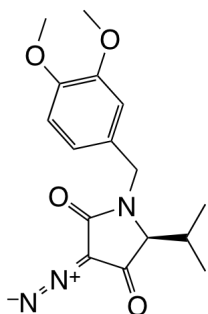


(S)-7-(cyclohexylmethyl)-6,7,12,13-tetrahydro-5H-indolo[2,3-a]pyrrolo[3,4-c]carbazol-5-one (Star 5) ¹H NMR (CDCl₃/MeOD, 400 MHz) δ 0.76-0.84 (m, 1H), 0.98-1.29 (m, 6H), 1.35-1.41 (m, 2H), 1.52-1.60 (m, 2H), 1.73-1.77 (d, 1H, *J* = 16Hz), 1.96-2.05 (m, 1H), 2.08-2.22 (m, 1H), 4.37-4.69 (m, 1H), 7.10-7.17 (m, 2H), 7.19-7.22 (m, 1H), 7.25-7.36 (m, 2H), 7.42-7.47 (m, 1H), 7.69-7.76 (m, 1H), 7.82 (s, 1H), 9.00-9.07 (m, 1H); ¹³C NMR (CDCl₃/MeOD, 400 MHz) δ 31.52, 34.49, 35.98, 36.72, 42.32, 55.01, 59.51, 87.93, 110.90, 111.53, 113.76, 119.33, 120.05, 121.84, 122.63, 122.98, 124.92, 125.17, 125.29, 125.45, 138.65, 139.39, 139.61, 163.24; LCMS: calculated [M+H]⁺ = 408.20, found = 408.3.

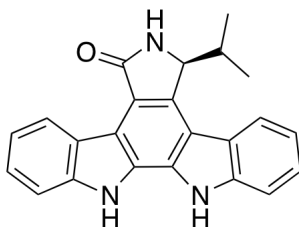


(S)-methyl 2-((3,4-dimethoxybenzyl)amino)-3-methylbutanoate (Star 6a) ¹H NMR (d₆ DMSO, 400 MHz) δ 0.83 (d, 3H, *J* = 8Hz), 0.88 (d, 3H, *J* = 8Hz), 1.80 (sep, 1H, *J* = 8Hz), 2.21

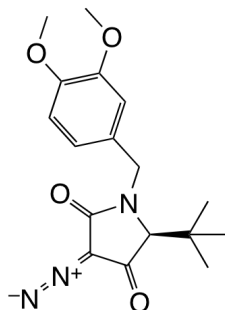
(s, 1H), 2.85 (d, 1H, $J = 8\text{Hz}$), 3.40 (d, 1H, $J = 16\text{Hz}$), 3.61 (s, 3H), 3.69 (d, 1H, $J = 16\text{Hz}$), 3.70 (s, 3H), 3.72 (s, 3H), 6.75 (d, 1H, $J = 8\text{Hz}$), 6.82 (d, 1H, $J = 4\text{Hz}$), 6.90 (s, 1H); ^{13}C NMR (d_6DMSO , 400 MHz) δ 19.34, 19.87, 31.66, 51.67, 51.73, 55.92, 55.97, 56.12, 66.36, 112.15, 112.18, 112.25, 120.49, 133.40, 148.33, 149.29, 175.65; LCMS: calculated $[\text{M}+\text{H}]^+ = 282.16$, found = 282.31.



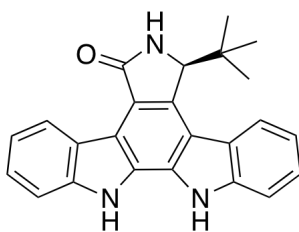
(S)-3-diazo-1-(3,4-dimethoxybenzyl)-5-isopropylpyrrolidine-2,4-dione (Star 6c) ^1H NMR (CDCl_3 , 400 MHz) δ 0.89 (d, 3H, $J = 8\text{Hz}$), 1.06 (d, 3H, $J = 8\text{Hz}$), 2.19 – 2.26 (m, 1H), 3.59 (d, 1H, $J = 4\text{Hz}$), 3.84 (s, 3H), 3.85 (d, 3H), 3.94 (d, 1H, $J = 16\text{Hz}$), 5.14 (d, 1H, 16Hz), 6.73 – 6.80 (m, 3H); ^{13}C NMR (CDCl_3 , 400 MHz) δ 0.19, 16.14, 18.08, 28.92, 44.55, 56.12, 56.19, 68.02, 111.36, 111.50, 120.85, 128.19, 149.10, 149.65, 162.41, 189.06; LCMS: calculated $[\text{M}+\text{H}]^+ = 318.14$, found = 318.26.



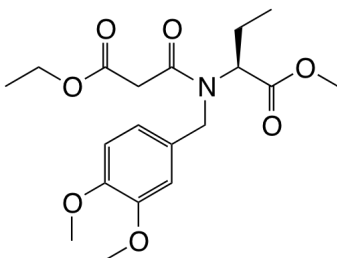
(S)-7-isopropyl-6,7,12,13-tetrahydro-5H-indolo[2,3-a]pyrrolo[3,4-c]carbazol-5-one (Star 6) ^1H NMR (d_6DMSO , 400 MHz) δ 0.24 (d, 3H, $J = 8\text{Hz}$), 1.33 (d, 3H, $J = 8\text{Hz}$), 2.76-2.83 (m, 1H), 5.19 (s, 1H), 7.20 (t, 1H, $J = 8\text{Hz}$), 7.28 (t, 1H, $J = 8\text{Hz}$), 7.42 (quin, $J = 8\text{Hz}$), 7.69 (d, 1H, $J = 8\text{Hz}$), 7.76 (d, 1H, $J = 8\text{Hz}$), 8.04 (d, 1H, $J = 8\text{Hz}$), 8.54 (s, 1H), 9.20 (d, 1H, $J = 8\text{Hz}$), 11.28 (s, 1H), 11.54 (s, 1H); ^{13}C NMR (DMSO , 400 MHz) δ 14.32, 21.83, 30.41, 62.00, 112.00, 112.71, 114.25, 115.97, 119.59, 119.80, 120.53, 122.40, 122.83, 123.42, 125.54, 125.74, 126.00, 126.17, 128.85, 137.04, 139.87, 140.08, 173.13; LCMS: calculated $[\text{M}+\text{H}]^+ = 354.42$, found = 354.3.



(S)-5-(tert-butyl)-3-diazo-1-(3,4-dimethoxybenzyl)pyrrolidine-2,4-dione (Star 7c) ^1H NMR (CDCl_3 , 400 MHz) δ 1.05 (s, 9H), 3.38 (s, 1H), 3.81 (s, 3H), 3.83 (s, 3H), 4.08 (d, 1H, $J = 16\text{Hz}$), 5.34 (d, 1H, $J = 16\text{Hz}$), 6.67 (s, 1H), 6.69 (d, 1H, $J = 4\text{Hz}$), 6.78 (d, 1H, $J = 8\text{Hz}$); ^{13}C NMR (CDCl_3 , 400 MHz) δ 27.09, 37.29, 48.46, 56.11, 56.18, 71.70, 77.27, 111.46, 111.47, 120.85, 128.45, 149.03, 149.63, 164.74, 189.54; LCMS: calculated $[\text{M}+\text{H}]^+ = 332.15$, found = 332.20.

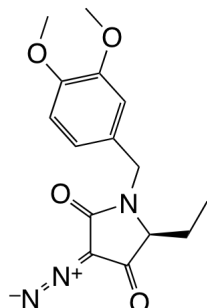


(S)-7-(tert-butyl)-6,7,12,13-tetrahydro-5H-indolo[2,3-a]pyrrolo[3,4-c]carbazol-5-one (Star 7) ^1H NMR (d_6 DMSO, 400 MHz) δ 0.90 (s, 9H), 5.11 (s, 1H), 7.18-7.22 (m, 2H), 7.37-7.40 (m, 2H), 7.69 (t, 2H, $J = 8\text{Hz}$), 8.30 (d, 1H, $J = 8\text{Hz}$), 8.46 (s, 1H), 9.22 (d, 1H, $J = 8\text{Hz}$), 11.27 (s, 1H), 11.50 (s, 1H); ^{13}C NMR (DMSO, 400 MHz) δ 27.64, 39.55, 65.65, 111.96, 112.35, 116.05, 116.18, 119.59, 119.65, 120.88, 123.40, 123.81, 123.95, 125.43, 125.82, 126.22, 126.56, 128.90, 135.79, 140.03, 140.09, 172.93; LCMS: calculated $[\text{M}+\text{H}]^+ = 368.17$, found = 368.3.

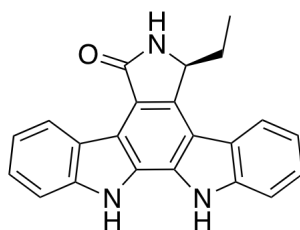


(S)-methyl 2-(N-(3,4-dimethoxybenzyl)-3-ethoxy-3-oxopropanamido)butanoate (Star 8b) ^1H NMR (CDCl_3 , 400 MHz) δ 0.80 (t, 3H, $J = 6\text{Hz}$), 1.21 (t, 3H, $J = 4\text{Hz}$), 1.77 – 1.82 (m, 1H), 1.95 – 2.00 (m, 1H), 3.39 (d, 1H, $J = 8\text{Hz}$), 3.58 (s, 3H), 3.79 – 3.86 (m, 6H), 4.10 – 4.16 (m, 2H), 4.41 – 4.59 (m, 3H), 6.70 – 6.86 (m, 3H); ^{13}C NMR (CDCl_3 , 400 MHz) δ 10.93, 11.31,

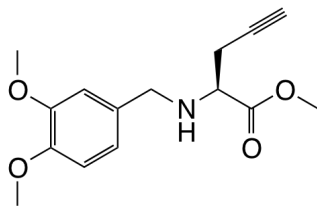
14.22, 41.78, 42.20, 46.39, 51.03, 52.20, 52.45, 56.03, 61.66, 61.78, 62.24, 110.03, 110.86, 111.42, 111.74, 119.05, 120.50, 128.85, 148.74, 149.53, 167.58, 171.41; LCMS: $[M+H]^+ = 382.18$, found = 382.18.



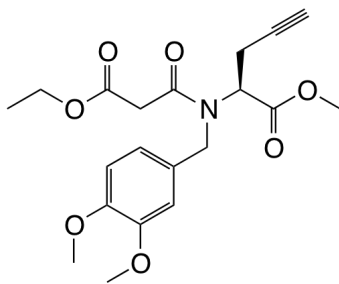
(S)-3-diazo-1-(3,4-dimethoxybenzyl)-5-ethylpyrrolidine-2,4-dione (Star 8c) ^1H NMR (d_6 DMSO, 400 MHz) δ 0.66 (t, 3H, $J = 8\text{Hz}$), 1.72 – 1.78 (m, 2H), 3.70 (s, 6H), 3.83 (t, 1H, $J = 4\text{Hz}$), 4.14 (d, 1H, $J = 16\text{Hz}$), 4.75 (d, 1H, $J = 16\text{Hz}$), 6.81 – 6.89 (m, 3H); ^{13}C NMR (DMSO, 400 MHz) δ 1.81, 7.68, 21.75, 44.25, 56.16, 64.86, 112.42, 112.50, 120.98, 129.40, 148.93, 149.47, 162.30, 189.92; LCMS: $[M+H]^+ = 304.12$, found = 304.30.



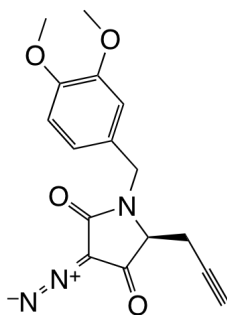
(S)-7-ethyl-6,7,12,13-tetrahydro-5H-indolo[2,3-a]pyrrolo[3,4-c]carbazol-5-one (Star 8) ^1H NMR (d_6 DMSO, 400 MHz) δ 0.83 (t, 3H, $J = 8\text{Hz}$), 1.74 (m, 1H), 2.31-2.36 (m, 1H), 5.20 (d, 1H, $J = 8\text{Hz}$), 7.20 (t, 1H, $J = 8\text{Hz}$), 7.28 (t, 1H, $J = 8\text{Hz}$), 7.38-7.46 (m, 2H), 7.68 (d, 1H, $J = 8\text{Hz}$), 7.75 (d, 1H, $J = 8\text{Hz}$), 8.08 (d, 1H, $J = 8\text{Hz}$), 9.21 (d, 1H, $J = 8\text{Hz}$), 11.36 (s, 1H), 11.62 (s, 1H); ^{13}C NMR (DMSO, 400 MHz) δ 9.89, 27.23, 57.91, 111.97, 112.67, 114.35, 116.08, 119.58, 119.62, 120.55, 122.33, 122.81, 123.45, 125.57, 125.98, 126.21, 128.80, 137.32, 139.88, 140.07, 172.51; LCMS: $[M+H]^+ = 340.14$, found = 340.18.



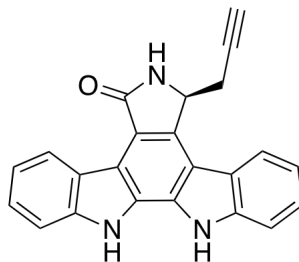
(S)-methyl 2-((3,4-dimethoxybenzyl)amino)pent-4-ynoate (Star 9a) ^1H NMR (CDCl_3 , 400 MHz) δ 2.00 – 2.02 (m, 1H), 2.57 – 2.59 (m, 1H), 3.42 (t, 1H, $J = 6\text{Hz}$), 3.63 (d, 1H, $J = 12\text{Hz}$), 3.72 (s, 3H), 3.79 (d, 1H, $J = 12\text{Hz}$), 3.83 (s, 3H), 3.85 (s, 3H), 6.76 – 6.89 (m, 3H); ^{13}C NMR (CDCl_3 , 400 MHz) δ 0.18, 23.48, 51.67, 51.88, 58.68, 71.28, 79.72, 111.19, 111.31, 111.63, 132.17, 148.39, 149.20, 173.85; LCMS: $[\text{M}+\text{H}]^+ = 378.13$, found = 378.28.



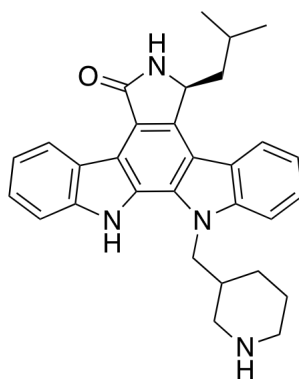
(S)-methyl 2-(N-(3,4-dimethoxybenzyl)-3-ethoxy-3-oxopropanamido)pent-4-ynoate (Star 9b) ^1H NMR (CDCl_3 , 400 MHz) δ 1.18 (t, 3H, $J = 8\text{Hz}$), 1.98 (s, 1H), 2.79 – 2.87 (m, 2H), 3.38 (q, 3H, $J = 16\text{Hz}$, $J = 8\text{Hz}$), 3.59 (s, 3H), 3.75 (d, 1H, $J = 8\text{Hz}$), 3.79 (s, 3H), 3.81 (s, 3H), 4.07 – 4.16 (m, 4H), 4.57 (d, 1H, $J = 16\text{Hz}$), 4.68 (d, 1H, $J = 16\text{Hz}$), 6.77 (d, 1H, $J = 8\text{Hz}$), 6.82 (d, 1H, $J = 8\text{Hz}$), 6.96 (s, 1H); ^{13}C NMR (CDCl_3 , 400 MHz) δ 14.24, 19.24, 41.60, 52.57, 53.65, 56.01, 58.88, 61.66, 70.79, 77.09, 77.41, 81.03, 110.65, 111.35, 119.81, 128.15, 148.90, 149.51, 167.04, 167.18, 169.38; LCMS: $[\text{M}+\text{H}]^+ = 392.20$, found = 392.0.



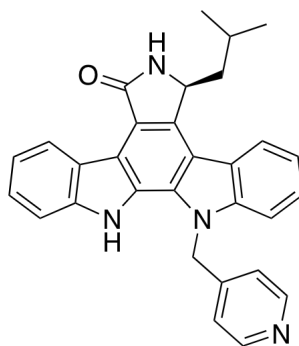
(S)-3-diazo-1-(3,4-dimethoxybenzyl)-5-(prop-2-yn-1-yl)pyrrolidine-2,4-dione (Star 9c) ^1H NMR (CDCl_3 , 400 MHz) δ 1.20 (t, 1H, $J = 8\text{Hz}$), 1.98 (s, 1H), 2.03 (t, 2H, $J = 4\text{Hz}$), 3.81 (s, 6H), 4.03 (d, 1H, $J = 16\text{Hz}$), 5.14 (d, 1H, $J = 16\text{Hz}$), 6.75 – 6.79 (m, 3H); ^{13}C NMR (CDCl_3 , 400 MHz) δ 19.90, 44.58, 56.11, 61.53, 72.68, 76.99, 111.38, 111.55, 120.90, 127.88, 149.20, 149.68, 162.18, 187.47; LCMS: $[\text{M}+\text{H}]^+ = 360.14$, found = 360.28.



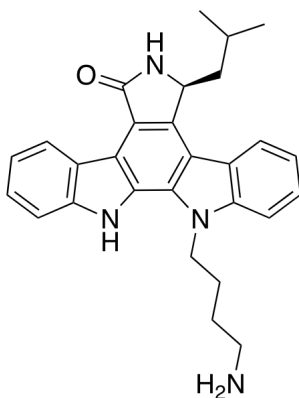
(S)-7-(prop-2-yn-1-yl)-6,7,12,13-tetrahydro-5H-indolo[2,3-a]pyrrolo[3,4-c]carbazol-5-one (Star 9) ^1H NMR (d_6 DMSO, 400 MHz) δ 2.44 (t, 1H, $J = 2.4\text{Hz}$), 3.10 (q, 2H, 17.2 Hz, $J = 16.4$), 5.40 (m, 1H), 7.21 (t, 1H, $J = 7.2\text{Hz}$), 7.29 (t, 1H, $J = 8\text{Hz}$), 7.41 (t, 1H, $J = 7.2\text{Hz}$), 7.46 (t, 1H, $J = 7.2\text{Hz}$), 7.69 (d, 1H, $J = 8\text{Hz}$), 7.77 (d, 1H, $J = 8\text{Hz}$), 8.11 (d, 1H, $J = 8\text{Hz}$), 8.49 (s, 1H), 9.18 (d, 1H, $J = 8\text{Hz}$), 11.31 (s, 1H), 11.56 (s, 1H); LCMS: calculated $[\text{M}+\text{H}]^+ = 350.12$, found = 350.20.



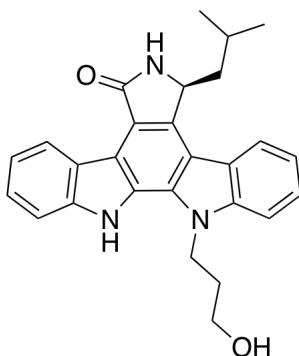
(7S)-7-isobutyl-12-(piperidin-3-ylmethyl)-6,7,12,13-tetrahydro-5H-indolo[2,3-a]pyrrolo[3,4-c]carbazol-5-one (Star 10, 3:1 ratio of N12 to N13 alylation product) ^1H NMR (d_6 DMSO, 400 MHz) δ 0.81 (t, 3H, $J = 8\text{Hz}$), 1.22 (t, 3H, $J = 8\text{Hz}$), 1.25 – 1.64 (m, 5H), 1.95 – 2.10 (m, 1H), 2.20 – 2.38 (m, 2H), 2.61 – 2.78 (m, 2H), 2.80 – 2.93 (m, 1H), 4.72 – 4.78 (m, 1H), 4.92 – 4.98 (m, 1H), 5.25 (d, 1H, $J = 8\text{Hz}$), 7.23 (t, 1H, $J = 8\text{Hz}$), 7.32 (t, 1H, $J = 8\text{Hz}$), 7.73 (d, 1H, $J = 8\text{Hz}$), 7.79 (d, 1H, $J = 8\text{Hz}$), 8.02 (d, 1H, $J = 8\text{Hz}$), 8.34 (s, 1H), 8.81 (s, 1H), 9.37 (d, 1H, $J = 8\text{Hz}$); LCMS: calculated $[\text{M}+\text{H}]^+ = 465.26$, found = 465.29.



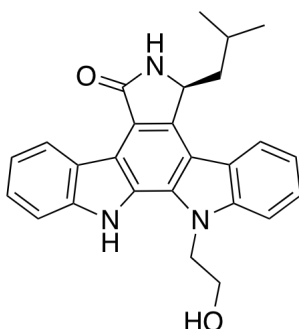
(S)-7-isobutyl-12-(pyridin-4-ylmethyl)-6,7,12,13-tetrahydro-5H-indolo[2,3-a]pyrrolo[3,4-c]carbazol-5-one (Star 11, 3:1 ratio of N12 to N13 alkylation product) ^1H NMR (d_6 DMSO, 400 MHz) δ 0.80 (d, 3H, $J = 6.4\text{Hz}$), 1.21 (d, 3H, $J = 6.4\text{Hz}$), 2.19 – 2.25 (m, 1H), 5.26 – 5.32 (m, 1H), 6.22 – 6.24 (m, 1H), 6.94 – 6.99 (m, 2H), 7.18 – 7.30 (m, 2H), 7.31 – 7.41 (m, 2H), 7.59 (t, 1H, $J = 8\text{Hz}$), 7.44 – 7.66 (m, 1H), 8.01 – 8.08 (m, 1H), 8.34 – 8.37 (m, 2H), 8.83 (s, 1H), 9.30 – 9.39 (m, 1H); LCMS: calculated $[\text{M}+\text{H}]^+ = 459.21$, found = 459.30.



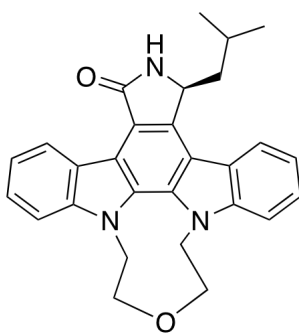
(S)-12-(4-aminobutyl)-7-isobutyl-6,7,12,13-tetrahydro-5H-indolo[2,3-a]pyrrolo[3,4-c]carbazol-5-one (Star 12) ^1H NMR (d_6 DMSO, 400 MHz) δ 0.81 (d, 3H, $J = 8\text{ Hz}$), 1.21 (d, 3H, $J = 4\text{ Hz}$), 1.32 (s, 1H), 1.49 – 1.62 (m, 2H), 1.84 – 1.90 (m, 2H), 2.03 – 2.08 (m, 1H), 2.21 (t, 1H, $J = 12\text{ Hz}$), 2.66 – 2.75 (m, 2H), 3.67 (s, 1H), 4.95 (b, 2H), 5.25 (d, 1H, $J = 8\text{ Hz}$), 7.21 (t, 1H, $J = 8\text{ Hz}$), 7.34 (t, 1H, $J = 8\text{ Hz}$), 7.42 (t, 1H, $J = 8\text{ Hz}$), 7.51 (t, 1H, $J = 8\text{ Hz}$), 7.70 (d, 1H, $J = 4\text{ Hz}$), 7.82 (d, 1H, $J = 8\text{ Hz}$), 8.03 (d, 1H, $J = 8\text{ Hz}$), .40 (s, 1H), 8.79 (s, 1H), 9.32 (d, 1H, $J = 4\text{ Hz}$); ^{13}C NMR (d_6 DMSO, 400 MHz) δ 22.30, 24.67, 25.60, 25.87, 28.13, 44.19, 44.79, 55.24, 110.90, 112.13, 114.30, 117.67, 119.18, 119.63, 120.62, 122.24, 122.31, 122.85, 125.50, 125.62, 125.85, 126.01, 129.40, 138.45, 140.80, 172.16; LCMS: calculated $[\text{M}+\text{H}]^+ = 439.24$, found = 439.32.



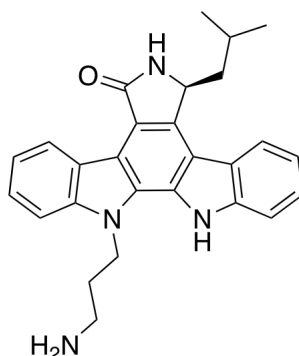
(S)-12-(3-hydroxypropyl)-7-isobutyl-6,7,12,13-tetrahydro-5H-indolo[2,3-a]pyrrolo[3,4-c]carbazol-5-one (Star 13), 2:1 ratio of N12 to N13 alkylation product) ^1H NMR (d_6 DMSO, 400 MHz) δ 0.78 – 0.81 (m, 3H), 1.99 – 2.22 (m, 3H), 1.24 – 1.28 (m, 1H), 2.02 – 2.05 (m, 4H), 4.85 – 4.96 (m, 2H), 5.09 – 5.20 (br, 1H), 5.25 (d, 1H, $J = 9.2\text{Hz}$), 6.60 – 6.67 (m, 1H), 6.79 – 6.82 (m, 2H), 7.22 – 7.32 (m, 1H), 7.40 – 7.58 (m, 2H), 7.70 (t, 1H, $J = 8.4\text{Hz}$), 8.03 (d, 1H, $J = 8\text{Hz}$), 8.78 (s, 1H), 9.30 – 9.34 (m, 1H), 11.63 – 11.83 (m, 1H); LCMS: calculated $[\text{M}+\text{H}]^+ = 426.21$, found = 426.33.



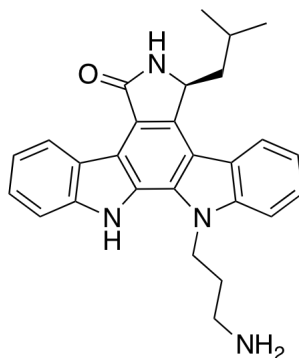
(S)-12-(2-hydroxyethyl)-7-isobutyl-6,7,12,13-tetrahydro-5H-indolo[2,3-a]pyrrolo[3,4-c]carbazol-5-one (Star 14) ^1H NMR (d_6 DMSO, 400 MHz) δ 0.81 (d, 3H, $J = 6.8\text{Hz}$), 1.21 (d, 3H, $J = 6.4\text{Hz}$), 1.24 – 1.27 (m, 1H), 1.99 – 2.05 (m, 1H), 2.22 (t, 1H, $J = 11.2\text{Hz}$), 3.90 (q, 2H, $J = 5.2\text{Hz}$, $J = 5.2\text{Hz}$), 4.92 (br, 1H), 5.25 (d, 1H, $J = 9.6\text{Hz}$), 7.21 (t, 1H, $J = 7.2\text{Hz}$), 7.31 (t, 1H, $J = 7.2\text{Hz}$), 7.45 (q, 2H, $J = 7.2\text{Hz}$, $J = 8\text{Hz}$), 7.70 (d, 1H, $J = 8.4\text{Hz}$), 7.77 (d, 1H, $J = 8\text{Hz}$), 8.02 (d, 1H, $J = 7.6\text{Hz}$), 8.77 (s, 1H), 9.35 (d, 1H, $J = 8\text{Hz}$), 11.60 (s, 1H); LCMS: calculated $[\text{M}+\text{H}]^+ = 412.19$, found = 412.30.



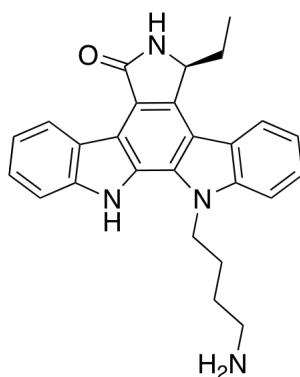
(S)-12,13-bis(diethylether)-7-isobutyl-6,7,12,13-tetrahydro-5H-indolo[2,3-a]pyrrolo[3,4-c]carbazol-5-one (Star 15) ^1H NMR (d_6 DMSO, 400 MHz) δ 0.79 (d, 3H, $J = 6.4\text{ Hz}$), 1.21 (d, 3H, $J = 6.4\text{ Hz}$), 2.00 – 2.054 (m, 1H), 2.19 (t, 1H, $J = 12\text{ Hz}$), 3.47 – 3.59 (m, 4H), 3.93 – 4.05 (m, 4H), 5.30 (d, 1H, $J = 7.6\text{ Hz}$), 7.32 (t, 1H, $J = 7.6\text{ Hz}$), 7.35 (t, 1H, $J = 7.2\text{ Hz}$), 7.46 (t, 1H, $J = 7.2\text{ Hz}$), 7.51 (t, 1H, $J = 7.6\text{ Hz}$), 7.74 (d, 1H, $J = 8.4\text{ Hz}$), 7.85 (d, 1H, $J = 8.4\text{ Hz}$), 8.05 (d, 1H, $J = 8.0\text{ Hz}$); LCMS: calculated $[\text{M}+\text{H}]^+ = 438.21$, found = 438.31.



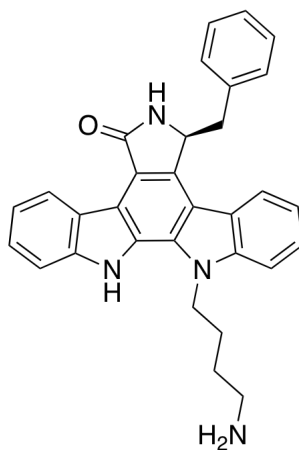
(S)-13-(3-aminopropyl)-7-isobutyl-6,7,12,13-tetrahydro-5H-indolo[2,3-a]pyrrolo[3,4-c]carbazol-5-one (Star 16) ^1H NMR (d_6DMSO , 400 MHz) δ 0.81 (d, 3H, $J = 4\text{Hz}$), 1.21 (d, 3H, $J = 4\text{Hz}$), 2.00 – 2.11 (m, 2H), 2.19 – 2.25 (m, 2H), 2.75 (t, 2H, $J = 6\text{Hz}$), 4.94 (t, 2H, $J = 6\text{Hz}$), 5.26 (d, 1H, $J = 8\text{Hz}$), 7.24 (t, 1H, $J = 8\text{Hz}$), 7.32 (t, 1H, $J = 8\text{Hz}$), 7.45 (t, 2H, $J = 8\text{Hz}$), 7.75 (t, 2H, $J = 8\text{Hz}$), 8.03 (d, 1H, $J = 8\text{Hz}$), 8.80 (s, 1H), 9.36 (d, 1H, $J = 8\text{Hz}$); ^{13}C NMR (d_6DMSO , 400 MHz) δ 22.32, 24.69, 25.86, 30.81, 37.42, 44.74, 55.28, 61.56, 94.62, 109.86, 112.91, 115.49, 116.52, 119.13, 119.76, 120.61, 122.09, 122.18, 123.02, 125.66, 125.93, 126.36, 127.15, 128.34, 138.65, 140.69, 141.11, 172.13; LCMS: calculated $[\text{M}+\text{H}]^+ = 425.23$, found = 425.34.



(S)-12-(3-aminopropyl)-7-isobutyl-6,7,12,13-tetrahydro-5H-indolo[2,3-a]pyrrolo[3,4-c]carbazol-5-one (Star 17) ^1H NMR (d_6DMSO , 400 MHz) δ 0.80 (d, 3H, $J = 4\text{Hz}$), 1.21 (d, 3H, $J = 4\text{Hz}$), 1.99 – 2.05 (m, 1H), 2.10 – 2.13 (m, 2H), 2.18 – 2.24 (m, 1H), 2.76 (t, 2H, $J = 6\text{Hz}$), 4.97 (t, 2H, $J = 6\text{Hz}$), 5.26 (d, 1H, $J = 8\text{Hz}$), 7.21 (t, 1H, $J = 8\text{Hz}$), 7.35 (t, 1H, $J = 8\text{Hz}$), 7.42 (t, 1H, $J = 8\text{Hz}$), 7.52 (t, 1H, $J = 8\text{Hz}$), 7.68 (d, 1H, $J = 8\text{Hz}$), 7.84 (d, 1H, $J = 8\text{Hz}$), 8.04 (d, 1H, $J = 8\text{Hz}$), 8.80 (s, 1H), 9.32 (d, 1H, $J = 8\text{Hz}$); ^{13}C NMR (d_6DMSO , 400 MHz) δ 22.32, 24.67, 25.85, 30.82, 37.46, 42.01, 44.77, 55.26, 110.75, 112.08, 114.27, 117.73, 119.27, 119.65, 120.75, 122.27, 122.36, 122.96, 125.71, 125.75, 125.88, 126.06, 129.61, 138.45, 140.86, 140.91, 172.15; LCMS: calculated $[\text{M}+\text{H}]^+ = 425.23$, found = 425.36.



(S)-12-(4-aminobutyl)-7-ethyl-6,7,12,13-tetrahydro-5H-indolo[2,3-a]pyrrolo[3,4-c]carbazol-5-one (Star 18) ^1H NMR (d_6 DMSO, 400 MHz) δ 0.84 (t, 3H, $J = 6.8$ Hz), 1.53 – 1.58 (m, 2H), 1.65 – 1.70 (m, 1H), 1.91 (t, 2H, $J = 7.2$ Hz), 2.34 – 2.40 (m, 1H), 2.70 (t, 2H, $J = 6.8$ Hz), 3.69 – 3.72 (m, 1H), 7.21 (t, 1H, $J = 8$ Hz), 7.30 (t, 1H, $J = 8$ Hz), 7.40 (t, 1H, $J = 7.6$ Hz), 7.51 (t, 1H, $J = 7.6$ Hz), 7.71 (d, 1H, $J = 8.4$ Hz), 7.81 (d, 1H, $J = 8.4$ Hz), 8.09 (d, 1H, $J = 8.4$), 8.65 (s, 1H), 9.32 (d, 1H, $J = 8$ Hz); ^{13}C NMR (d_6 DMSO, 400 MHz) δ 10.03, 25.67, 27.27, 28.12, 44.18, 57.78, 108.33, 110.66, 110.69, 110.75, 110.80, 112.12, 114.43, 114.47, 117.50, 119.68, 122.35, 125.54, 129.37, 137.36, 140.77, 140.79, 155.45, 165.90, 169.63, 172.33; LCMS: calculated $[\text{M}+\text{H}]^+ = 411.21$, found = 411.32.



(S)-12-(4-aminobutyl)-7-benzyl-6,7,12,13-tetrahydro-5H-indolo[2,3-a]pyrrolo[3,4-c]carbazol-5-one (Star 19) ^1H NMR (d_6 DMSO, 400 MHz) δ 1.53 – 1.59 (m, 2H), 1.90 – 1.94 (m, 2H), 2.70 – 2.73 (m, 2H), 3.20 – 3.24 (m, 2H), 3.56 – 3.59 (m, 2H), 4.93 – 4.98 (m, 2H),

5.58 (s, 1H), 6.90 (d, 2H, $J = 8\text{Hz}$), 6.98 – 7.01 (m, 3H), 7.14 (t, 1H, $J = 8\text{Hz}$), 7.36 – 7.40 (m, 2H), 7.55 (t, 1H, $J = 8\text{Hz}$), 7.68 (d, 1H, $J = 8\text{Hz}$), 7.86 (d, 1H, $J = 8\text{Hz}$), 8.32 (d, 1H, $J = 8\text{Hz}$), 8.49 (s, 1H), 9.18 (d, 1H, $J = 8\text{Hz}$); ^{13}C NMR (d_6DMSO , 400 MHz) δ 26.14, 28.00, 31.36, 39.25, 44.21, 57.18, 82.56, 94.61, 110.88, 112.11, 114.66, 117.39, 119.51, 120.06, 120.77, 122.38, 122.56, 122.75, 125.51, 125.72, 125.98, 126.81, 128.31, 129.29, 130.14, 136.53, 137.13, 140.76, 140.83, 166.36, 172.00; LCMS: calculated $[\text{M}+\text{H}]^+ = 473.23$, found = 473.30.

Chapter 4 – Future Directions and Conclusions

Introduction

The combination of a repertoire of potent and selective inhibitors and robust methods for engineering functional AS alleles have enabled the application of this technique to nearly any kinase. The benefits of AS technology will be maximized if investigators from diverse scientific backgrounds are able to routinely apply this technique to address important questions in their respective fields. Thus, a significant future direction for our lab is to continue the dissemination of the tools and information necessary for others to use the AS technique. Another important goal will be to facilitate more widespread use of AS kinases *in vivo*. To address this, new inhibitors must be developed that retain potency and selectivity, but have enhanced PK properties. Finally, another direction in which our work will develop is the design of therapeutic kinase inhibitors that are based on structure-activity relationships we have identified in the course of studies with AS-kinase inhibitors. In this concluding chapter I describe preliminary work toward optimizing the *in vivo* properties of PP inhibitors to facilitate their use in mice. I also describe work towards developing a new statalog inhibitor that is a potent and extremely selective Flt3 kinase inhibitor and may serve as the basis for new therapeutic Acute Myeloid Leukemia (AML) drugs.

Optimizing the *in vivo* properties of PP inhibitors. Lourido *et al* recently reported that *Toxoplasma gondii* Calcium-Dependent Protein Kinase 1 (CDPK1) is essential for host-cell invasion by the eukaryotic parasite⁶¹. They also noted that CDPK1 unexpectedly contains a naturally occurring glycine gatekeeper residue making it sensitive to AS-kinase inhibitors such as 3MB-PP1. To address whether AS-kinase inhibitors might be used to target CDPK1 for the treatment of toxoplasmosis, the human disease caused by *T. gondii* infection, Sibley and co-workers sought to assess their efficacy in a mouse model

of infection. Thus, we initiated a collaboration to design new inhibitors with improved *in vivo* properties. Importantly, we hope these new compounds will also serve as tools for targeting AS kinases in experimental organisms such as mice and rats.

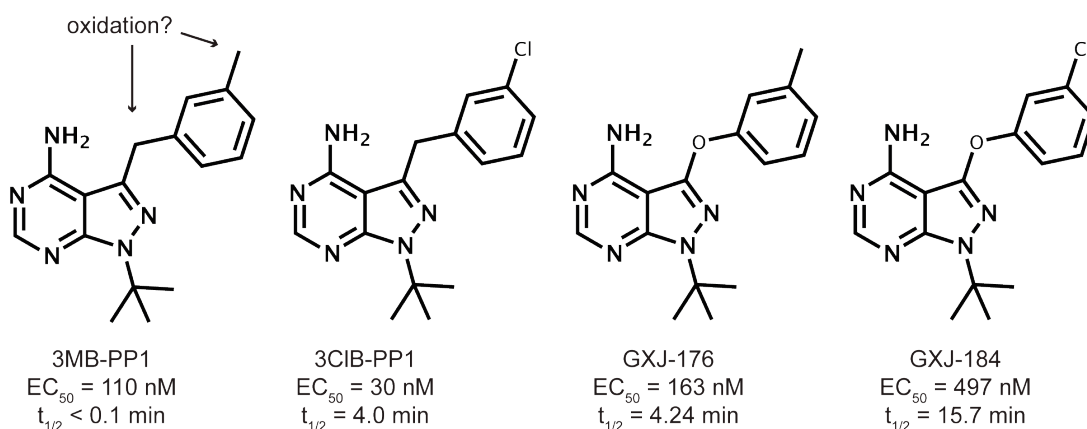


Figure 17. PP inhibitors designed to have enhanced metabolic stability and retain potency. EC_{50} values are for inhibition of parasite growth in host cells. Half-lives are for compound stability in the presence of rat liver microsomes.

We hypothesize that the two benzylic positions present in 3MB-PP1 may be susceptible to oxidation by P450 enzymes *in vivo*⁶². In previous work, we showed that oxidation at one of these positions reduces the potency of 3MB-PP1 toward CDPK1 and presumably against AS kinases as well⁶³. Most published reports using AS kinases *in vivo* have utilized 1NA-PP1, a PP inhibitor that does not have either of the problematic benzylic positions. However, 1NA-PP1 is not a potent inhibitor of CDPK1, does not target all AS kinases, and is the least selective commonly used AS-kinase inhibitor. Thus, we hoped to design new PP inhibitors lacking the problematic benzylic positions while retaining potency and selectivity for CDPK1 and diverse AS kinases.

We synthesized a panel of compounds based on the structure of 3MB-PP1 where we replaced the 3-methyl group with a chlorine atom (3CIB-PP1), the benzylic methylene position with an oxygen atom (GXJ-176), or combined both substitutions (GXJ-184). We then measured the stability of each compound in the presence of rat liver microsomes, a common technique for predicting drug metabolism *in vitro*. 3MB-PP1 levels decrease to

undetectable amounts at the first time point, indicating this compound is indeed very rapidly consumed in the presence of metabolic enzymes. As we predicted, replacement of either benzylic carbon is stabilizing, resulting in half-lives of 4.0 min for 3CIB-PP1 and 4.24 min for GXJ-176 (Figure 17). The removal of both positions yields a multiplicative increase in stability as GXJ-184 has a measured half-life of 15.7 min. Importantly all three new PP derivatives retain similar or greater potency (within ~ 5-fold) for inhibition of parasite growth in host cells (Figure 17).

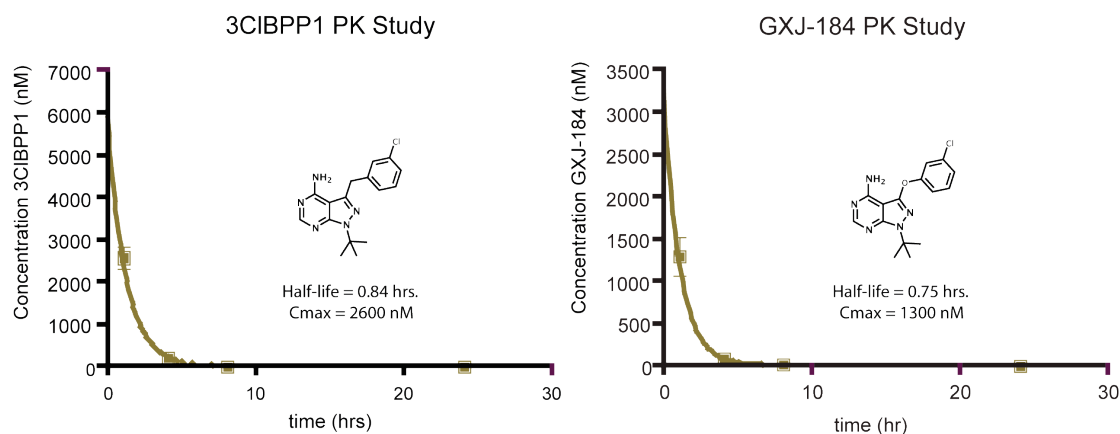


Figure 18. Serum half-life concentration in mice treated with 3CIB-PP1 or GXJ-184

Next, we sought to verify that the enhanced microsomal stability of our compounds is relevant *in vivo* and leads to an increase in sustained drug concentrations in blood serum of treated mice. We administered healthy mice with intraperitoneal injections of 20mg/kg 3CIB-PP1 or GXJ-184 and measured serum drug concentrations at 1hr, 4hrs, 8hrs, and 24hrs post-treatment. To our surprise there is very little difference between 3CIB-PP1 and GXJ-184 maximum serum concentrations or half-lives (Figure 18). In fact, 3CIB-PP1 actually achieved two-fold greater concentration than GXJ-184 despite a four-fold greater microsomal clearance rate.

Another unexplained observation is that 3MB-PP1 protects mice against *Toxoplasma gondii* infection despite its near-instantaneous clearance in rat liver microsomes⁶³. Thus, one of our future goals is to understand the lack of correlation between microsomal stability, *in vivo* stability, and efficacy in preventing infection in mice. One possibility is that the *in vivo* product of metabolized 3MB-PP1 is active against CDPK1. It is also possible that another property of the inhibitors, such as blood

plasma protein binding or blood-brain barrier penetration, is much more important than metabolic clearance *in vivo*. We will examine these possibilities and determine the most important properties for optimizing the activity of PP inhibitors *in vivo*. We hope these studies will lead to a potent and selective inhibitor of CDPK1 that can be used as a therapeutic treatment for toxoplasmosis as well as a chemical tool for studying AS kinases in mice.

Re-purposing staralogs as therapeutic Flt3 inhibitors. Acute Myeloid Leukemia (AML) is an extremely aggressive hematologic malignancy characterized by the abnormal growth of improperly differentiated myeloid progenitor cells⁶⁴. Mutations in the FMS-like Tyrosine Kinase 3 (Flt3) gene occur in approximately one quarter⁶⁵ of all AML patients and indicate a poor prognosis for both disease-free survival and overall survival⁶⁶. The most common Flt3 mutations associated with AML enhance Flt3 kinase activity either through disruption of the auto-inhibitory juxtamembrane (JM) domain by insertion of internal tandem duplications (ITD)⁶⁷ or by stabilization of the catalytically active kinase conformation⁶⁸. Furthermore, expression of Flt3-ITD is sufficient to induce a myeloproliferative disorder in a mouse bone marrow transplant model⁶⁹. Taken together, this evidence suggests Flt3 might serve as a therapeutic drug target for the treatment of AML.

A number of small molecule Flt3 kinase inhibitors have entered clinical trials as single agents or in combination therapy for the treatment of AML. These drugs include promiscuous kinase inhibitors such as PKC412 and Sunitinib, as well as more targeted molecules such as AC220. A major limitation of all known Flt3 inhibitors is the propensity for drug treatment to induce drug-resistant mutations in the Flt3 kinase domain^{70,71}. This observation suggests Flt3 signaling is critical for AML cell proliferation and that a repertoire of structurally diverse molecules may be important for overcoming the strong evolutionary pressure to develop resistance mutations. For example, resistance mutations in the Flt3 activation loop are thought to bias the conformation of the kinase towards the active state, thus reducing the potency of inhibitors such as AC220 that bind to the inactive conformation⁷⁰. However, different mutations have been identified that provide resistance against PKC412, which binds Flt3 in the active conformation⁷². Thus,

it is important that we identify a panel of diverse inhibitors that can be used sequentially, or in combination, to overcome the evolutionary pressure for AML cells to develop resistant Flt3 mutations.

Another weakness of current Flt3 inhibitors is that they all potently target c-Kit, a Type III RTK that plays a key role in normal hematopoiesis. In the absence of Flt3, c-Kit is essential for the development of normal white blood cells in mice⁷³. In the clinic, potent Flt3 inhibitors have been shown to reduce the levels of undifferentiated cancer cells, however, they fail to allow the regeneration of healthy white blood cells that are required for complete remission^{74,75}. We hypothesize this may be due to inadvertent inhibition of c-Kit in combination with the on-target inhibition of Flt3 kinase. Thus, in the context of therapeutic Flt3 inhibition we suggest that c-Kit is an anti-target whose inhibition must be avoided. To make this possible we sought to identify inhibitor scaffolds that retained potency against Flt3 but were inactive toward c-Kit.

Staralogs are potent Flt3 inhibitors

We previously demonstrated that C7-modified staralogs are extremely selective inhibitors of engineered AS kinases but do not potently inhibit any known WT human kinases. However, we also observed that **Star 12** (C7-*iso*-butyl) weakly inhibited Flt3 (41% inhibition) and the oncogenic mutant Flt3 D835Y (55% inhibition) at a concentration of 1 μ M (Appendix 3). Importantly, **Star 12** did not exhibit any significant activity against other Type III receptor tyrosine kinases (RTKs), including the important anti-target c-Kit. One notable difference between Flt3 and all other Type III RTKs is that Flt3 possesses a phenylalanine gatekeeper whereas other Type III RTKs have threonine or leucine residues. We hypothesized that the planar benzene ring of the phenylalanine side chain might rotate to accommodate binding of staralogs with bulky C7 substituents. Thus we asked if we could identify a staralog with enhanced potency and selectivity for Flt3 over c-Kit by exploiting the unique complementarity of C7 modified staralogs and the Flt3 ATP-binding pocket.

We measured IC₅₀ values for a panel of staralogs against Flt3 and discovered that several were modestly potent having IC₅₀ values in the low micromolar range. In particular, staralogs with smaller C7 groups such as isopropyl (**Star 6**) and ethyl (**Star 8**) had IC₅₀ values of ~ 2 μM. To identify more potent inhibitors we synthesized several new molecules bearing C7 methyl groups and either N12-H (**Star 22**), N12-butylamine (**Star 23**) or N12-butanol (**Star 26**) substituents. We included the N12 substitutions because we previously observed that polar groups at this position enhance potency against AS kinase by forming a hydrogen bond interaction with a conserved asparagine residue (Src Asn391, Figure 12). As predicted, all three compounds were significantly more potent with **Star 23** having an IC₅₀ of 82 nM, while **Star 23** and **Star 26** had IC₅₀ values of 14 nM and 11 nM, respectively. Thus, we applied structure-activity relationships that we identified in the course of developing AS-kinase inhibitors to rapidly generate potent inhibitors of Flt3 kinase.

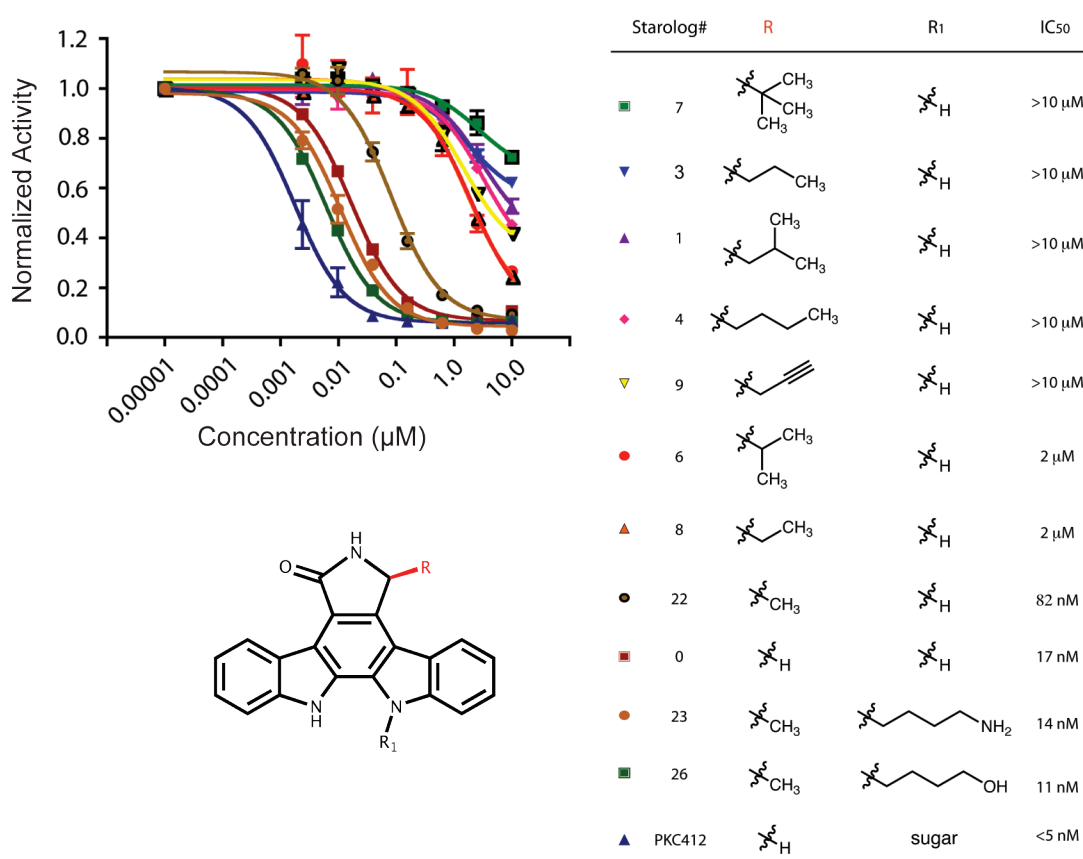


Figure 19. Dose-response curves and IC₅₀ values for staralogs against Flt3 kinase.

Star 23 is a potent Flt3 inhibitor in cells

To determine if **Star 23** is a potent inhibitor of Flt3 in cells we measured the ability of **Star 23** to inhibit the proliferation of IL3-dependent Ba/F3 cells and IL3-independent Ba/F3 cells driven by Flt3-ITD or Flt3 D835Y (Figure 20A). As we hoped, **Star 23** inhibited the proliferation of Ba/F3 cells dependent on Flt3 signaling, but showed very little activity against the parental IL3-dependent cells. To further verify this activity was due to on-target Flt3 inhibition we prepared lysates from the **Star 23** – treated Ba/F3 Flt3-ITD cells and probed Flt3 auto-phosphorylation. As we expected, phospho-Flt3 levels decreases sharply at ~300 nM, near the IC₅₀ of the proliferation assay, suggesting inhibition of cell growth is due to Flt3 inhibition.

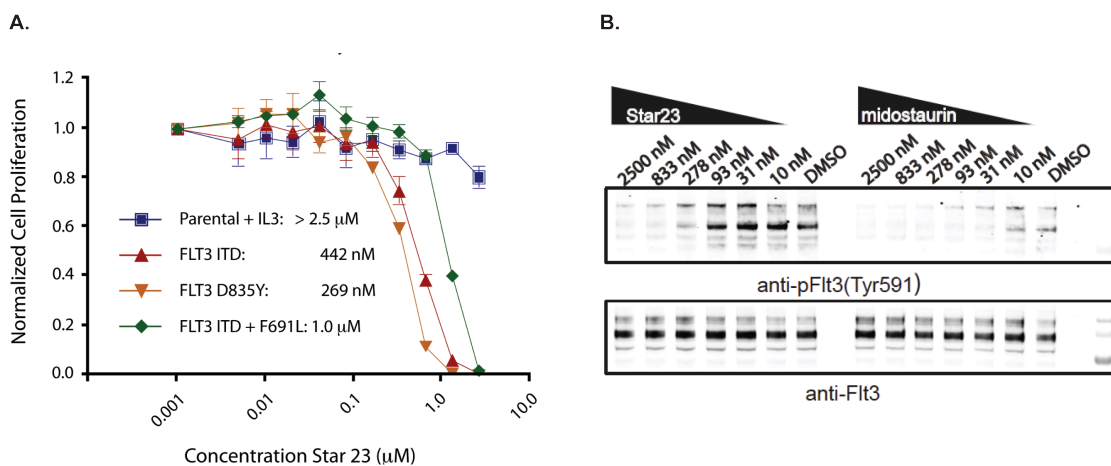


Figure 20. Star 23 activity against Flt3-driven Ba/F3 cells (A) Inhibition of Ba/F3 cell proliferation by Star 23 (B) Western blot of pFlt3 in Flt3-ITD Ba/F3 cells treated with Star 23 or midostaurin (PKC412).

Star 23 selectively targets human AML cells over Kit or Bcr-Abl driven cell lines. A

primary motivation to develop a new Flt3 inhibitor is to identify a new therapeutic that avoids inhibition of the anti-target c-Kit and thereby allows recovery of normal white blood cells in AML patients. The clinical compound PKC412 is a potent Flt3 inhibitor but also targets c-Kit, albeit less potently (7 to 55 – fold selectivity, Figure 21).

Additionally, the PKC412 metabolic product CPG52421 is a major species *in vivo* and has even worse selectivity for (2 to 7 – fold, Figure 21). Unfortunately, CPG52421 represents ~90% of the total amount of PKC412 and its metabolic byproducts *in vivo*^{74,76}. Thus, the most active pharmacological component in PKC412-treated patients has very little selectivity for Flt3 over c-Kit. In contrast, we observed 17 to 47 – fold selectivity for **Star 23** – mediated inhibition of Flt3-driven AML cell lines over c-Kit driven HMC1.1 cells (Figure 21). Thus, we anticipate the greater selectivity of **Star 23** for Flt3 over c-Kit will allow suppression of aberrant Flt3 signaling while not affecting c-Kit signaling essential for proper development of healthy white blood cells. We hope to test this hypothesis directly by measuring the ability of bone marrow colonies to form in the presence of **Star 23** at concentrations required to abrogate Flt3 signaling.

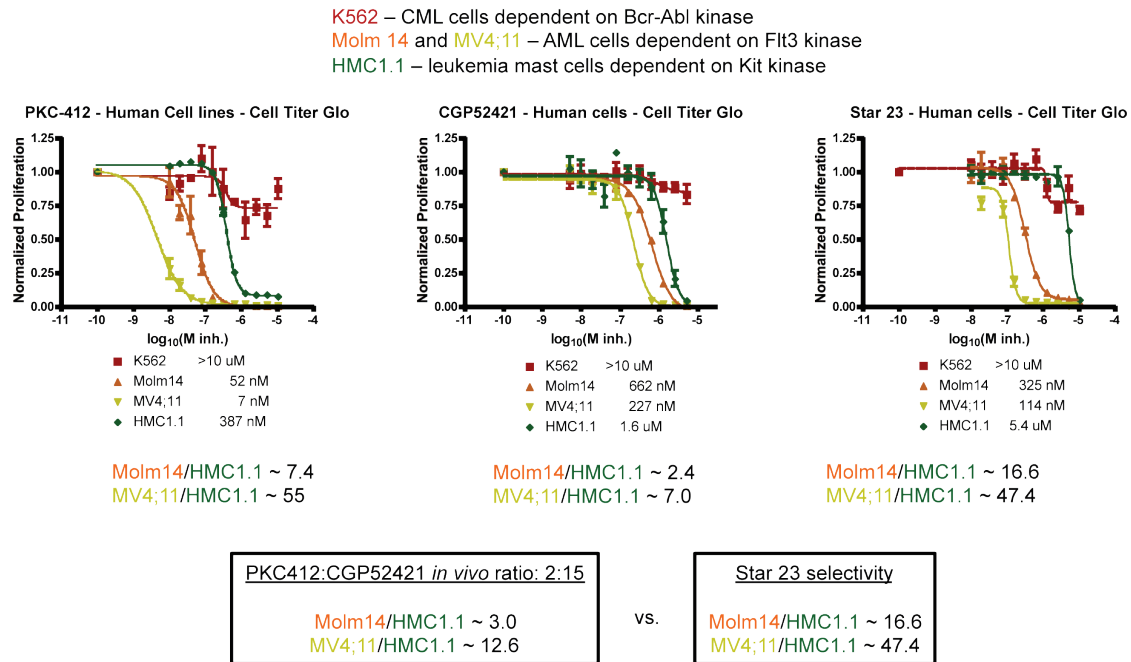
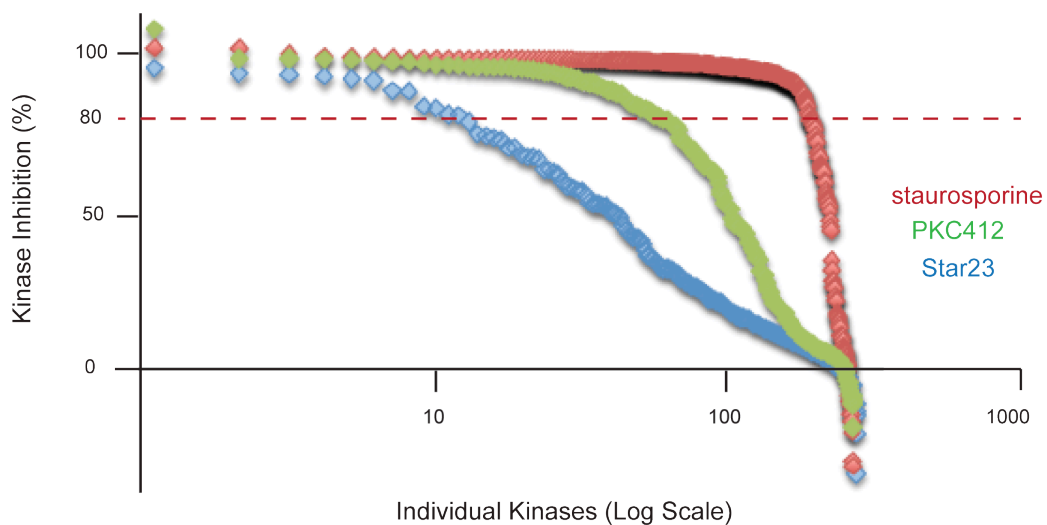


Figure 21. Dose-dependent proliferation of leukemia cell lines in the presence of PKC412, CPG52421, or **Star 23**. Proliferation of Molm14 and MV4;11 cells is driven by aberrant Flt3 signaling. Proliferation of K562 and HMC1.1 is driven by Br-Abl and Kit signaling, respectively.

Star 23 is extremely selective for Flt3 over other human kinases

To determine if the smaller C7 substituent of **Star 23** retained similar selectivity to other staralogs, we screened it against a panel of 308 human kinases (Figure 22A). **Star 23** was extremely selective and only inhibited >80% activity of 12 kinases (including Flt3 and Flt3D835Y) at a concentration of 500 nM. By comparison, clinical Flt3 inhibitors PKC412 and sunitinib each inhibit >80% activity of 63 and 43 WT kinases, respectively⁴². Importantly **Star 23** did not inhibit other kinases, such as c-Kit and Pdgfr, which modulate hematopoiesis. Taken together our results demonstrate that the C7-methyl group of **Star 23** allows targeting of Flt3, but prevents binding to nearly all other human kinases. Additionally, we observed that the only tyrosine kinases identified in our screen contain unusual phenylalanine gatekeepers. Although it remains to be more fully investigated, we hypothesize that C7-staralogs allow specific targeting of tyrosine kinases with phenylalanine gatekeepers. These results give confidence that **Star 23** or a similar molecule may represent a more selective Flt3 inhibitor and this selectivity may contribute to increased therapeutic efficacy.

A.



B.

Kinase	% Inhibition	Gatekeeper	Class
CaMKIID	81	Phe	CAMK
Flt3	95	Phe	TK
Flt3 D835Y	92	Phe	TK
MELK	93	Leu	CAMK
TrkA	79	Phe	TK
TrkB	81	Phe	TK
TrkC	94	Phe	TK
Pkd1	94	Met	CAMK
Pkd2	97	Met	CAMK
Pkd3	84	Met	CAMK
Rsk3	83	Leu	CAMK
Mst1	89	Met	STE
Mst2	89	Met	STE

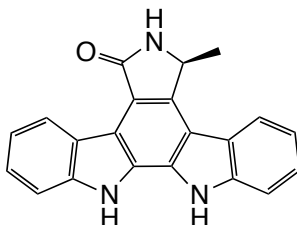
Figure 22. Selectivity of **Star 23** (A) Kinase inhibition profile of **Star 23** with PKC412 and staurosporine included for comparison. (B) List of the kinase name, % inhibition, gatekeeper and phylogeny of each of the thirteen kinases most potently inhibited by **Star 23**.

Conclusion

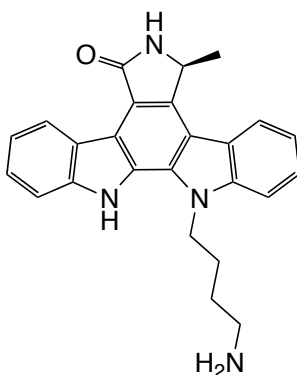
In our work to develop more efficacious AS-kinase inhibitors we often focused on developing more selective molecules that do not target WT kinases. However, our future work will involve exploiting the inherent sensitivity of Flt3 for indolocarbazoles to develop a potent Flt3 inhibitor as a potential therapeutic for the treatment of AML. A key feature of this strategy is that C7-substituents allow for molecules that retain potency against Flt3 but dial out activity against the AML anti-target c-Kit. Additionally, we will also work to optimize the PK properties of PP inhibitors to allow for *in vivo* targeting of CDPK1 for the prevention toxoplasmosis. Finally, these optimized PP inhibitors will expand our ability to use AS technology in mouse models of human disease. This advance will greatly aid in the understanding of developmental biology, behavioral processes, and will help in the validation of therapeutic drug targets.

Experimental Methods

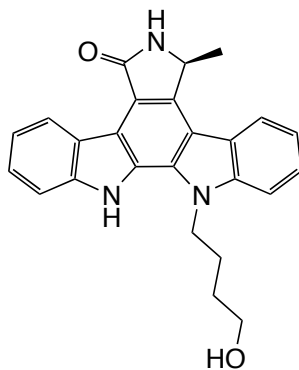
Compound Characterization



(S)-7-methyl-6,7,12,13-tetrahydro-5H-indolo[2,3-a]pyrrolo[3,4-c]carbazol-5-one (Star 22) ^1H NMR (d_6 DMSO, 400 MHz) δ 1.61 (d, 3H, $J = 4\text{Hz}$), 5.27 (q, 1H, $J = 8\text{Hz}$), 7.20 (t, 1H, $J = 8\text{Hz}$), 7.29 (t, 1H, $J = 8\text{Hz}$), 7.45 (t, 1H, $J = 8\text{Hz}$), 7.69 (d, 1H, $J = 8\text{Hz}$), 7.77 (d, 1H, $J = 8\text{Hz}$), 8.13 (d, 1H, $J = 8\text{Hz}$), 8.51 (s, 1H), 9.19 (d, 1H, $J = 8\text{Hz}$), 11.26 (s, 1H), 11.51 (s, 1H); ^{13}C NMR (d_6 DMSO, 400 MHz) δ 21.32, 52.62, 112.01, 112.69, 114.29, 116.17, 118.96, 119.61, 120.59, 122.32, 122.37, 122.72, 123.49, 125.60, 125.74, 125.95, 126.17, 128.76, 139.22, 139.87, 140.05, 171.88; LCMS: calculated $[\text{M}+\text{H}]^+ = 326.12$, found = 326.3.



(S)-12-(4-aminobutyl)-7-methyl-6,7,12,13-tetrahydro-5H-indolo[2,3-a]pyrrolo[3,4-c]carbazol-5-one (Star 23) ^1H NMR (d_6 DMSO, 400 MHz) δ 1.51 – 1.56 (m, 2H), 1.60 (d, 3H, $J = 4\text{Hz}$), 1.86 – 1.95 (m, 2H), 2.71 (t, 2H, $J = 8\text{Hz}$), 4.94 (t, 2H, $J = 6\text{Hz}$), 5.29 (q, 1H, $J = 8\text{Hz}$), 7.20 (t, 1H, $J = 6\text{Hz}$), 7.32 (t, 1H, $J = 8\text{Hz}$), 7.40 (t, 1H, $J = 8\text{Hz}$), 7.51 (t, 1H, $J = 8\text{Hz}$), 7.71 (d, 1H, $J = 8\text{Hz}$), 7.81 (d, 1H, $J = 8\text{Hz}$), 8.15 (d, 1H, $J = 8\text{Hz}$), 8.54 (s, 1H), 9.32 (d, 1H, $J = 8\text{Hz}$); ^{13}C NMR (d_6 DMSO, 400 MHz) δ 21.32, 26.60, 28.15, 30.41, 44.15, 52.48, 110.75, 112.11, 114.40, 117.61, 119.03, 119.63, 120.68, 122.24, 122.51, 122.90, 125.46, 125.66, 125.84, 126.01, 128.74, 129.36, 139.24, 140.76, 171.74; LCMS: calculated $[\text{M}+\text{H}]^+ = 397.20$, found = 397.30.



(S)-12-(4-hydroxybutyl)-7-methyl-6,7,12,13-tetrahydro-5H-indolo[2,3-a]pyrrolo[3,4-c]carbazol-5-one (Star 26) ^1H NMR (d_6 DMSO, 400 MHz) δ 1.47 (quin, 2H, $J = 8\text{Hz}$), 1.61 (d, 3H, 3H), 3.36 – 3.40 (m, 2H), 4.65 (br, 1H), 4.93 (t, 2H, $J = 6\text{Hz}$), 5.29 (q, 1H, $J = 8\text{Hz}$), 7.21 (t, 1H, $J = 8\text{Hz}$), 7.32 (t, 1H, $J = 8\text{Hz}$), 7.42 (t, 1H, $J = 8\text{Hz}$), 7.51 (t, 1H, $J = 8\text{Hz}$), 7.70 (d, 1H, $J = 8\text{Hz}$), 7.81 (d, 1H, $J = 8\text{Hz}$), 8.15 (d, 1H, $J = 8\text{Hz}$), 8.54 (s, 1H), 9.32 (d, 1H, $J = 8\text{Hz}$), 11.61 (s, 1H); ^{13}C NMR (d_6 DMSO, 400 MHz) δ 21.30, 27.87, 29.75, 44.49, 52.49, 61.17, 110.80, 112.04, 114.43, 117.54, 118.96, 119.67, 120.62, 122.19, 122.50, 122.88, 125.47, 125.66, 125.89, 126.02, 129.34, 139.32, 140.65, 140.85, 171.74; LCMS: calculated $[\text{M}+\text{H}]^+ = 398.18$, found = 398.28.

Appendices

Appendix 1 – Tables of AS kinases reported in peer-reviewed publications

Information provided in tables: organism, kinase, reference, gatekeeper mutation, stabilizing suppressor mutation (red), inhibitor sensitizing mutation (green), concentration and identity of inhibitor used.

<i>S. Pombe</i> Kinases			
15			
Kinase	Ref	GK	Inhib.
Hhp1	17	M84G	1NM-PP1
Cdc2	17	F84G	0.5µM 1NM-PP1
Cdk9	17	T120G	10µM1NM-PP1
Cka1	17	F117G	5µM 9Ch-ANPUR
Crk1	17	L87G	30µM 3BrB-PP1
Ksg1	17	L177G	5µM 1NM-PP1
Nak1	17	M77G	40µM 3BrB-PP1
Orb6	17	M170G	5µM 3BrB-PP1
Pat1	17	L95A	10µM 1NM-PP1
Plo1	17	L117G	10µM 3BrB-PP1
Ppk37	17	M537G	30µM 1NM-PP1
Prp4	17	F238A	30µM 3BrB-PP1
Shk1	17	M460A	20µM 3BrB-PP1
Sid2	17	M285G	40µM 3BrB-PP1
Ark1	17,77	L166A S229A	5µM 1NM-PP1

<i>S. Cerevisiae</i> Kinases			
26			
Kinase	Ref	GK	Inhib.
Pho85	78,79	F82G	5uM 1NA-PP1
Elm1	80	T200G	25uM 1NM-PP1
Kin28	81	L83G	6μM 1NA-PP1
Srb10	81	Y236G	24μM 1NA-PP1
Cla4	27	M640A & T710A	1NM-PP1
Cdc15	82	L99G	10μM 1NM-PP1
Cdc28	4	F88G	1NM-PP1
Mps1	83	M516G	1NM-PP1
Ipl1	84	M181G & T244A	1NA-PP1
Ime2	85	M146G	1NA-PP1
Mek1	86,87	Q247G	1NA-PP1
Ire1	19	L745G	1NM-PP1
Prk1	88	M108G & C175A	40μM 1NA-PP1
Apg1	89	M102A	1NA-PP1
Cbk1	90	M429A	1NA-PP1
Hog1	91,92	T100G	1NM-PP1
Fus3	4	Q93G	1NM-PP1
Tpk1	93	M164G	1NM-PP1
Tpk2	93	M147G	1NM-PP1
Tpk3	93	M165G	1NM-PP1
Sch9	94	T492G	1NM-PP1
Tos3	95	L135G	2,3-dMB-PP1
Cdc7	96	L120A & V181A	15μM PP1
Cdc5	7,97	L158G, C96V	CMK
Snf1	98	I132G	2NM-PP1
Bur1	26	L149G	6μM 3MB-PP1

Mammalian Tyr Kinases

18

Kinase	Ref	GK	Conc. Used μM	Inhib.
v-Src	6	I338G	0.25	1NA-PP1
CSK	99	T266G	10	3IB-PP1
Fyn	4	T339G	0.005 (in vitro)	1NA-PP1
Lck	100	T316G	10	1NA-PP1
TrkA	101	F592A	0.1	1NM-PP1
TrkB	101	F616A	0.1	1NM-PP1
TrkC	101	F617A	0.1	1NM-PP1
Bcr-Abl	20	T316A	2	1NA-PP1
v-ErbB	102	T210A	2	1NA-PP1
Jak1	103	M956G	40	1NM-PP1
Jak3	103	M902G	40	1NM-PP1
Zap70	25	M414A C405V	10	3MB-PP1
Syk	15	M442A M429L R428Q	6	2,3DMB-PP1
EphB1	35	T697G	0.25	1NA-PP1
EphB2	35	T699A	0.25	1NA-PP1
EphB3	35	T706A	0.25	1NA-PP1
Ret	34	V805A	0.1	1NA-PP1
Yes	104	T346G	10	1NM-PP1

Mammalian Ser/Thr Kinases					
21					
Kinase	Ref	GK	supressor	Conc. used in cells (μ M)	Inhib.
Cdk1	105	F80G	n	0.6	1NM-PP1
Cdk2	106	F80G	n	10	3MB-PP1
Cdk7	107	F91G	n	5	3MB-PP1
PKA α	108	M120A	n	10	1NM-PP1
PKA β	108	M120G & K46I	Y	10	1NM-PP1
PKC ϵ	109	M486A	n	1	1NA-PP1
GRK2	7,110	L271G & C221V	Y	2.5	1NA-PP1
JNK1	111	M108G & L168A	Inhib	1	1NM-PP1
JNK2	112	M108G	n	10	1NM-PP1
CaMIK α	113,114	F89G	n	5	1NM-PP1
Irel α	115	I642G	n	5	1NM-PP1
Plk1	116,117	C67V & L130G	Y	10	3MB-PP1
Mps1	118,119	M602A	n	5	3MB-PP1
Lkb	120	M129G	n	10	1NM-PP1
Akt1	21,22	M227G	n	2.5	3IB-PP1, PrIDZ
Akt2	21,22	M225G	n	2.5	PrIDZ
Akt3	21,22	M229G	n	2.5	PrIDZ
Pdk1	121	L159G	n	2	Cpac-BX
Mekk1	7	I1304G, C1238V	Y	N.D.	N.D.
Pkd1	41	M665A	n	1	1NA-PP1

Plant Kinases			
<i>3</i>			
Kinase	Ref	GK	Inhib.
MPK4	122	Y124G	100µM 1NA-PP1
Pto	7,123	Y114A, L681I	10µM 1NM-PP1 10 µM 3MB-PP1
LeMPK3	124	T123A	1µM Bn-PP1(in vitro)

<i>C. Elegans</i>			
<i>1</i>			
Kinase	Ref	GK	Inhib.
Sad1	125	L123A	33µM 1NA-PP1

Appendix 2 – Profiling of PP inhibitors

Legend

< 40% Inhibition
40% - 80% Inhibition
≥ 80% Inhibition

			<u>Conc. (nM)</u>				
		<u>Compound</u>	1000	1000	1000	1000	1000
			1NAPP1	1NMPP1	3MBPP1	3IB-PP1 (17)	3MSB-PP1 (18)
ABL1	Activity	Km app	26	14	16	-6	-10
ABL1 E255K	Activity	Km app	24	14	17	8	8
ABL1 G250E	Activity	Km app	18	9	13	24	19
ABL1 T315I	Activity	Km app	8	5	8	-2	-2
ABL1 Y253F	Activity	Km app	29	14	18	19	13
ABL2 (Arg)	Activity	Km app	19	16	13	5	3
ACVR1 (ALK2)	Binding					20	13
ACVR1B (ALK4)	Activity	Km app	65	-3	5	25	9

ACVR2B	Binding							
ADRBK1 (GRK2)	Activity	Km app	3	3	-1	12	9	
ADRBK2 (GRK3)	Activity	Km app	6	-3	-6	3	3	
AKT1 (PKB alpha)	Activity	Km app	0	2	-1	-6	-6	
AKT2 (PKB beta)	Activity	Km app	-1	-2	0	6	6	
AKT3 (PKB gamma)	Activity	Km app	9	1	1	2	1	
ALK	Activity	Km app	1	3	-1	5	8	
AMPK A1/B1/G1	Activity	Km app	2	1	-2	-18	-1	
AMPK A2/B1/G1	Activity	Km app	9	4	8	10	12	
AURKA (Aurora A)	Activity	Km app	6	0	4	0	-2	
AURKB (Aurora B)	Activity	Km app	5	7	3	5	8	
AURKC (Aurora C)	Activity	Km app	6	2	6	-10	-12	
AXL	Activity	Km app	4	2	3	2	-1	
BLK	Activity	Km app	38	16	15	12	11	
BMPR1A (ALK3)	Binding							
BMX	Activity	Km app	26	52	25	41	47	
BRAF	Binding						14	12
BRAF	Activity	100	29	19	26	8	11	
BRAF V599E	Binding						9	2
BRAF V599E	Activity	100	17	9	32	12	11	
BRSK1 (SAD1)	Activity	Km app	9	8	7	2	1	
BTK	Activity	Km app	49	61	39	19	20	
CAMK1 (CaMK1)	Activity	10	-16	-20	12	-17	-21	
CAMK1 (CaMK1)	Activity	100						
CAMK1D (CaMKI delta)	Activity	Km app	-2	-5	-5	-1	3	

CAMK2A (CaMKII alpha)	Activity	Km app	2	1	-3	12	14
CAMK2B (CaMKII beta)	Activity	Km app	14	15	9	19	21
CAMK2D (CaMKII delta)	Activity	Km app	4	0	-2	15	15
CAMK4 (CaMKIV)	Activity	Km app	-6	10	-5	-2	-1
CAMKK1 (CAMKKA)	Binding					9	6
CAMKK2 (CaMKK beta)	Binding					1	1
CDC42 BPA (MRCKA)	Activity	Km app	-2	-2	5	6	4
CDC42 BPB (MRCKB)	Activity	Km app	9	2	3	2	2
CDK1/cyclin B	Activity	Km app	2	2	3	8	10
CDK2/cyclin A	Activity	Km app	8	9	11	2	1
CDK5/p25	Activity	Km app	2	2	3	6	7
CDK5/p35	Activity	Km app	0	-2	2	10	16
CDK7/cyclin H/MNAT1	Activity	Km app	-5	14	-15	12	8
CDK8/cyclin C	Binding					12	16
CDK9/cyclin K	Binding					4	3
CDK9/cyclin T1	Activity	Km app	3	-2	-4	4	8
CHEK1 (CHK1)	Activity	Km app	3	6	4	-6	-6
CHEK2 (CHK2)	Activity	Km app	12	7	9	-3	-3
CHUK (IKK alpha)	Activity	10	4	-20	-12		
CHUK (IKK alpha)	Activity	Km app				3	-1
CLK1	Activity	Km app	7	7	7	13	12
CLK2	Activity	Km app	10	10	14	32	38
CLK3	Activity	Km app	4	7	6	1	5
CLK4	Binding						
CSF1R (FMS)	Activity	Km	40	28	20	30	19

		app					
CSK	Activity	Km app	28	29	17	28	27
CSNK1A1 (CK1 alpha 1)	Activity	Km app	12	1	13	18	17
CSNK1D (CK1 delta)	Activity	Km app	38	14	70	90	89
CSNK1E (CK1 epsilon)	Activity	Km app	91	96	85	100	100
CSNK1G1 (CK1 gamma 1)	Activity	Km app	0	2	-2	6	3
CSNK1G2 (CK1 gamma 2)	Activity	Km app	-2	-1	-2	14	11
CSNK1G3 (CK1 gamma 3)	Activity	Km app	0	2	2	6	4
CSNK2A1 (CK2 alpha 1)	Activity	Km app	6	7	3	5	5
CSNK2A2 (CK2 alpha 2)	Activity	Km app	4	3	1	4	3
DAPK1	Activity	Km app	-3	12	3	2	-1
DAPK3 (ZIPK)	Activity	Km app	0	2	-1	2	-3
DCAMKL2 (DCK2)	Activity	Km app	2	1	-1	7	9
DDR1	Binding						
DDR2	Binding					6	4
DMPK	Binding					6	7
DNA-PK	Activity	Km app					
DYRK1A	Activity	Km app	4	2	3	-3	-4
DYRK1B	Activity	Km app	12	11	10	-10	-9
DYRK3	Activity	Km app	0	2	0	3	3
DYRK4	Activity	Km app	2	2	1	1	2
EEF2K	Activity	Km app	2	3	1	20	18
EGFR (ErbB1)	Activity	Km app	28	24	36	56	65
EGFR (ErbB1) L858R	Activity	Km app	40	29	34	48	27

EGFR (ErbB1) L861Q	Activity	Km app	34	17	30	34	20
EGFR (ErbB1) T790M	Activity	Km app	48	38	44	66	81
EGFR (ErbB1) T790M L858R	Activity	Km app	65	53	56	66	55
EPHA1	Activity	Km app	93	83	71	48	47
EPHA2	Activity	Km app	75	43	44	22	13
EPHA3	Binding						
EPHA3	Activity	Km app	45	18	21	12	4
EPHA4	Activity	Km app	83	43	46	36	25
EPHA5	Activity	Km app	86	56	61	40	21
EPHA7	Binding					6	8
EPHA8	Activity	Km app	67	51	40	39	24
EPHB1	Activity	Km app	63	44	43	34	27
EPHB2	Activity	Km app	78	58	58	38	25
EPHB3	Activity	Km app	48	35	52	31	14
EPHB4	Activity	Km app	73	62	63	45	25
ERBB2 (HER2)	Activity	Km app	9	19	25	21	32
ERBB4 (HER4)	Activity	Km app	10	38	35	63	85
FER	Activity	Km app	29	24	15	12	15
FES (FPS)	Activity	Km app	20	13	4	15	15
FGFR1	Activity	Km app	13	8	17	7	7
FGFR2	Activity	Km app	16	10	12	11	9
FGFR3	Activity	Km app	1	4	-3	14	15
FGFR3 K650E	Activity	Km app	5	2	4	25	22

FGFR4	Activity	Km app	14	-2	5	20	15
FGR	Activity	Km app	71	42	55	52	33
FLT1 (VEGFR1)	Activity	Km app	5	5	4	10	9
FLT3	Activity	Km app	13	12	20	28	35
FLT3 D835Y	Activity	Km app	16	14	-2	1	13
FLT4 (VEGFR3)	Activity	Km app	9	8	20	21	17
FRAP1 (mTOR)	Activity	Km app	0	0	-3	6	-5
FRK (PTK5)	Activity	Km app	89	47	74	60	33
FYN	Activity	Km app	45	37	32	37	39
GRK4	Activity	Km app	-10	-9	-12	-3	-5
GRK5	Activity	Km app	-4	1	-5	4	3
GRK6	Activity	Km app	-5	-4	-6	1	-1
GRK7	Activity	Km app	-4	-6	-6	-2	-3
GSG2 (Haspin)	Activity	Km app				28	49
GSK3A (GSK3 alpha)	Activity	Km app	5	6	2	9	11
GSK3B (GSK3 beta)	Activity	Km app	4	5	7	-3	-3
HCK	Activity	Km app	59	31	31	17	11
HIPK1 (Myak)	Activity	Km app	1	0	-1	5	5
HIPK2	Activity	Km app				4	5
HIPK3 (YAK1)	Activity	Km app					
HIPK4	Activity	Km app	9	9	8	12	10
IGF1R	Activity	Km app	4	7	2	11	10
IKBKB (IKK beta)	Activity	Km	4	5	4	5	6

		app						
		Km app						
IKBKE (IKK epsilon)	Activity	Km app	1	-2	-4	-1	-6	
INSR	Activity	Km app	7	6	4	4	4	
INSRR (IRR)	Activity	Km app	-6	-5	-6	24	21	
IRAK1	Activity	Km app				7	11	
IRAK4	Activity	Km app	5	2	4	-3	-2	
ITK	Activity	Km app	6	4	3	6	4	
JAK1	Activity	Km app	0	-6	-3	5	3	
JAK2	Activity	Km app	-2	-1	4	-8	-10	
JAK2 JH1 JH2	Activity	Km app	3	4	4	-3	-2	
JAK2 JH1 JH2 V617F	Activity	Km app	-6	-5	-7	7	6	
JAK3	Activity	Km app	-6	-6	-5	3	8	
KDR (VEGFR2)	Activity	Km app	24	21	41	25	21	
KIT	Activity	Km app	38	24	21	-4	-5	
KIT T670I	Activity	Km app	7	5	10	-2	-1	
KIT V654A	Binding					3	6	
LCK	Activity	Km app	52	35	36	24	20	
LIMK1	Binding					0	-5	
LIMK2	Binding					-3	1	
LRRK2	Activity	Km app	13	-7	5	-13	3	
LRRK2 G2019S	Activity	Km app	19	10	1	4	8	
LTK (TYK1)	Activity	Km app	-2	1	-2	0	1	
LYN A	Activity	Km app	82	55	59	49	39	
LYN B	Activity	Km app	81	55	55	43	33	

MAP2K1 (MEK1)	Binding				22	38	
MAP2K1 (MEK1)	Activity	100	5	15	9	1	4
MAP2K1 (MEK1) S218D S222D	Binding				18	28	
MAP2K2 (MEK2)	Binding				12	21	
MAP2K2 (MEK2)	Activity	100	14	8	8	-4	0
MAP2K3 (MEK3)	Binding				16	14	
MAP2K6 (MKK6)	Binding				7	10	
MAP2K6 (MKK6)	Activity	100	4	4	3	-11	-16
MAP2K6 (MKK6) S207E T211E	Binding				17	9	
MAP3K10 (MLK2)	Binding				11	13	
MAP3K11 (MLK3)	Binding				0	1	
MAP3K14 (NIK)	Binding				-1	-2	
MAP3K2 (MEKK2)	Binding				31	15	
MAP3K3 (MEKK3)	Binding				62	35	
MAP3K5 (ASK1)	Binding				6	5	
MAP3K7/MAP3K7IP1 (TAK1-TAB1)	Binding				2	4	
MAP3K8 (COT)	Activity	100	14	10	12	26	22
MAP3K9 (MLK1)	Activity	Km app	1	3	0	-6	0
MAP4K2 (GCK)	Activity	Km app	7	2	4	4	6
MAP4K4 (HGK)	Activity	Km app	92	56	28	8	1
MAP4K5 (KHS1)	Activity	Km app	69	31	38	26	30
MAPK1 (ERK2)	Activity	Km app	4	6	3	2	0
MAPK10 (JNK3)	Binding				21	18	
MAPK10 (JNK3)	Activity	100	4	5	6	-6	-7
MAPK11 (p38 beta)	Activity	Km app	12	15	16	14	15
MAPK12 (p38 gamma)	Activity	Km app	1	2	2	6	8
MAPK13 (p38 delta)	Activity	Km app	2	3	4	11	11
MAPK14 (p38 alpha)	Activity	100	15	26	24	7	12

MAPK14 (p38 alpha) Direct	Activity	Km app	[Hatched]			-1	-1
MAPK3 (ERK1)	Activity	Km app	6	4	5	9	7
MAPK8 (JNK1)	Binding		[Hatched]			1	3
MAPK8 (JNK1)	Activity	100	-7	-11	-5	-7	3
MAPK9 (JNK2)	Binding		[Hatched]			15	18
MAPK9 (JNK2)	Activity	100	0	6	4	9	3
MAPKAPK2	Activity	Km app	-2	0	-1	-6	-6
MAPKAPK3	Activity	Km app	2	-1	3	-1	-1
MAPKAPK5 (PRAK)	Activity	Km app	-2	0	0	1	1
MARK1 (MARK)	Activity	Km app	6	4	3	10	10
MARK2	Activity	Km app	11	8	7	14	13
MARK3	Activity	Km app	[Hatched]			1	-12
MARK4	Activity	Km app	[Hatched]			-2	-1
MATK (HYL)	Activity	Km app	-2	0	-3	13	10
MELK	Activity	Km app	21	17	16	16	16
MERTK (cMER)	Activity	Km app	5	5	7	21	19
MET (cMet)	Activity	Km app	-2	-1	0	3	3
MET M1250T	Activity	Km app	-2	-5	-4	3	3
MINK1	Activity	Km app	89	52	37	40	28
MKNK1 (MNK1)	Activity	Km app	[Hatched]				
MKNK2 (MNK2)	Binding		[Hatched]				
MLCK (MLCK2)	Binding		[Hatched]			6	4
MST1R (RON)	Activity	Km app	2	2	3	-2	-2
MST4	Activity	Km app	25	13	13	1	3
MUSK	Activity	Km	-3	2	-2	28	29

		app						
MYLK (MLCK)	Binding						2	1
		Km						
MYLK2 (skMLCK)	Activity	app	0	5	-2	-3	3	
		Km						
NEK1	Activity	app	9	8	10	-8	1	
		Km						
NEK2	Activity	app	8	6	9	5	3	
		Km						
NEK4	Activity	app	3	3	3	8	5	
		Km						
NEK6	Activity	app	8	3	0	3	3	
		Km						
NEK7	Activity	app	3	4	-1	24	25	
		Km						
NEK9	Activity	app	-6	-5	-8	2	2	
		Km						
NLK	Binding						34	20
		Km						
NTRK1 (TRKA)	Activity	app	4	10	16	40	33	
		Km						
NTRK2 (TRKB)	Activity	app	6	10	46	63	62	
		Km						
NTRK3 (TRKC)	Activity	app	20	12	34	66	66	
		Km						
NUAK1 (ARK5)	Activity	app				3	10	
		Km						
PAK1	Activity	app				20	26	
		Km						
PAK2 (PAK65)	Activity	app	-3	11	9	6	5	
		Km						
PAK3	Activity	app	7	7	3	11	3	
		Km						
PAK4	Activity	app	16	1	17	2	9	
		Km						
PAK6	Activity	app	14	10	11	14	14	
		Km						
PAK7 (KIAA1264)	Activity	app	8	8	4	10	13	
		Km						
PASK	Activity	app	2	3	3	-2	2	
		Km						
PDGFRA (PDGFR alpha)	Activity	app	7	3	10	11	9	
		Km						
PDGFRA D842V	Activity	app	0	-4	3	3	3	
		Km						
PDGFRA T674I	Activity	app	-1	5	-2	20	21	
		Km						

		app						
PDGFRA V561D	Activity	Km app	20	15	29	22	15	
PDGFRB (PDGFR beta)	Activity	Km app	12	-4	9	-2	-2	
PDK1	Activity	100	3	0	2	18	18	
PDK1 Direct	Activity	Km app				-1	1	
PHKG1	Activity	Km app	6	7	5	5	5	
PHKG2	Activity	Km app	-1	0	2	-9	-5	
PI4KA (PI4K alpha)	Activity	10				1	-7	
PI4KB (PI4K beta)	Activity	Km app				17	14	
PIK3C2A (PI3K-C2 alpha)	Activity	Km app				-1	4	
PIK3C2B (PI3K-C2 beta)	Activity	10				11	-1	
PIK3C2B (PI3K-C2 beta)	Activity	100						
PIK3C3 (hVPS34)	Activity	Km app				-13	-9	
PIK3CA/PIK3R1 (p110 alpha/p85 alpha)	Activity	Km app	0	-35	-29	-14	-4	
PIK3CD/PIK3R1 (p110 delta/p85 alpha)	Activity	Km app				13	8	
PIK3CG (p110 gamma)	Activity	Km app	12	4	10	10	-9	
PIM1	Activity	Km app	-4	-2	0	1	6	
PIM2	Activity	Km app	1	0	2	-8	-7	
PKN1 (PRK1)	Activity	Km app	8	12	5	-7	5	
PLK1	Activity	Km app	5	4	6	1	-6	
PLK2	Activity	Km app	7	13	9	-3	4	
PLK3	Activity	Km app	16	5	8	-6	-7	
PRKACA (PKA)	Activity	Km app	12	41	38	56	53	
PRKCA (PKC alpha)	Activity	Km app	13	6	8	-3	0	

PRKCB1 (PKC beta I)	Activity	Km app	5	6	0	7	7
PRKCB2 (PKC beta II)	Activity	Km app	-4	1	-5	9	7
PRKCD (PKC delta)	Activity	Km app	4	6	9	-1	3
PRKCE (PKC epsilon)	Activity	Km app	-2	2	1	26	30
PRKCG (PKC gamma)	Activity	Km app	4	-2	2	3	6
PRKCH (PKC eta)	Activity	Km app	2	3	4	8	15
PRKCI (PKC iota)	Activity	Km app	11	7	7	13	15
PRKCN (PKD3)	Activity	Km app	69	65	72	77	100
PRKCQ (PKC theta)	Activity	Km app	22	15	17	5	12
PRKCZ (PKC zeta)	Activity	Km app	1	5	-4	1	3
PRKD1 (PKC mu)	Activity	Km app	59	56	65	79	102
PRKD2 (PKD2)	Activity	Km app	75	83	83	85	101
PRKG1	Activity	Km app	-1	0	0	7	6
PRKG2 (PKG2)	Activity	Km app	4	6	4	-4	0
PRKX	Activity	Km app	4	4	5	1	2
PTK2 (FAK)	Activity	Km app	20	11	10	12	10
PTK2B (FAK2)	Activity	Km app	5	1	-2	4	1
PTK6 (Brk)	Activity	Km app	98	55	87	9	11
RAF1 (cRAF) Y340D Y341D	Binding					28	22
RAF1 (cRAF) Y340D Y341D	Activity	100	14	1	10	38	22
RET	Activity	Km app	79	65	67	47	46
RET V804L	Activity	Km app	11	15	10	3	2
RET Y791F	Activity	Km app	84	70	71	55	48

RIPK2	Binding					75	57
ROCK1	Activity	Km app	-1	6	0	5	3
ROCK2	Activity	Km app	3	3	-2	-13	-9
ROS1	Activity	Km app	6	5	1	11	13
RPS6KA1 (RSK1)	Activity	Km app	1	0	4	4	1
RPS6KA2 (RSK3)	Activity	Km app	4	3	3	-5	-6
RPS6KA3 (RSK2)	Activity	Km app	3	4	2	4	2
RPS6KA4 (MSK2)	Activity	Km app	25	12	11	3	8
RPS6KA5 (MSK1)	Activity	Km app	5	2	6	8	10
RPS6KA6 (RSK4)	Activity	Km app	1	5	6	2	7
RPS6KB1 (p70S6K)	Activity	Km app	4	4	4	0	-1
SGK (SGK1)	Activity	Km app	0	2	1	-9	-8
SGK2	Activity	Km app	6	5	0	-2	-7
SGKL (SGK3)	Activity	Km app	-1	-1	-1	-5	-3
SLK	Binding					5	5
SNF1LK2	Activity	Km app				9	7
SPHK1	Activity	Km app				-4	-2
SPHK2	Activity	10				-36	2
SPHK2	Activity	100					
SRC	Activity	Km app	65	27	36	16	7
SRC N1	Activity	Km app	61	21	28	23	13
SRMS (Srm)	Activity	Km app	22	7	11	22	21
SRPK1	Activity	Km app	5	5	4	6	4
SRPK2	Activity	Km app	0	0	3	-3	1

STK16 (PKL12)	Binding				11	3	
STK17A (DRAK1)	Binding				10	6	
STK22B (TSSK2)	Activity	Km app	2	4	2	6	4
STK22D (TSSK1)	Activity	Km app	5	4	5	0	1
STK23 (MSSK1)	Activity	Km app	6	5	6	4	3
STK24 (MST3)	Activity	Km app	22	9	9	0	4
STK25 (YSK1)	Activity	Km app	11	1	5	-2	-3
STK3 (MST2)	Activity	Km app	13	4	3	5	8
STK33	Binding				3	1	
STK4 (MST1)	Activity	Km app	14	8	5	12	18
SYK	Activity	Km app	7	10	4	-10	-3
TAOK2 (TAO1)	Activity	Km app	3	-1	1	-4	2
TAOK3 (JIK)	Binding				9	6	
TBK1	Activity	Km app	7	8	5	9	9
TEC	Binding				3	3	
TEK (Tie2)	Activity	Km app	-2	0	-4	-5	3
TGFBR1 (ALK5)	Binding						
TNK2 (ACK)	Binding				29	31	
TTK	Binding				0	0	
TXK	Activity	Km app					
TYK2	Activity	Km app	0	0	1	10	10
TYRO3 (RSE)	Activity	Km app	9	3	2	24	21
WEE1	Binding				-3	-1	
WNK2	Binding				-3	-4	
YES1	Activity	Km app	54	42	52	42	39
ZAK	Binding				1	1	

ZAP70

Activity	Km app
	-7
	-5
	-6
	14
	10

Appendix 3 – Profiling of staralog inhibitors

Kinase Tested	Star 12	Star 14	Star 23
	% Inhibition		
ACVR1 (ALK2)	2	-1	47
ACVR2B	12	-1	9
BMPR1A (ALK3)	4	1	9
CAMKK1 (CAMKKA)	5	6	17
CAMKK2 (CaMKK beta)	20	9	26
CDK8/cyclin C	9	3	-8
CDK9/cyclin K	13	1	6
CLK4	21	10	48
DDR1	2	3	3
DDR2	-2	-5	5
DMPK	13	-2	52
EPHA3	14	-5	3
EPHA7	9	0	1
KIT V654A	6	-1	4
LIMK1	6	7	1
LIMK2	11	7	-2
MAP2K1 (MEK1) S218D S222D	5	-2	5
MAP2K3 (MEK3)	-11	5	10
MAP2K6 (MKK6) S207E T211E	6	-3	19
MAP3K10 (MLK2)	8	4	3
MAP3K11 (MLK3)	10	-3	11
MAP3K14 (NIK)	5	6	2
MAP3K2 (MEKK2)	10	-7	26
MAP3K3 (MEKK3)	5	-2	26
MAP3K5 (ASK1)	12	8	10

MAP3K7/MAP3K7IP1 (TAK1-TAB1)	9	-9	6
MKNK2 (MNK2)	6	-1	14
MLCK (MLCK2)	15	0	29
MYLK (MLCK)	21	15	52
NLK	9	1	11
RIPK2	4	-6	10
SLK	6	1	1
STK16 (PKL12)	11	-1	5
STK17A (DRAK1)	16	2	12
STK33	10	0	58
TAOK3 (JIK)	8	-4	1
TEC	4	-2	7
TGFBR1 (ALK5)	3	0	7
TNK2 (ACK)	10	1	16
TTK	2	1	31
WEE1	7	-6	31
WNK2	6	3	4
ZAK	2	0	0
CAMK1 (CaMK1)	-14	0	-3
CDK7/cyclin H/MNAT1	-2	-3	-18
CDK9/cyclin T1	-6	3	-8
CHUK (IKK alpha)	-12	2	8
DAPK1	0	7	-1
GSG2 (Haspin)	-16	-3	10
IRAK1	-9	12	7
LRRK2	-16	1	30
LRRK2 G2019S	10	-2	49
NUAK1 (ARK5)	2	-3	62
PI4KA (PI4K alpha)	-14	-4	-12

PI4KB (PI4K beta)	-16	-4	-24
PIK3C2A (PI3K-C2 alpha)	-2	1	1
PIK3C2B (PI3K-C2 beta)	6	-1	-7
PIK3C3 (hVPS34)	-11	0	15
PIK3CA/PIK3R1 (p110 alpha/p85 alpha)	0	8	-12
PIK3CD/PIK3R1 (p110 delta/p85 alpha)	-9	1	-12
PIK3CG (p110 gamma)	-15	2	-37
SPHK1	12	17	0
SPHK2	-4	-3	-2
ABL1	-2	1	-2
ABL1 E255K	2	8	0
ABL1 G250E	-2	3	2
ABL1 T315I	1	7	-1
ABL1 Y253F	-3	2	-11
ABL2 (Arg)	-3	2	-5
ACVR1B (ALK4)	-13	7	-2
ADRBK1 (GRK2)	7	-11	1
ADRBK2 (GRK3)	9	5	-3
AKT1 (PKB alpha)	15	7	14
AKT2 (PKB beta)	16	16	7
AKT3 (PKB gamma)	11	16	14
AMPK A1/B1/G1	10	8	26
AMPK A2/B1/G1	13	13	21
AURKA (Aurora A)	8	51	19
AURKB (Aurora B)	8	20	41
AURKC (Aurora C)	7	8	19
AXL	35	0	33
BLK	4	6	6

BMX	-2	-5	14
BRAF	-8	2	12
BRAF V599E	-10	4	30
BRSK1 (SAD1)	-3	0	35
BTK	-5	-5	10
CAMK1D (CaMKI delta)	-1	5	4
CAMK2A (CaMKII alpha)	5	3	49
CAMK2B (CaMKII beta)	14	6	20
CAMK2D (CaMKII delta)	24	12	81
CAMK4 (CaMKIV)	-10	21	16
CDC42 BPA (MRCKA)	9	6	23
CDC42 BPB (MRCKB)	11	3	18
CDK1/cyclin B	2	5	10
CDK2/cyclin A	5	6	12
CDK5/p25	-3	0	14
CDK5/p35	2	3	5
CHEK1 (CHK1)	11	18	25
CHEK2 (CHK2)	7	3	30
CLK1	5	2	-1
CLK2	3	5	-5
CLK3	4	8	20
CSF1R (FMS)	4	7	27
CSK	-9	0	0
CSNK1A1 (CK1 alpha 1)	-7	-16	2
CSNK1D (CK1 delta)	0	1	0
CSNK1E (CK1 epsilon)	-4	-4	8
CSNK1G1 (CK1 gamma 1)	0	-2	-3
CSNK1G2 (CK1 gamma 2)	4	6	4
CSNK1G3 (CK1 gamma 3)	-1	3	2

CSNK2A1 (CK2 alpha 1)	-5	-1	12
CSNK2A2 (CK2 alpha 2)	5	4	3
DAPK3 (ZIPK)	9	10	21
DCAMKL2 (DCK2)	3	8	-1
DNA-PK	0	9	11
DYRK1A	6	18	5
DYRK1B	2	8	18
DYRK3	-11	-2	24
DYRK4	5	5	1
EEF2K	0	-2	-5
EGFR (ErbB1)	-5	1	-5
EGFR (ErbB1) L858R	-15	-13	6
EGFR (ErbB1) L861Q	-1	3	3
EGFR (ErbB1) T790M	7	11	63
EGFR (ErbB1) T790M L858R	7	5	70
EPHA1	0	5	-1
EPHA2	-2	0	3
EPHA4	-2	-2	5
EPHA5	0	2	-3
EPHA8	-6	-1	-3
EPHB1	-4	-2	0
EPHB2	-2	5	-2
EPHB3	0	2	-3
EPHB4	-4	-1	-7
ERBB2 (HER2)	-5	-15	4
ERBB4 (HER4)	-2	2	-6
FER	0	10	14
FES (FPS)	6	8	-4
FGFR1	5	5	5

FGFR2	-20	3	14
FGFR3	1	4	-18
FGFR3 K650E	5	0	3
FGFR4	1	-5	-6
FGR	0	9	15
FLT1 (VEGFR1)	-7	6	-2
FLT3	41	1	95
FLT3 D835Y	55	14	92
FLT4 (VEGFR3)	-4	7	13
FRAP1 (mTOR)	-6	-4	-2
FRK (PTK5)	-3	10	2
FYN	1	7	-7
GRK4	8	17	-7
GRK5	2	3	6
GRK6	4	-3	11
GRK7	-2	3	45
GSK3A (GSK3 alpha)	-2	8	6
GSK3B (GSK3 beta)	14	17	3
HCK	0	6	7
HIPK1 (Myak)	-2	-2	13
HIPK2	0	3	30
HIPK3 (YAK1)	-1	4	7
HIPK4	1	3	20
IGF1R	-5	0	9
IKBKB (IKK beta)	3	4	20
IKBKE (IKK epsilon)	5	2	-2
INSR	1	2	8
INSRR (IRR)	8	5	8
IRAK4	16	19	-3

ITK	-4	-3	-7
JAK1	-4	-2	1
JAK2	-3	1	17
JAK2 JH1 JH2	11	8	25
JAK2 JH1 JH2 V617F	0	5	3
JAK3	4	5	55
KDR (VEGFR2)	-5	-1	15
KIT	3	1	12
KIT T670I	2	1	4
LCK	-2	1	7
LTK (TYK1)	-2	2	6
LYN A	0	4	10
LYN B	-1	3	5
MAP2K1 (MEK1)	17	14	21
MAP2K2 (MEK2)	10	13	17
MAP2K6 (MKK6)	0	5	14
MAP3K8 (COT)	13	12	11
MAP3K9 (MLK1)	27	25	73
MAP4K2 (GCK)	12	10	14
MAP4K4 (HGK)	2	-4	67
MAP4K5 (KHS1)	-2	11	7
MAPK1 (ERK2)	10	16	13
MAPK10 (JNK3)	24	26	27
MAPK11 (p38 beta)	0	6	-7
MAPK12 (p38 gamma)	-1	-1	-2
MAPK13 (p38 delta)	6	6	-5
MAPK14 (p38 alpha)	-5	4	9
MAPK14 (p38 alpha) Direct	-5	-5	2
MAPK3 (ERK1)	11	12	9

MAPK8 (JNK1)	2	4	-16
MAPK9 (JNK2)	4	5	-14
MAPKAPK2	2	10	-1
MAPKAPK3	9	16	5
MAPKAPK5 (PRAK)	-1	5	-4
MARK1 (MARK)	9	11	41
MARK2	-2	1	42
MARK3	-2	0	74
MARK4	13	6	70
MATK (HYL)	-5	-2	3
MELK	27	25	93
MERTK (cMER)	1	0	2
MET (cMet)	15	14	35
MET M1250T	-2	-1	12
MINK1	4	6	57
MKNK1 (MNK1)	7	4	14
MST1R (RON)	-2	0	25
MST4	19	19	30
MUSK	8	-5	-1
MYLK2 (skMLCK)	15	22	40
NEK1	1	11	34
NEK2	2	8	1
NEK4	4	10	41
NEK6	5	6	1
NEK7	-3	-12	-2
NEK9	5	-3	-2
NTRK1 (TRKA)	4	4	79
NTRK2 (TRKB)	6	6	81
NTRK3 (TRKC)	17	10	94

PAK1	1	-4	16
PAK2 (PAK65)	6	14	6
PAK3	16	15	2
PAK4	-4	4	1
PAK6	12	11	0
PAK7 (KIAA1264)	1	15	3
PASK	8	6	17
PDGFRA (PDGFR alpha)	14	5	24
PDGFRA D842V	4	5	23
PDGFRA T674I	19	3	9
PDGFRA V561D	13	5	52
PDGFRB (PDGFR beta)	-2	1	12
PDK1	13	4	19
PDK1 Direct	8	3	56
PHKG1	15	15	74
PHKG2	0	2	63
PIM1	60	25	51
PIM2	7	6	10
PKN1 (PRK1)	19	10	50
PLK1	-5	-3	10
PLK2	4	10	14
PLK3	-6	13	3
PRKACA (PKA)	-2	8	8
PRKCA (PKC alpha)	-1	3	67
PRKCB1 (PKC beta I)	10	6	36
PRKCB2 (PKC beta II)	4	4	57
PRKCD (PKC delta)	-1	-3	31
PRKCE (PKC epsilon)	-11	3	27
PRKCG (PKC gamma)	7	11	67

PRKCH (PKC eta)	1	2	20
PRKCI (PKC iota)	2	6	12
PRKCN (PKD3)	1	13	84
PRKCQ (PKC theta)	12	14	29
PRKCZ (PKC zeta)	7	9	8
PRKD1 (PKC mu)	6	14	94
PRKD2 (PKD2)	5	9	97
PRKG1	-2	5	23
PRKG2 (PKG2)	14	6	56
PRKX	8	5	52
PTK2 (FAK)	3	5	21
PTK2B (FAK2)	-4	0	34
PTK6 (Brk)	0	4	-4
RAF1 (cRAF) Y340D Y341D	-9	3	15
RET	-4	-1	42
RET V804L	-1	5	62
RET Y791F	-2	3	33
ROCK1	2	2	20
ROCK2	-4	10	25
ROS1	-1	-1	68
RPS6KA1 (RSK1)	9	10	51
RPS6KA2 (RSK3)	20	6	83
RPS6KA3 (RSK2)	23	13	59
RPS6KA4 (MSK2)	8	9	38
RPS6KA5 (MSK1)	2	5	22
RPS6KA6 (RSK4)	33	13	75
RPS6KB1 (p70S6K)	5	4	29
SGK (SGK1)	-17	7	9
SGK2	9	14	9

SGKL (SGK3)	0	8	5
SNF1LK2	9	17	23
SRC	10	9	8
SRC N1	-2	2	1
SRMS (Srm)	6	17	6
SRPK1	18	3	7
SRPK2	18	17	0
STK22B (TSSK2)	3	1	12
STK22D (TSSK1)	2	4	13
STK23 (MSSK1)	-11	-5	2
STK24 (MST3)	-6	-1	7
STK25 (YSK1)	-5	-2	16
STK3 (MST2)	0	-1	89
STK4 (MST1)	-1	-7	89
SYK	2	6	4
TAOK2 (TAO1)	-2	9	6
TBK1	-4	2	8
TEK (Tie2)	3	2	5
TXK	-2	-8	3
TYK2	-6	-8	10
TYRO3 (RSE)	16	-3	43
YES1	1	8	-6
ZAP70	3	11	0

References

1. Manning, G., Whyte, D. B., Martinez, R. & Hunter, T. The protein kinase complement of the human genome. *Science* (2002).
2. Lampson, M. A. & Kapoor, T. M. Unraveling cell division mechanisms with small-molecule inhibitors. *Nat. Chem. Biol.* **2**, 19–27 (2006).
3. Davies, S. P., Reddy, H., Caivano, M. & Cohen, P. Specificity and mechanism of action of some commonly used protein kinase inhibitors. *Biochem. J.* **351**, 95–105 (2000).
4. Bishop, A. C. ...Shokat, K. M. A chemical switch for inhibitor-sensitive alleles of any protein kinase. *Nature* **407**, 395–401 (2000).
5. Liu, Y. *et al.* Structural basis for selective inhibition of Src family kinases by PP1. *Chem. Biol.* **6**, 671–678 (1999).
6. Bishop, A. C., Kung, C., Shah, K. & Witucki, L. Generation of monospecific nanomolar tyrosine kinase inhibitors via a chemical genetic approach. *Journal of the ...* (1999).
7. Zhang, C. *et al.* A second-site suppressor strategy for chemical genetic analysis of diverse protein kinases. *Nat. Methods* **2**, 435–441 (2005).
8. Garske, A. L., Peters, U., Cortesi, A. T., Perez, J. L. & Shokat, K. M. Chemical genetic strategy for targeting protein kinases based on covalent complementarity. *Proc. Natl. Acad. Sci. U.S.A.* **108**, 15046–15052 (2011).
9. Azam, M., Seeliger, M. A., Gray, N. S., Kuriyan, J. & Daley, G. Q. Activation of tyrosine kinases by mutation of the gatekeeper threonine. *Nat. Struct. Mol. Biol.* **15**, 1109–1118 (2008).
10. Hanke, J. H. *et al.* Discovery of a Novel, Potent, and Src Family-selective Tyrosine Kinase Inhibitor: STUDY OF Lck- AND FynT-DEPENDENT T CELL ACTIVATION. *J. Biol. Chem.* **271**, 695–701 (1996).
11. Liu, Y., Shah, K., Yang, F., Witucki, L. & Shokat, K. M. A molecular gate which controls unnatural ATP analogue recognition by the tyrosine kinase v-Src. *Bioorg. Med. Chem.* **6**, 1219–1226 (1998).
12. Zuccotto, F., Ardini, E., Casale, E. & Angiolini, M. Through the ‘gatekeeper door’: exploiting the active kinase conformation. *J. Med. Chem.* **53**, 2681–2694 (2010).
13. Branford, S., Rudzki, Z., Walsh, S. & Grigg, A. High frequency of point mutations clustered within the adenosine triphosphate-binding region of BCR/ABL in patients with chronic myeloid leukemia or Ph-positive (2002).
14. Schindler, T. *et al.* Crystal structure of Hck in complex with a Src family-selective tyrosine kinase inhibitor. *Mol. Cell* **3**, 639–648 (1999).
15. Miller, A. L., Zhang, C., Shokat, K. M. & Lowell, C. A. Generation of a novel system for studying spleen tyrosine kinase function in macrophages and B cells. *J. Immunol.* **182**, 988–998 (2009).
16. Hunter, T. & Plowman, G. D. The protein kinases of budding yeast: six score and more. *Trends Biochem. Sci.* (1997).
17. Cipak, L. *et al.* Generation of a set of conditional analog-sensitive alleles of essential protein kinases in the fission yeast *Schizosaccharomyces pombe*. *Cell Cycle* **10**, 3527–3532 (2011).
18. Holt, L. J. *et al.* Global analysis of Cdk1 substrate phosphorylation sites provides insights into evolution. *Science* **325**, 1682–1686 (2009).
19. Papa, F. R., Zhang, C., Shokat, K. & Walter, P. Bypassing a kinase activity with an ATP-competitive drug. *Science* **302**, 1533–1537 (2003).
20. Wong, S. Sole BCR-ABL inhibition is insufficient to eliminate all myeloproliferative disorder cell populations. *Proceedings of the National Academy of Sciences* **101**, 17456–17461 (2004).
21. Okuzumi, T. *et al.* Inhibitor hijacking of Akt activation. *Nat. Chem. Biol.* **5**, 484–493 (2009).
22. Okuzumi, T. *et al.* Synthesis and evaluation of indazole based analog sensitive Akt inhibitors. *Mol Biosyst* **6**, 1389–1402 (2010).
23. Zhang, C. & Shokat, K. M. Enhanced selectivity for inhibition of analog-sensitive protein kinases through scaffold optimization. *Tetrahedron* **63**, 5832–5838 (2007).
24. Blair, J. A., Rauh, D., Kung, C., Yun, C. H. & Fan, Q. W. Structure-guided development of affinity probes for tyrosine kinases using chemical genetics. *Nature chemical ...* (2007).
25. Au-Yeung, B. B. *et al.* A genetically selective inhibitor demonstrates a function for the kinase

- Zap70 in regulatory T cells independent of its catalytic activity. *Nat. Immunol.* **11**, 1085–1092 (2010).
26. Liu, Y. *et al.* Phosphorylation of the transcription elongation factor Spt5 by yeast Bur1 kinase stimulates recruitment of the PAF complex. *Mol. Cell. Biol.* **29**, 4852–4863 (2009).
 27. Drubin, D. G., Weiss, E. L., Bishop, A. C. & Shokat, K. M. Chemical genetic analysis of the budding-yeast p21-activated kinase Cla4p. *Nat. Cell Biol.* **2**, 677–685 (2000).
 28. Bain, J. *et al.* The selectivity of protein kinase inhibitors: a further update. *Biochem. J.* **408**, 297 (2007).
 29. Beis, I. & Newsholme, E. A. The contents of adenine nucleotides, phosphagens and some glycolytic intermediates in resting muscles from vertebrates and invertebrates. *Biochem. J.* **152**, 23–32 (1975).
 30. Knight, Z. A. & Shokat, K. M. Features of selective kinase inhibitors. *Chem. Biol.* **12**, 621–637 (2005).
 31. Cheng, Y. C. & Prusoff, W. H. Relationship between the inhibition constant (K₁) and the concentration of inhibitor which causes 50 per cent inhibition (I₅₀) of an enzymatic reaction. *Biochemical pharmacology* (1973).
 32. Sánchez-Ruiloba, L. *et al.* Protein Kinase D Intracellular Localization and Activity Control Kinase D-interacting Substrate of 220-kDa Traffic through a Postsynaptic Density-95/Discs Large/Zonula Occludens-1-binding Motif. *J. Biol. Chem.* **281**, 18888–18900 (2006).
 33. Liljedahl, M., Maeda, Y., Colanzi, A., Ayala, I. & Van Lint, J. Protein kinase D regulates the fission of cell surface destined transport carriers from the trans-Golgi network. *Cell* (2001).
 34. Savitt, J. *et al.* The in vivo response of stem and other undifferentiated spermatogonia to the reversible inhibition of glial cell line-derived neurotrophic factor signaling in the adult. *Stem Cells* **30**, 732–740 (2012).
 35. Soskis, M. J. *et al.* A chemical genetic approach reveals distinct EphB signaling mechanisms during brain development. *Nat. Neurosci.* **15**, 1645–1654 (2012).
 36. Tarcsay, A. & Keserű, G. M. Contributions of molecular properties to drug promiscuity. *J. Med. Chem.* **56**, 1789–1795 (2013).
 37. McGovern, S. L., Helfand, B. T., Feng, B. & Shoichet, B. K. A Specific Mechanism of Nonspecific Inhibition. *J. Med. Chem.* **46**, 4265–4272 (2003).
 38. Seeliger, M. A. *et al.* High yield bacterial expression of active c-Abl and c-Src tyrosine kinases. *Protein Sci.* **14**, 3135–3139 (2005).
 39. Witucki, L. A. *et al.* Mutant tyrosine kinases with unnatural nucleotide specificity retain the structure and phospho-acceptor specificity of the wild-type enzyme. *Chem. Biol.* **9**, 25–33 (2002).
 40. Zheng, X. F., Florentino, D., Chen, J., Crabtree, G. R. & Schreiber, S. L. TOR kinase domains are required for two distinct functions, only one of which is inhibited by rapamycin. *Cell* **82**, 121–130 (1995).
 41. Zhang, C. *et al.* Structure-guided Inhibitor Design Expands the Scope of Analog-Sensitive Kinase Technology. *ACS Chem. Biol.* (2013). doi:10.1021/cb400376p
 42. Anastassiadis, T., Deacon, S. W., Devarajan, K., Ma, H. & Peterson, J. R. Comprehensive assay of kinase catalytic activity reveals features of kinase inhibitor selectivity. *Nat. Biotechnol.* **29**, 1039–1045 (2011).
 43. Tamaoki, T. *et al.* Staurosporine, a potent inhibitor of protein kinase. *Biochemical and Biophysical Research Communications* **135**, 397–402 (1986).
 44. Wood, J. L., Petsch, D. T., Stoltz, B. M. & Hawkins, E. M. Total synthesis and protein kinase activity of C (7) methyl derivatives of K252a. *Synthesis* (1999).
 45. Raghavan, S. & Danishefsky, S. J. First total synthesis of staurosporine and ent-staurosporine. *Journal of the American ...* (1995).
 46. Wood, J. L., Stoltz, B. M. & Dietrich, H. J. Total synthesis of (+)-and (-)-K252a. *Journal of the American ...* (1995).
 47. Tanramluk, D., Schreyer, A., Pitt, W. R. & Blundell, T. L. On the origins of enzyme inhibitor selectivity and promiscuity: a case study of protein kinase binding to staurosporine. *Chem Biol Drug Des* **74**, 16–24 (2009).
 48. Xu, Z.-B. *et al.* Catalytic domain crystal structure of protein kinase C-theta (PKCtheta). *J. Biol. Chem.* **279**, 50401–50409 (2004).
 49. Kleinschroth, J., Hartenstein, J. & Rudolph, C. Non-glycosidic/non-aminoalkyl-substituted

- indolocarbazoles as inhibitors of protein kinase C. *Bioorganic & medicinal ...* (1993).
50. Levinson, N. M., Seeliger, M. A., Cole, P. A. & Kuriyan, J. Structural basis for the recognition of c-Src by its inactivator Csk. *Cell* **134**, 124–134 (2008).
 51. Van Hoecke, A. *et al.* EPHA4 is a disease modifier of amyotrophic lateral sclerosis in animal models and in humans. *Nat. Med.* **18**, 1418–1422 (2012).
 52. Egea, J. *et al.* Regulation of EphA 4 kinase activity is required for a subset of axon guidance decisions suggesting a key role for receptor clustering in Eph function. *Neuron* **47**, 515–528 (2005).
 53. Joung, J. K. & Sander, J. D. TALENs: a widely applicable technology for targeted genome editing. *Nat. Rev. Mol. Cell Biol.* **14**, 49–55 (2013).
 54. Bishop, A. C. *et al.* Design of allele-specific inhibitors to probe protein kinase signaling. *Curr. Biol.* **8**, 257–266 (1998).
 55. Dalva, M. B. *et al.* EphB receptors interact with NMDA receptors and regulate excitatory synapse formation. *Cell* **103**, 945–956 (2000).
 56. Li, M. Z. & Elledge, S. J. Harnessing homologous recombination in vitro to generate recombinant DNA via SLIC. *Nat. Methods* **4**, 251–256 (2007).
 57. Breitenlechner, C. B. *et al.* Crystal structures of active SRC kinase domain complexes. *J. Mol. Biol.* **353**, 222–231 (2005).
 58. McCoy, A. J., Grosse-Kunstleve, R. W. & Adams, P. D. Phaser crystallographic software. ... *applied crystallography* (2007).
 59. Emsley, P., Lohkamp, B. & Scott, W. G. Features and development of Coot. ... *Section D: Biological ...* (2010).
 60. Adams, P. D. *et al.* PHENIX: a comprehensive Python-based system for macromolecular structure solution. *Acta Crystallogr. D Biol. Crystallogr.* **66**, 213–221 (2010).
 61. Lourido, S. *et al.* Calcium-dependent protein kinase 1 is an essential regulator of exocytosis in *Toxoplasma*. *Nature* **465**, 359–362 (2010).
 62. Baer, B. R., DeLisle, R. K. & Allen, A. Benzylic oxidation of gemfibrozil-1-O-beta-glucuronide by P450 2C8 leads to heme alkylation and irreversible inhibition. *Chem. Res. Toxicol.* **22**, 1298–1309 (2009).
 63. Lourido, S. *et al.* Optimizing Small Molecule Inhibitors of Calcium-Dependent Protein Kinase 1 to Prevent Infection by *Toxoplasma gondii*. *J. Med. Chem.* (2013). doi:10.1021/jm4001314
 64. McKenzie, S. B. Advances in understanding the biology and genetics of acute myelocytic leukemia. *Clin Lab Sci* **18**, 28–37 (2005).
 65. Stirewalt, D. L. & Radich, J. P. The role of FLT3 in haematopoietic malignancies. *Nat. Rev. Cancer* **3**, 650–665 (2003).
 66. Mattison, R. J., Ostler, K. R., Locke, F. L. & Godley, L. A. Implications of FLT3 mutations in the therapy of acute myeloid leukemia. *Rev Recent Clin Trials* **2**, 135–141 (2007).
 67. Nakao, M. *et al.* Internal tandem duplication of the flt3 gene found in acute myeloid leukemia. *Leukemia* **10**, 1911–1918 (1996).
 68. Yamamoto, Y. *et al.* Activating mutation of D835 within the activation loop of FLT3 in human hematologic malignancies. *Blood* **97**, 2434–2439 (2001).
 69. Kelly, L. M. *et al.* FLT3 internal tandem duplication mutations associated with human acute myeloid leukemias induce myeloproliferative disease in a murine bone marrow transplant model. *Blood* **99**, 310–318 (2002).
 70. Smith, C. C. *et al.* Validation of ITD mutations in FLT3 as a therapeutic target in human acute myeloid leukaemia. *Nature* **485**, 260–263 (2012).
 71. Weisberg, E. *et al.* FLT3 inhibition and mechanisms of drug resistance in mutant FLT3-positive AML. *Drug Resist. Updat.* **12**, 81–89 (2009).
 72. Opatz, S. *et al.* Exome sequencing identifies recurring FLT3 N676K mutations in core-binding factor leukemia. *Blood* (2013). doi:10.1182/blood-2013-01-476473
 73. Mackarehtschian, K. *et al.* Targeted disruption of the flk2/flt3 gene leads to deficiencies in primitive hematopoietic progenitors. *Immunity* **3**, 147–161 (1995).
 74. Fischer, T. *et al.* Phase IIB trial of oral Midostaurin (PKC412), the FMS-like tyrosine kinase 3 receptor (FLT3) and multi-targeted kinase inhibitor, in patients with acute myeloid leukemia and high-risk myelodysplastic syndrome with either wild-type or mutated FLT3. *J. Clin. Oncol.* **28**, 4339–4345 (2010).

75. Cortes, J. E. 767 Phase 1 AML Study of AC220, a Potent and Selective Second Generation FLT3 Receptor Tyrosine Kinase Inhibitor. (2008).
76. Levis, M. *et al.* Plasma inhibitory activity (PIA): a pharmacodynamic assay reveals insights into the basis for cytotoxic response to FLT3 inhibitors. *Blood* **108**, 3477–3483 (2006).
77. Hauf, S. *et al.* Aurora controls sister kinetochore mono-orientation and homolog bi-orientation in meiosis-I. *EMBO J* **26**, 4475–4486 (2007).
78. Carroll, A. S., Bishop, A. C., DeRisi, J. L., Shokat, K. M. & O'Shea, E. K. Chemical inhibition of the Pho85 cyclin-dependent kinase reveals a role in the environmental stress response. *Proceedings of the National Academy of Sciences* **98**, 12578–12583 (2001).
79. Kung, C., Kenski, D. M., Krukenberg, K., Madhani, H. D. & Shokat, K. M. Selective kinase inhibition by exploiting differential pathway sensitivity. *Chem. Biol.* **13**, 399–407 (2006).
80. Sreenivasan, A., Bishop, A. C., Shokat, K. M. & Kellogg, D. R. Specific inhibition of Elm1 kinase activity reveals functions required for early G1 events. *Mol. Cell. Biol.* **23**, 6327–6337 (2003).
81. Liu, Y. *et al.* Two cyclin-dependent kinases promote RNA polymerase II transcription and formation of the scaffold complex. *Mol. Cell. Biol.* **24**, 1721–1735 (2004).
82. D'Aquino, K. E. *et al.* The protein kinase Kin4 inhibits exit from mitosis in response to spindle position defects. *Mol. Cell* **19**, 223–234 (2005).
83. Jones, M. H., Huneycutt, B. J., Pearson, C. G. & Zhang, C. Chemical genetics reveals a role for Mps1 kinase in kinetochore attachment during mitosis. *Current ...* (2005).
84. Pinsky, B. A., Kung, C., Shokat, K. M. & Biggins, S. The Ipl1-Aurora protein kinase activates the spindle checkpoint by creating unattached kinetochores. *Nat. Cell Biol.* **8**, 78–83 (2006).
85. Benjamin, K. R., Zhang, C., Shokat, K. M. & Herskowitz, I. Control of landmark events in meiosis by the CDK Cdc28 and the meiosis-specific kinase Ime2. (2003).
86. Wan, L., de los Santos, T., Zhang, C., Shokat, K. & Hollingsworth, N. M. Mek1 kinase activity functions downstream of RED1 in the regulation of meiotic double strand break repair in budding yeast. (2004).
87. Niu, H. *et al.* Regulation of meiotic recombination via Mek1-mediated Rad54 phosphorylation. *Mol. Cell* **36**, 393–404 (2009).
88. Sekiya-Kawasaki, M. *et al.* Dynamic phosphoregulation of the cortical actin cytoskeleton and endocytic machinery revealed by real-time chemical genetic analysis. *J. Cell Biol.* **162**, 765–772 (2003).
89. Abeliovich, H., Zhang, C., Dunn, W. A., Shokat, K. M. & Klionsky, D. J. Chemical genetic analysis of Apg1 reveals a non-kinase role in the induction of autophagy. *Mol. Biol. Cell* **14**, 477–490 (2003).
90. Weiss, E. L. The *Saccharomyces cerevisiae* Mob2p-Cbk1p kinase complex promotes polarized growth and acts with the mitotic exit network to facilitate daughter cell-specific localization of Ace2p transcription factor. *J. Cell Biol.* **158**, 885–900 (2002).
91. Klein, M. *et al.* Design, synthesis and characterization of a highly effective inhibitor for analog-sensitive (as) kinases. *PLoS ONE* **6**, e20789 (2011).
92. Westfall, P. J. & Thorner, J. Analysis of mitogen-activated protein kinase signaling specificity in response to hyperosmotic stress: use of an analog-sensitive HOG1 allele. *Eukaryotic Cell* **5**, 1215–1228 (2006).
93. Budhwar, R., Fang, G. & Hirsch, J. P. Kelch repeat proteins control yeast PKA activity in response to nutrient availability. *Cell Cycle* **10**, 767–770 (2011).
94. Yorimitsu, T., Zaman, S., Broach, J. R. & Klionsky, D. J. Protein kinase A and Sch9 cooperatively regulate induction of autophagy in *Saccharomyces cerevisiae*. *Mol. Biol. Cell* **18**, 4180–4189 (2007).
95. Rubenstein, E. M. *et al.* Access denied: Snf1 activation loop phosphorylation is controlled by availability of the phosphorylated threonine 210 to the PP1 phosphatase. *J. Biol. Chem.* **283**, 222–230 (2008).
96. Wan, L., Zhang, C., Shokat, K. M. & Hollingsworth, N. M. Chemical inactivation of cdc7 kinase in budding yeast results in a reversible arrest that allows efficient cell synchronization prior to meiotic recombination. *Genetics* **174**, 1767–1774 (2006).
97. Snead, J. L. *et al.* A coupled chemical-genetic and bioinformatic approach to Polo-like kinase pathway exploration. *Chem. Biol.* **14**, 1261–1272 (2007).

98. Young, E. T., Zhang, C., Shokat, K. M., Parua, P. K. & Braun, K. A. The AMP-activated protein kinase Snf1 regulates transcription factor binding, RNA polymerase II activity, and mRNA stability of glucose-repressed genes in *Saccharomyces cerevisiae*. *J. Biol. Chem.* **287**, 29021–29034 (2012).
99. Schoenborn, J. R., Tan, Y. X., Zhang, C., Shokat, K. M. & Weiss, A. Feedback circuits monitor and adjust basal Lck-dependent events in T cell receptor signaling. *Sci Signal* **4**, ra59 (2011).
100. Denzel, A. *et al.* Cutting Edge: A Chemical Genetic System for the Analysis of Kinases Regulating T Cell Development. *The Journal of ...* (2003).
101. Chen, X. *et al.* A chemical-genetic approach to studying neurotrophin signaling. *Neuron* **46**, 13–21 (2005).
102. Fan, Q.-W., Zhang, C., Shokat, K. M. & Weiss, W. A. Chemical genetic blockade of transformation reveals dependence on aberrant oncogenic signaling. *Curr. Biol.* **12**, 1386–1394 (2002).
103. Haan, C., Rolvering, C., Raulf, F., Kapp, M. & Drückes, P. Jak1 has a dominant role over Jak3 in signal transduction through γ c-containing cytokine receptors. *Chem. Biol.* (2011).
104. Su, T. *et al.* A kinase cascade leading to Rab11-FIP5 controls transcytosis of the polymeric immunoglobulin receptor. *Nat. Cell Biol.* **12**, 1143–1153 (2010).
105. Gravells, P., Tomita, K., Booth, A., Poznansky, J. & Porter, A. C. G. Chemical genetic analyses of quantitative changes in Cdk1 activity during the human cell cycle. *Human Molecular Genetics* (2013). doi:10.1093/hmg/ddt133
106. Merrick, K. A. *et al.* Switching Cdk2 On or Off with Small Molecules to Reveal Requirements in Human Cell Proliferation. *Mol. Cell* **42**, 624–636 (2011).
107. Merrick, K. A. *et al.* Distinct activation pathways confer cyclin-binding specificity on Cdk1 and Cdk2 in human cells. *Mol. Cell* **32**, 662–672 (2008).
108. Niswender, C. M. *et al.* Protein engineering of protein kinase A catalytic subunits results in the acquisition of novel inhibitor sensitivity. *J. Biol. Chem.* **277**, 28916–28922 (2002).
109. Qi, Z.-H. *et al.* Protein kinase C epsilon regulates gamma-aminobutyrate type A receptor sensitivity to ethanol and benzodiazepines through phosphorylation of gamma2 subunits. *J. Biol. Chem.* **282**, 33052–33063 (2007).
110. Kenski, D. M., Zhang, C., Zastrow, von, M. & Shokat, K. M. Chemical genetic engineering of G protein-coupled receptor kinase 2. *J. Biol. Chem.* **280**, 35051–35061 (2005).
111. Das, M. *et al.* Suppression of p53-dependent senescence by the JNK signal transduction pathway. *Proc. Natl. Acad. Sci. U.S.A.* **104**, 15759–15764 (2007).
112. Jaeschke, A. *et al.* JNK2 is a positive regulator of the cJun transcription factor. *Mol. Cell* **23**, 899–911 (2006).
113. Wei, F. *et al.* Forebrain overexpression of CaMKII abolishes cingulate long term depression and reduces mechanical allodynia and thermal hyperalgesia. *Mol Pain* **2**, 21 (2006).
114. Wang, H. *et al.* Inducible protein knockout reveals temporal requirement of CaMKII reactivation for memory consolidation in the brain. *Proc. Natl. Acad. Sci. U.S.A.* **100**, 4287–4292 (2003).
115. Lin, J. H. *et al.* IRE1 signaling affects cell fate during the unfolded protein response. *Science* **318**, 944–949 (2007).
116. Burkard, M. E. *et al.* Chemical genetics reveals the requirement for Polo-like kinase 1 activity in positioning RhoA and triggering cytokinesis in human cells. *Proc. Natl. Acad. Sci. U.S.A.* **104**, 4383–4388 (2007).
117. Burkard, M. E. *et al.* Plk1 self-organization and priming phosphorylation of HsCYK-4 at the spindle midzone regulate the onset of division in human cells. *PLoS Biol.* **7**, e1000111 (2009).
118. Maciejowski, J. *et al.* Mps1 directs the assembly of Cdc20 inhibitory complexes during interphase and mitosis to control M phase timing and spindle checkpoint signaling. *J. Cell Biol.* **190**, 89–100 (2010).
119. Sliedrecht, T., Zhang, C., Shokat, K. M. & Kops, G. J. P. L. Chemical genetic inhibition of Mps1 in stable human cell lines reveals novel aspects of Mps1 function in mitosis. *PLoS ONE* **5**, e10251 (2010).
120. Lo, B. *et al.* Lkb1 regulates organogenesis and early oncogenesis along AMPK-dependent and -independent pathways. *The Journal of cell ...* (2012).
121. Tamgüney, T., Zhang, C., Fiedler, D., Shokat, K. & Stokoe, D. Analysis of 3-phosphoinositide-dependent kinase-1 signaling and function in ES cells. *Experimental Cell Research* **314**, 2299–


- 2312 (2008).
122. Brodersen, P. *et al.* Arabidopsis MAP kinase 4 regulates salicylic acid- and jasmonic acid/ethylene-dependent responses via EDS1 and PAD4. *Plant J.* **47**, 532–546 (2006).
 123. Salomon, D. *et al.* Bypassing kinase activity of the tomato Pto resistance protein with small molecule ligands. *J. Biol. Chem.* **284**, 15289–15298 (2009).
 124. Salomon, D., Zhang, C., Shokat, K. M. & Sessa, G. Sensitizing plant protein kinases to specific inhibition by ATP-competitive molecules. *Methods Mol. Biol.* **779**, 185–197 (2011).
 125. Kim, J. S. M. *et al.* A chemical-genetic strategy reveals distinct temporal requirements for SAD-1 kinase in neuronal polarization and synapse formation. *Neural Dev* **3**, 23 (2008).

Publishing Agreement

It is the policy of the University to encourage the distribution of all theses, dissertations, and manuscripts. Copies of all UCSF theses, dissertations, and manuscripts will be routed to the library via the Graduate Division. The library will make all theses, dissertations, and manuscripts accessible to the public and will preserve these to the best of their abilities, in perpetuity.

Please sign the following statement:

I hereby grant permission to the Graduate Division of the University of California, San Francisco to release copies of my thesis, dissertation, or manuscript to the Campus Library to provide access and preservation, in whole or in part, in perpetuity.



Author Signature

9/4/2013
Date